LIÈGE université
Sciences Appliquées

Some Effects of Evaporation in Binary Mixtures

Ramin RABANI

A thesis submitted in partial fulfillment of the requirements
for the degree of Doctor of Philosphy (Phd) in Engineering Science

Supervisor: Prof. Pierre DAUBY

Co-supervisor: Prof. Jean-Philippe PONTHOT

DOCTORAL COLLEGE IN AEROSPACE AND MECHANICS

NOVEMBER 2020

LIÈGE université
Sciences Appliquées

Some Effects of Evaporation in Binary Mixtures

Ramin RABANI

JURY MEMBERS:

Dr. Thomas DESAIVE (Chairman)

Prof. Benoît HAUT

Prof. Jean BRAGARD

Prof. Jean-Philippe PONTHOT (Co-supervisor)

Dr. Hatim MACHRAFI

Prof. Pierre DAUBY (Supervisor)

The presented research was financially supported by F.R.S.-FNRS ("DITRASOL" PDR T.0123.16) and BELSPO ("EVAPORATION" MAP-PRODEX project)).

Abstract

Evaporation of thin films of polymer solutions or of a partially miscible binary mixtures have many industrial applications related for instance to painting, coating, inkjet printing, or the fabrication of photovoltaic devices. Thus, a detailed understanding of the physical mechanisms that drive and influence structure formation in such films is of high scientific and industrial value.

This thesis explores different physical phenomena involved in such systems, and aims at producing novel insights into the dynamics of thin evaporating film of binary mixtures. Four different questions are analyzed, that correspond to four published, or to be published papers. The first two are concerned with polymer solutions, while partially miscible mixtures are analyzed in the other two.

First, we examine the formation of a skin layer at the free surface of a thin evaporating film of a polymer solution. A composition-dependent diffusion coefficient is considered in the liquid phase, which allows describing the gelation and skin formation at the liquid-gas interface. In addition, a realistic model of the evaporation flux, which is based on thermodynamic principles, is proposed. As interesting result, a possible immediate gelation, which is related to a very high evaporation flux, is predicted by our approach. This immediate gelation thus prevents all Marangoni convection in the system.

In the second subject, Rayleigh-Bénard-Marangoni instabilities in a thin evaporating film of a polymer solution are analyzed and the importance of concentration dependent diffusion coefficient, viscosity, and relaxation time is examined using the framework of linear stability theory. The analysis is non-trivial because evaporative mass loss naturally leads to a time-dependent

reference solution. As a key result of the linear stability analysis, we emphasize the presence of two distinct modes of instability in the system. The first one is monotonic, and corresponds to stationary convective cells. The conditions for its appearance are shown to be in good agreement with previous experimental work. The second mode of instability is oscillatory and is related to the viscoelastic properties of polymer solutions. Regions in the parameter space are identified, where an oscillatory instability should occur. This provides interesting indications on the conditions under which this phenomenon could be observed in future experiments.

The third question considered in the thesis consists in exploring the possibility of phase separation in a sessile drop of a partially miscible binary mixture. First, experimental results obtained in the context of a collaboration with ULB (Brussels) are presented. Then a 1-D diffusive model is built to describe the beginning of evaporation in such systems. This model considers the physics of the gas layer above the mixture and its interactions with the liquid. An important result consists in the numerical determination of some conditions that are required for phase separation to occur during the evaporation of the liquid phase.

In the last studied problem, we focus on the dynamics of phase separation and evaporation phenomena in a thin evaporating film of a partially miscible binary mixture. A 2-D diffusive and non-isothermal phase-field model is introduced and numerically solved to describe the dynamics of the system and to assess the competition between evaporation and phase separation. Depending on the leading mechanism, different types of morphology can appear in the separating mixture, which are analyzed in detail. We also examine the mid- and long-term evolution of the system. At last, we describe an experimental setup and the associated results obtained in our collaboration with ULB, that nicely confirm our theoretical and numerical predictions

about the morphologies that can be created by evaporation and phase separation.

Résumé

L'évaporation de films minces de solutions de polymères, ou de mélanges binaires partiellement miscibles a de nombreuses applications industrielles liées, par exemple, à la peinture, à l'enduction, à l'impression par jet d'encre, ou à la fabrication de composants photovoltaïques. Il en résulte que la connaissance détaillée des mécanismes physiques qui régissent et influencent la formation de structure dans de tels films est d'un grand intérêt scientifique et industriel.

Cette thèse explore différents mécanismes physiques impliqués dans de tels systèmes et a pour but de fournir de nouvelles connaissances dans la dynamique de l'évaporation de films minces de mélanges binaires. Quatre questions distinctes sont analysées, correspondant à quatre travaux publiés, ou en voie de l'être. Les deux premières se rapportent à des solutions de polymères, alors que ce sont des mélanges binaires partiellement miscibles qui sont envisagés dans les deux autres.

Tout d'abord, on examine la formation d'une « peau » à la surface libre d'un film de solution de polymères qui s'évapore. Un coefficient de diffusion qui dépend de la composition est pris en compte dans la phase liquide, ce qui permet de décrire la gélification et la formation d'une peau à l'interface liquide-gaz. En outre, on propose un modèle réaliste du flux d'évaporation, basé sur des principes thermodynamiques. Comme résultat intéressant, on met en évidence la possibilité d'une gélification immédiate de l'interface, reliée à un flux d'évaporation très important. La survenue de ce phénomène empêche dès lors toute convection de Marangoni dans le système.

Dans le second sujet de la thèse, on s'intéresse aux instabilités de Rayleigh-Bénard-Marangoni dans un film mince d'une solution de polymères qui

s'évapore et, dans le cadre d'une étude de stabilité linéaire, on examine l'importance de la dépendance par rapport à la composition du mélange des coefficients de diffusion, de viscosité et du temps de relaxation. L'analyse est non triviale parce que la perte de masse par évaporation conduit naturellement à une solution de référence qui dépend du temps. Comme résultat important de l'étude de stabilité linéaire, nous avons mis en évidence la présence de deux modes distincts d'instabilité. Le premier est monotone et correspond à des cellules de convection stationnaires. On montre en outre que les conditions d'apparition de ce mode sont en bon accord avec des résultats expérimentaux antérieurs. Le second mode d'instabilité est oscillant et est relié aux propriétés de viscoélasticité des solutions de polymères. Les domaines de l'espace des paramètres dans lesquels les instabilités oscillantes sont possibles sont déterminés. Ceci fournit des indications intéressantes sur les conditions sous lesquelles le phénomène pourrait être observé dans de futures expériences.

La troisième question envisagée dans la thèse consiste à examiner la possibilité de séparation de phases dans une goutte sessile constituée d'un mélange binaire partiellement miscible. D'abord, des résultats expérimentaux obtenus dans le cadre d'une collaboration avec l'ULB (Bruxelles) sont présentés. Ensuite, un modèle 1-D diffusif est construit afin de décrire le début de l'évaporation dans de tels systèmes. Ce modèle considère la physique de la couche de gaz surplombant le mélange binaire et ses interactions avec celui-ci. Un résultat important consiste en la détermination numérique de certaines conditions qui sont requises pour que la séparation de phases puisse effectivement se produire pendant l'évaporation.

Dans le dernier problème étudié, nous nous intéressons à la dynamique de l'évaporation et de la séparation de phases dans une mince couche d'un

mélange binaire partiellement miscible qui s'évapore. Un modèle à champ de phase 2-D, diffusif et non isotherme est construit et résolu numériquement afin de décrire la dynamique du système et d'évaluer la compétition entre évaporation séparation de phases. En fonction du mécanisme dominant, différents types de morphologies apparaissent dans la couche et sont étudiés en détail. Nous examinons également le comportement à moyen et long terme du système. Enfin, nous décrivons un dispositif expérimental et les résultats correspondant obtenus dans le cadre de notre collaboration avec l'ULB. Ces résultats confirment de manière convaincante nos prédictions théoriques et numériques à propos des morphologies qui peuvent être engendrées par l'évaporation et la séparation de phases.

Acknowledgements

Foremost I would like to thank my supervisor Pierre Dauby for guiding me through my PhD. I am also very grateful for his support and understanding during the challenges I encountered in my PhD as well as his patience in combination with his time for countless discussions, which made the doctoral journey a truly enjoyable, productive, and enlightening one.

In addition to my official supervisor, I am greatly indebted to my colleague Hatim Machrafi for the guidance and suggestions he has so kindly provided while I was working on this thesis. I have also benefited from many fruitful discussions with him.

I am grateful to Pierre Colinet, Benoit Haut, and Hosein Sadafi for the valuable meetings, discussions and collaboration by undertaking experimental studies in the TIPs research group at ULB. With their collaboration, I was able to observe real phenomena in the experiments that was enriching for my study.

I would like to thank my friends and colleagues, Sarah, Simon, and Vincent for providing a decent environment in the office for scientific discussions and friendly talks.

I am forever grateful to my father and mother instilling in me many values that were very useful during my PhD. My elder brother Mehran and my twin brother Mehrdad for their loves and support.

Last but not least, I would like to thank my wife Mona for unceasing love and support. She has always encouraged and assisted me in my PhD.

List of publications

- Ramin Rabani, Hatim Machrafi, Pierre Dauby, *Effect of including a gas layer on the gel formation process during the drying of a polymer solution*, Eur. Phys. J. E 40 (10) (2017) 89.

- Ramin Rabani, Hatim Machrafi, Pierre Dauby, *Influence of composition dependent diffusion coefficient, viscosity and relaxation time on evaporative Rayleigh–Bénard–Marangoni instabilities induced by solvent evaporation in a polymer solution*, Microgravity Sci. Technol. 31, 615–628 (2019).

- Hosein Sadafi, Ramin Rabani, Sam Dehaeck, Hatim Machrafi, Benoit Haut, Pierre Dauby, Pierre Colinet, *Evaporation induced demixing in binary sessile drops*, Colloids and Surfaces A: Physicochemical and Engineering Aspects, (2020) 125052.

- Ramin Rabani, Hosein Sadafi, Hatim Machrafi, Monavar Abbasi, Benoit Haut, Pierre Dauby, *Morphology of phase separation during the evaporation of a thin film of a partially miscible binary mixture*, Colloids and Surfaces A: Physicochemical and Engineering Aspects (Submitted).

Contents

List of Figures

List of Tables

Introduction

Evaporation is a universal phenomenon that occurs in nature, for instance in the evaporation process of water drops in clouds, or in our daily life when the transition from liquid water to gaseous steam takes place when we boil a kettle of water. They are also present in many industrial contexts including coatings and painting technologies [1-3], ink-jet printing [4-6], the manufacturing of membranes [7-9], and many functional materials that are created thanks to evaporative self-assembly. Therefore, evaporation remains a very challenging topics for scientists and engineers.

Evaporation of a volatile component at the free surface of a solution generates a temperature gradient in the liquid due to the latent heat absorption. When the fluid is a mixture, this evaporation also generates a concentration gradient due to the volatility difference between components. Thus, evaporation can actually generate thermal and solutal instabilities in mixtures, which are an interesting type of hydrodynamic instabilities. The hydrodynamical instabilities [10-12] have drawn the attention of scientists and researchers for many years and their studies aims at determining the boundaries in the parameter space of the stability and instability domains, and also to analyze to behavior of the fluid after an instability has occurred. The fundamentals of hydrodynamic instability, both theoretical and

experimental, were presented particularly by Helmholtz, Kelvin, Reynolds, Rayleigh, Taylor, and Bénard during the past centuries.

When a liquid layer of a mixture with a free surface is subjected to temperature and concentration gradients (typically due to the evaporation at free surface), convection can be induced by two mechanism: Rayleigh-Bénard instability [12, 13] (buoyancy-driven convection) and Bénard-Marangoni instability [12, 14] (surface tension-driven convection). Rayleigh-Bénard instability is caused by the variation of density with respect to temperature and concentration while Bénard-Marangoni instability can occur by temperature and concentration changes of surface tension at free surface. When both mechanisms are present, the problem is commonly referred to as the Rayleigh-Bénard-Marangoni instability [12, 15, 16].

Beside the aforementioned hydrodynamic instabilities, evaporation in a mixture of liquids (binary and ternary mixtures) can lead to different phase transitions or phase changes in the system, such as the sol-gel or the demixing transitions that will be analyzed in this thesis.

The sol-gel transition (also known as gelation) is a change from a liquid phase to a gel phase [17, 18]. To achieve a gel state, we need at least two components, one should be a fluid (solvent) while the other component is not a fluid (solute). The initial phase is effectively formed by a liquid (for instance, water) in which a solute (usually colloidal particles) is dispersed, in colloidal solution, or a polymer is dissolved, in polymer solution [17, 18]. This initial fluid state is usually called “sol”, for “solution”. In determined conditions (e.g., for certain temperature, concentration, and/or pH), the sol goes through the sol-gel transition and a gel phase is created. The so-called gel point is the critical point where the transition occurs, from the fluid-like behavior to a viscoelastic behavior [17, 19]. It is important to emphasize that

several physical properties are effectively drastically changed at the gel point [17, 19], such as viscosity, diffusion coefficient, weight average, relaxation time and so on. For instance, in the polymer solution, at the gel point, the appearance of a three dimensional network induces a viscosity divergence and the emergence of elasticity in the solution, that is also known as gelation.

In demixing, or phase separation phenomena, the phase transition is from a mixed state to a demixed state [20-22]. In this situation, it is necessary to have at least two liquid components. Either temperature variations (sufficient cooling of a mixture), or concentration changes (adding/removing some components in the mixture), or both as in the case of evaporation, can in certain circumstances drastically modify the interactions between the components of a fluid mixture. As a consequence, some thermodynamic properties of the mixture, such as the free energy, are modified accordingly: the components become immiscible and the liquid phases start to separate in the system. From a thermodynamic point of view, the demixing conditions on temperature and concentrations are described by a phase diagram. When a well-mixed mixture crosses the phase boundary to enter the miscibility gap, either in the meta-stable region or the unstable region, phase separation takes place [20-22].

The overall aim of this thesis is to build an understanding of some physical processes and phenomena that occur during the evaporation of a binary mixture, specifically in a thin film, including skin formation (gelation), hydrodynamic instabilities, and demixing (phase separation). By using a combination of mathematical modelling, experimental set-up, and numerical approaches, valuable insights into the dynamics of evaporating binary mixtures are obtained in different problems.

The present manuscript takes the form of a “paper-thesis”, of which four chapters consist of four published, or to be published papers and thus describe the truly original research work. After the present introduction, the manuscript is divided into two main Parts, which are devoted to the study of evaporation in binary mixtures in the following two situations:

- Part I: Thin evaporating film of a polymer solution
- Part II: Phase separation in thin evaporating film of a partially miscible binary mixture

In each Part, an introduction is first proposed, that describe the corresponding general context and present the questions that are going to be analyzed. The two chapters of each Part then consist of the text of the two associated papers. In Part I, the two papers respectively describe skin formation and hydrodynamic instabilities in a polymer solution. In Part II, the two papers are concerned demixing (phase separation) in a partially miscible binary mixture.

Finally, the conclusion of the thesis is presented. In this part of the manuscript, the main results are first summarized and further discussed. Then some limitations of our approach are discussed and possible interesting avenues of future work are mentioned.

References

[1] C. Park, J. Yoon, E.L. Thomas, Enabling nanotechnology with self assembled block copolymer patterns, Polymer, 44 (2003) 6725-6760.

[2] S. Walheim, E. Schäffer, J. Mlynek, U. Steiner, Nanophase-separated polymer films as high-performance antireflection coatings, Science, 283 (1999) 520-522.

[3] K.-D. Bouzakis, N. Michailidis, G. Skordaris, E. Bouzakis, D. Biermann, R. M'Saoubi, Cutting with coated tools: Coating technologies, characterization methods and performance optimization, CIRP annals, 61 (2012) 703-723.

[4] B.J. De Gans, P.C. Duineveld, U.S. Schubert, Inkjet printing of polymers: state of the art and future developments, Advanced materials, 16 (2004) 203-213.

[5] J.A. Lim, W.H. Lee, H.S. Lee, J.H. Lee, Y.D. Park, K. Cho, Self-organization of ink-jet-printed triisopropylsilylethynyl pentacene via evaporation-induced flows in a drying droplet, Advanced functional materials, 18 (2008) 229-234.

[6] A. Kamyshny, M. Ben-Moshe, S. Aviezer, S. Magdassi, Ink-jet printing of metallic nanoparticles and microemulsions, Macromolecular Rapid Communications, 26 (2005) 281-288.

[7] L. Martinez-Diez, F. Florido-Diaz, M. Vazquez-Gonzalez, Study of evaporation efficiency in membrane distillation, Desalination, 126 (1999) 193-198.

[8] A. Alkhudhiri, N. Darwish, N. Hilal, Membrane distillation: A comprehensive review, Desalination, 287 (2012) 2-18.

[9] E. Curcio, E. Drioli, Membrane distillation and related operations—a review, Separation and Purification Reviews, 34 (2005) 35-86.

[10] F. Charru, Hydrodynamic instabilities, Cambridge University Press2011.

[11] S.W. Haan, Weakly nonlinear hydrodynamic instabilities in inertial fusion, Physics of Fluids B: Plasma Physics, 3 (1991) 2349-2355.

[12] P. Colinet, J.C. Legros, M.G. Velarde, Nonlinear dynamics of surface-tension-driven instabilities, Wiley-vch Berlin2001.

[13] G. Freund, W. Pesch, W. Zimmermann, Rayleigh-Bénard convection in the presence of spatial temperature modulations, Journal of fluid mechanics, 673 (2011) 318.

[14] J. Margerit, P. Colinet, G. Lebon, C.S. Iorio, J.C. Legros, Interfacial nonequilibrium and Benard-Marangoni instability of a liquid-vapor system, Physical Review E, 68 (2003) 041601.

[15] V. Regnier, P. Dauby, G. Lebon, Linear and nonlinear Rayleigh–Bénard–Marangoni instability with surface deformations, Physics of Fluids, 12 (2000) 2787-2799.

[16] O. Touazi, E. Chénier, F. Doumenc, B. Guerrier, Simulation of transient Rayleigh–Bénard–Marangoni convection induced by evaporation, International journal of heat and mass transfer, 53 (2010) 656-664.

[17] P. Innocenzi, The sol to gel transition, Springer2016.

[18] P. Papon, J. Leblond, P.H. Meijer, Physics of Phase Transitions, Springer2002.

[19] L. Guo, Gelation and micelle structure changes of aqueous polymer solutions, (2003).

[20] S.Z. Cheng, Phase transitions in polymers: the role of metastable states, Elsevier2008.

[21] L.M. Robeson, Polymer blends, A Comprehensive Review, (2007).

[22] S. Puri, V. Wadhawan, Kinetics of phase transitions, CRC press2009.

I Thin evaporating film of a polymer solution

Chapter 1

Introduction to papers 1 and 2

1.1 General context

Evaporating films of polymer solutions, colloidal suspensions, and emulsions, when the solvent evaporates, are commonly encountered in our daily life. For example, several interesting phenomena happen in a cup filled with hot coffee [1] (Fig. 1-1) including convection and a thin skin layer on top of the hot coffee.

In addition to this daily routine interest, it is a rather practical but important issue to know how the evaporation process affects many modern technologies, such as painting (Fig. 1-2-a), fabrication of electronic components (Fig. 1-2-b), and ink-jet printing (Fig. 1-2-c) [2-6]. Evaporation can lead to aggregation of polymer at the free interface of a polymer solution. Under certain conditions, this accumulation of polymer will be sufficiently important to induce the formation of a viscous skin at the free surface. From an industrial point of view, for instance in painting technology, the residual stress, which emerges when a thin film of the polymer solution is dried on a substrate, is significantly influenced by the procedure of skin formation [7].

In ink-jet printing, the form of the final deposit, when solvent-rich ink is dried, is significantly related to the skin formation phenomena [8]. Beside this skin formation, the evaporation of solvent can also trigger hydrodynamic instabilities [9-12], which can give rise to nontrivial spatial distributions of polymer and influence the final phase of the dried film. Therefore, it is of great interest and an important challenge to further understand the dynamics of skin formation and the appearance of convective patterns that happen during the evaporation process of a polymer solution.

Fig. 1-1. Misty thin skin that covers the hot water surface. The patterns move through the skins due to the convection flow [1].

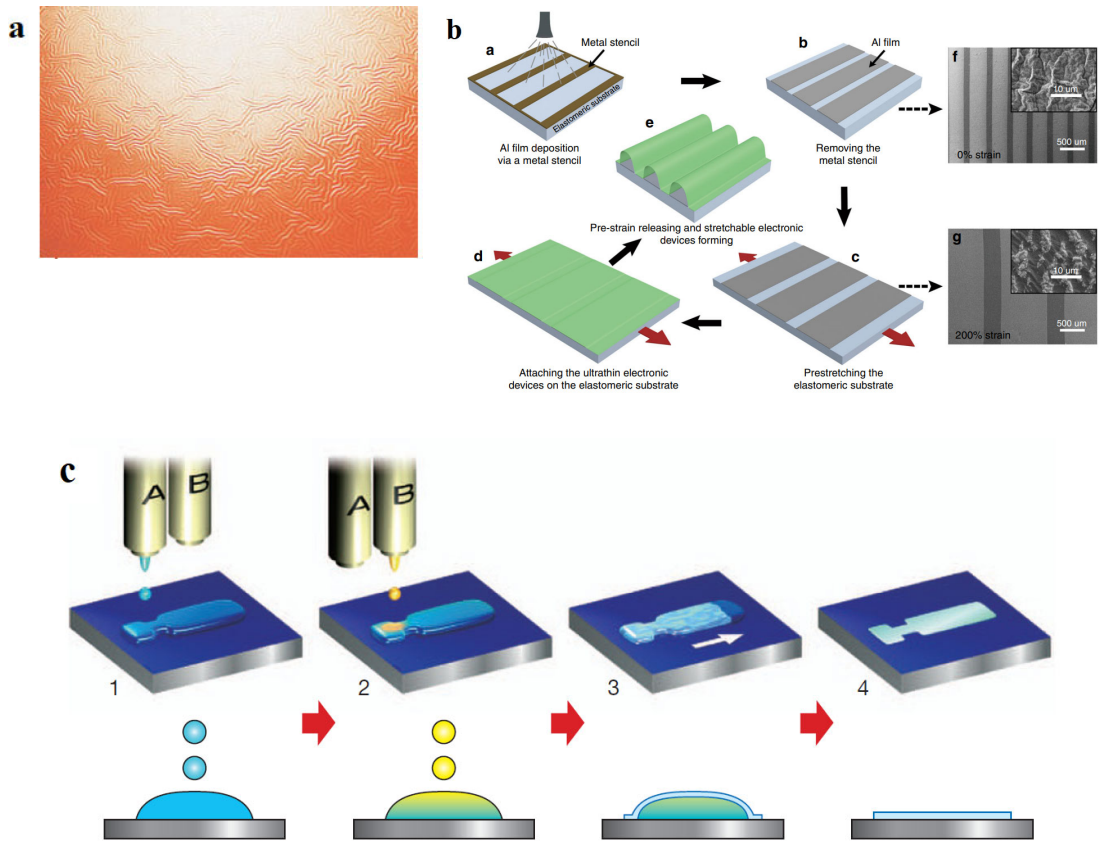

Fig. 1-2. a) Wrinkling of the outer surface of a paint coating due to the to the rapid formation of a skin [13], b) Fabrication process for the stretchable electronic devices [14], c) Inkjet printing of organic single-crystal thin film [5].

1.2 Skin formation during the evaporation process

The depletion of solvent due to evaporation can lead to the formation of a solute (polymer or colloidal particles)-rich layer at the liquid-gas interface and subsequently a viscous skin can form when the solute concentration becomes sufficiently high near the free surface (Fig. 1-3). This viscous skin becomes a gel phase when the solute concentration reaches a certain value, which is called the gelation concentration. During the gelation process, a linear polymer chain crosslinks either with itself to form intramolecular cycles, or with another chain to create branched chains [15]. Note that the microscopic gelation process and the formation of branch chains will not be examined in details here and only the effect of gelation on the global physical

properties of an evaporative polymer solution will be considered in this thesis. The elastic energy of the gel, when gelation takes place, has a significant effect on the physical properties of the polymer solution such as the diffusion coefficient and the viscosity, which are not constant and can significantly change [16-19].

Whatever the nature of the skin layer is, when and how such a skin layer is formed is a significant and interesting question in controlling the evaporation process of a thin liquid film. There are several research studies concerning the skin formation phenomenon in an evaporative liquid film, of which we now briefly discuss some of the most important ones.

The first mathematical studies over the skin formation, because of the evaporation of the solvent component, in a polymer solution were performed by Lawrence [20, 21] and de Gennes [22]. Ozawa et al. [18] suggested a diffusive model for the drying dynamics of a polymer solution taking into account the effect of skin formation due to the gelation at the free surface. The model involved a set of nonlinear partial differential equations and a phenomenological expression for the diffusion coefficient of the polymer solution. The authors emphasized that the drying dynamics of polymer solutions is effectively associated with the gelation at the free surface, which results in a significant increase of the diffusion coefficient of a polymer solution.

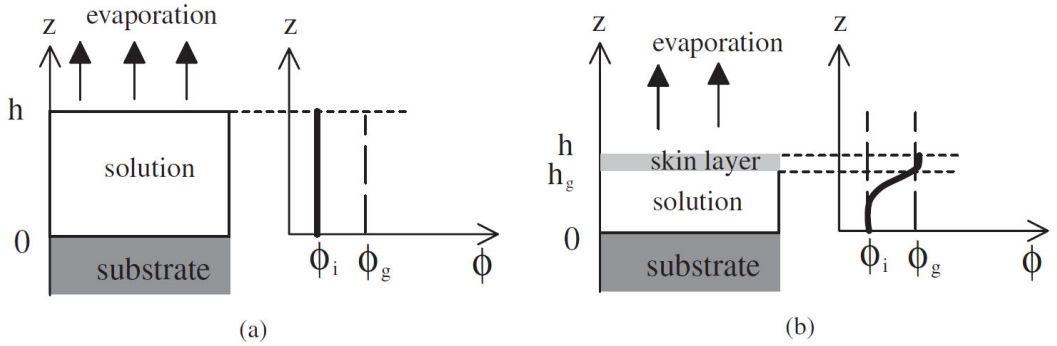

Fig. 1-3. Schematic of thin evaporating film of a polymer solution (left) and a profile of polymer concentration ∅ (right) for an initial situation (a) and a situation after skin formation (b) [18]. $\emptyset_i$ and $\emptyset_g$ are respectively the initial concertation and the gelation concentration. h is the total height of the solution and the possible skin, h_g is the thickness of the liquid part.

Münch et al. [23] modeled the one-dimensional development of a thin layer during the spin coating of a single polymer species blended in a solvent. The main interest of this research study was in controlling the appearance and development of skin formation where the solvent evaporates at the free surface. In another work, Hennessy et al. [24] developed a model for the solvent evaporation in a thin liquid film consisting of a volatile solvent and one or more non-volatile solutes. They tracked the volume fraction of the solvent using a diffusion model, coupled this with mass transfer across the moving interface. They also made the quantitative predictions about the drying dynamics and the skin formation at the free surface.

1.3 Hydrodynamic instability of a thin evaporating film

1.3.1 Thermal and solutal instabilities

In pure liquids or binary mixtures, evaporation at the upper surface creates a temperature gradient induced by cooling through latent heat absorption. In the case of binary mixtures, this evaporation also generates a concentration gradient because of a difference in components volatility. Because the

density and surface tension of the binary mixture typically depend on temperature and concentration, buoyancy forces and/or surface tension variations can destabilize the liquid layer and lead to pattern formation [25]. Therefore, temperature and concentration gradients can trigger different instabilities which come in two flavors, the thermal and solutal type.

Thermal and solutal instabilities have been described in many research studies. The earliest studies regarding the pure liquid layer subject to heating from below were conducted by Bénard [26, 27]. His early experiments indicated that sufficiently large temperature gradients can result in the onset of convection within the layer. Later theoretical analysis of Bénard's experiments by Rayleigh [28] indicated that this convection could be driven by thermally induced density variations within the fluid layer. Nevertheless, experimental studies conducted by Block [29] suggested a different mechanism for convection based on thermally induced gradients in the surface tension. A mathematical analysis by Pearson [30] two years later verified Block's claims for the surface tension-driven flow (Bénard-Marangoni convection). Pearson clarified that, for the most common pure liquids, the Marangoni effect or buoyancy was the main motor of the thermal instability for layer thicknesses respectively lower or higher than approximately 1 cm. Berg et al. [31] emphasized how evaporation can result in the onset of thermal convection in fluid layers that are not heated from below. The temperature gradient in this system is the consequence of evaporative cooling at the surface of the fluid. A comprehensive theoretical study of evaporating layers of pure fluid has been conducted by Burelbach et al. [32]. This study was then extended by Sultan et al. [33] by taking into account the diffusion of vapor in the overlaying gas. Another interesting theoretical model of the evaporation of a pure liquid layer was obtained by Haut and Colinet [34]. Their analysis predicted that the existence of an inert

gas highly triggers the appearance of surface-tension-driven instabilities. An experimental study of the evaporation of a polymer solution (polyisobutylene/toluene) was performed by Toussaint et al. [35]. In the experimental process, the solution, initially maintained at the ambient temperature, is poured in a dish located in an extractive hood (Fig. 1-4). The convective patterns start to appear when the evaporation of solvent begins, at the very beginning of the experiment. For small thicknesses, the cell patterns induced by surface tension disappear due to a thin viscous skin that spreads over the entire surface. In contrast, a succession of cells and rolls was detected and after a while (a few hundred seconds), the buoyancy driven convection was the only dominant process under the thin viscous skin (Fig. 1-5).

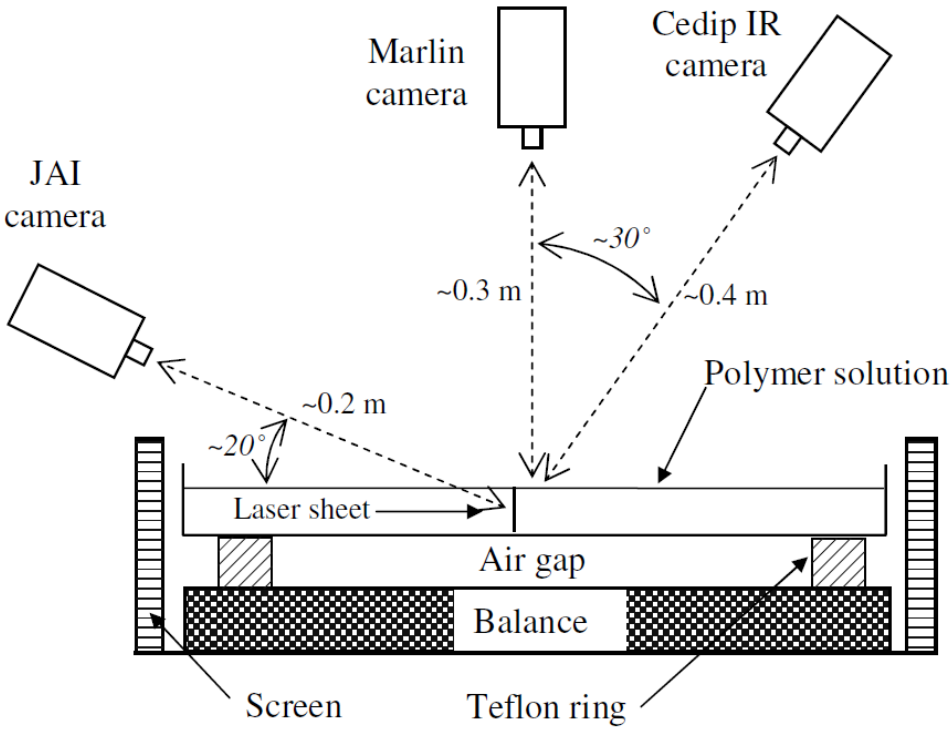

Fig. 1-4. Schematic of experimental setup [35].

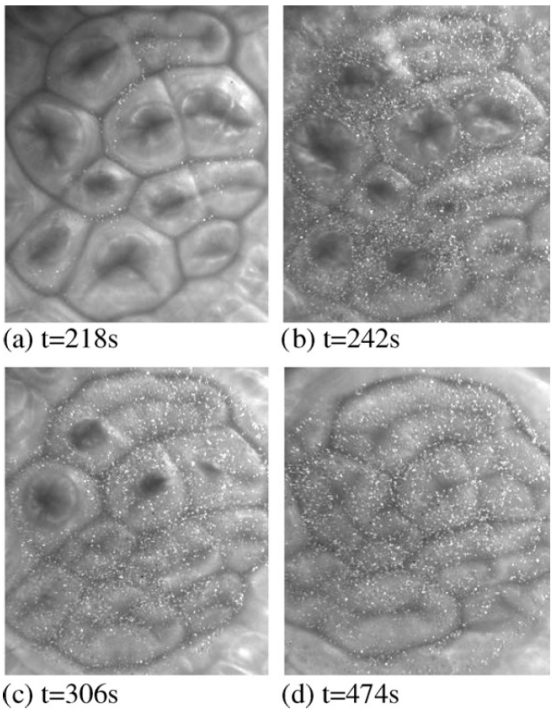

Fig. 1-5. Skin formation [35]. Focus on a few cells at four time slots for the structure. The surface is distributed with aluminum powder between photos (a) and (b); photo (b): the aluminum powder had converged at the boundary of convective cells where the skin begins to form; photos (c) and (d): the skin overflows the entire surface, while convection is still active under the thin viscous skin.

A linear analysis of the thermal instability for one-component system based on a non-normal approach was proposed one year later by Doumenc et al. [9] to describe the experimental work presented by Toussaint et al. [35]. Doumenc et al. showed that their linear instability analysis follows the experimental observations well.

When the fluid is a binary solution, the process of evaporation is also linked to the solutal Rayleigh-Bénard-Marangoni instability through the fact that non-uniform removal of solvent can generate the necessary gradients in composition that drive the formation of convection cells. The experimental and theoretical studies of evaporating binary mixtures have given evidence to suggest that convection is primarily driven by a solutal instability rather than its thermal counterpart [10, 12, 36]. Ha and Lai [37] investigated

theoretically the onset of Marangoni instability because of the evaporation of a two-component droplet using a quasi-steady approximation. Machrafi et al. [11] considered buoyancy and surface tension impacts, of thermal and solutal origin, in their linear stability analysis. Their findings showed that the onset of convection was driven by the solutal Bénard-Marangoni mechanism.

An important issue, in complex fluids when one of the components is non-volatile (for example in a polymer solution or a colloidal solution), is that the physical properties often depend significantly on the solvent concentration, so that the ratio between destabilizing and stabilizing forces changes continually during the evaporation process. Practical results of this can be important and several experimental works have mentioned a possible connection between solutal convection and wrinkles or surface corrugations observed on dried films (Fig. 1-6) [12, 38]. De Gennes [22, 39] developed a theoretical approach to describe the impact of the solvent removal in a thin evaporating film of a polymer solution on the convective instabilities and their role in the surface corrugation formation. He indicated that in an evaporating film, a ‘‘plume” of solvent-rich fluid induces a local depression in surface tension, and the surface forces tend to strengthen the plume. His calculations showed that the solutal critical thickness is much smaller than the thermal one and thus the concentration impacts should overcome the thermal impacts. Trouette et al. [40] analyzed the onset of solutal convection for a thin evaporating film of a polymer solution submitted to the removal of solvent at the liquid-gas interface. A model was created considering the change of the viscosity with the solute concentration, a constant evaporative flux, and a non-deformable interface. Their results revealed a substantial effect of the concentration-dependent viscosity on the threshold of convection (Fig. 1-7).

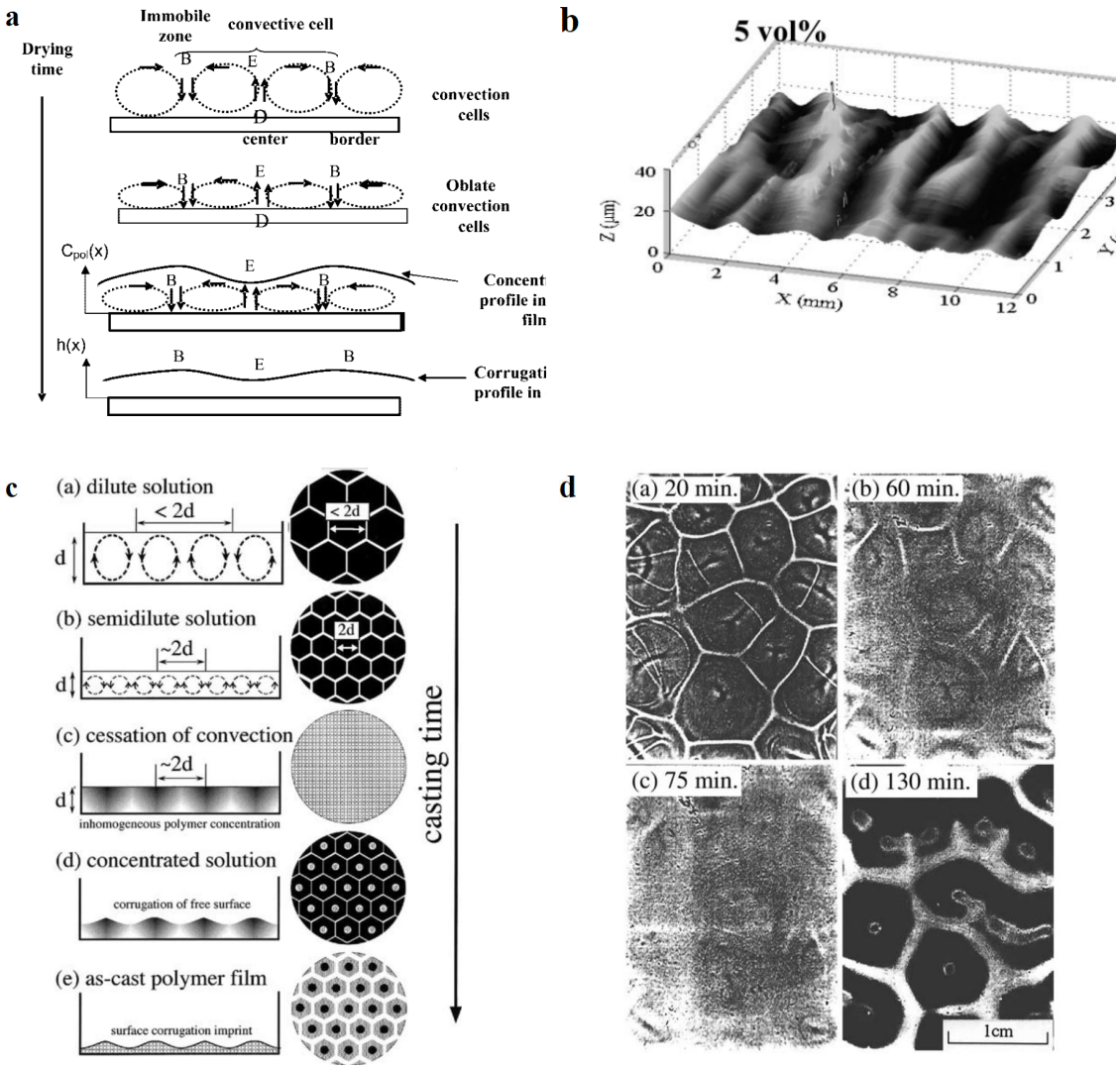

Fig. 1-6. a) Scheme of formation mechanism of surface corrugation via the evolution of convective cells into a concentration profile [12] and b) (Top)Three-dimensional morphology profiles of the surface corrugation of films prepared by the evaporation of polystyrene in toluene solutions [12], c) Schematic illustration for change in side and through views of a casting solution [12] and d) Experimental results for change in pattern of casting polymer solution with solvent evaporation [12].

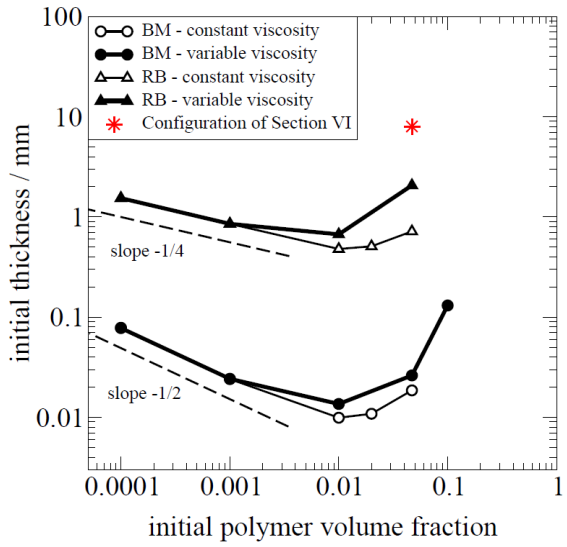

Fig. 1-7. Critical thickness as a function of the initial polymer volume fraction for the polyisobutylene (PIB)/toluene solution [40].

1.3.2 Linear stability of time-dependent reference solutions

It is not straightforward to study an evaporating layer of fluid mathematically, because of the evaporative mass loss, typically leading to time dependent solutions. Within the framework of the linear stability analysis, this usually implies that the reference solution about which the system is linearized depends on the time. Hence, the linear problem for the perturbations with respect to the reference solution becomes non-autonomous in the time changing. In some situations, it is possible to simplify the stability problem by trying to obtain a transformation that separate the time and space parameters or by seeking a similarity solution in specific time schemes, see Smolka and Witelski [41] and Kang and Choi [42].

Relating to the condition where it is not possible to deal with the linear stability problem analytically, an approximate method should be used or some simplified assumptions about the reference solution should be made. One possibility is to consider the linearized problem as an initial value

problem, which can be solved numerically. The stability of the system is then deduced by taking a suitable norm for the perturbation. In some cases, this norm can be associated with a physical quantity such as energy; see, for example, Doumenc et al. [43], Shen [44], or Warner et al. [45]. Such a numerical approach was taken by Foster [46] to study convection in a layer of fluid that is uniformly cooled from above. A shortcoming of this approach is that the growth of a perturbation will depend sensitively on its initial condition.

One method for avoiding the difficulties associated with a time-dependent reference solution is to modify the problem in some manner that removes this dependence. To study the stability of an evaporating solvent-polymer mixture, Souche & Clarke [47] introduce an artificial flux boundary condition at the substrate which compensates for the loss of solvent due to evaporation. A similar approach was also taken by Sultan et al. [33]. The shortcoming of this approach is that it is not easy to evaluate how the artificial modification of the problem affects the stability of the system.

An alternative method for the analysis of a non-autonomous stability problem is the so-called frozen-time approach, which is according to the assumption that the reference solution evolves so slowly in comparison with the perturbations that it can be frozen. The time variable in the reference solution is then considered as an extra system variable. This leads the stability problem to become independent and it gives the possibility that the routine methods from linear stability theory to be used. The frozen-time approach has been already adapted in several studies for evaporating mixtures; see, for instance, Haut and Colinet [34], Serpetsi and Yiantsios [48], Doumenc et al. [49] and Machrafi et al. [10, 11, 36]. In this thesis (Chapter 3), we use the same approach for the linear stability analysis of an evaporative polymer solution layer.

1.4 Research aims of the first part of the thesis

The mechanisms of skin formation and hydrodynamic instability in the context of the evaporative polymer solutions can be further understood by systematic mathematical investigations of these systems. The attractiveness of a mathematical study comes from its potential to provide detailed quantitative insights into the experimental results. The aim of the first part of this thesis is, hence, to study mathematically the role of these physical mechanisms in the context of evaporating mixtures.

In Chapter 2, which is a paper published in The European Physical Journal E, we describe the interplay between evaporation and skin formation in a thin evaporative film of a polymer solution consisting of a volatile solvent and non-volatile polymer. Therefore, a diffusive one-dimensional model is proposed and the exchange of solvent with the gas phase is described using a thermodynamics-based expression for the evaporation flux. Moreover, a composition-dependent diffusion coefficient is introduced, which allows describing the gelation and skin formation at the liquid-gas interface. Note, however, that in our analysis, we don't consider convective transport or any hydrodynamic effects. Let us also emphasize that our model of the evaporation flux is based on a local equilibrium at the liquid-gas interface and is more realistic than previous studies regarding the drying of a thin film of polymer solution. Another interesting and important result is that the possibility of an abrupt gelation at the free surface which may lead to the system stabilization by preventing all Marangoni convection.

In Chapter 3, which is a paper published in Microgravity Science and Technology, we analyze the onset of convection in an evaporative thin film of a polymer solution with one volatile component. The main effort of this study focuses on the fact that evaporative mass loss introduces a natural time

dependence in the solutions simultaneously with composition dependent diffusion coefficient, viscosity and relaxation time, which make the linear stability analysis of the system more attractive. Note that we do not investigate the formation of skin layer in this study due to the fact that convection occurs before the system reaches the gelation and skin formation conditions at the free surface. Moreover, deformations in the liquid-gas interface from the flat state are also neglected since we assume the surface tension of the polymer solution is sufficiently strong.

In this study, two main modes of instability are observed. The first one is the monotonic mode of instability corresponding to the steady convection cells which is similar to the thermal-Marangoni instability studied by Pearson [30] for the first time. We show that the variations of the liquid properties with the change of concentration during the evaporation process, in contrast with many analyses considering constant properties, can effectively change the onset of convection. The second mode, which is an interesting new issue and has not been properly addressed in the literature, is the possibility of an oscillatory instability of convection during the drying of a polymer solution.

1.5 References

[1] T. Umeki, M. Ohata, H. Nakanishi, M. Ichikawa, Dynamics of microdroplets over the surface of hot water, Sci Rep, 5 (2015) 8046.

[2] S. Howison, J. Moriarty, J. Ockendon, E. Terrill, S. Wilson, A mathematical model for drying paint layers, Journal of Engineering Mathematics, 32 (1997) 377-394.

[3] M. Fujii, Issues and Approaches Imposed on Ink Jet Technologies for the Progress of Printed Electronics, Transactions of The Japan Institute of Electronics Packaging, 3 (2010) 35-39.

[4] R. Das, A. Chanda, Fabrication and Properties of Spin-Coated Polymer Films, Nano-size Polymers, Springer2016, pp. 283-306.

[5] H. Minemawari, T. Yamada, H. Matsui, J. Tsutsumi, S. Haas, R. Chiba, R. Kumai, T. Hasegawa, Inkjet printing of single-crystal films, Nature, 475 (2011) 364-367.

[6] P.L. Evans, L.W. Schwartz, R.V. Roy, A Mathematical Model for Crater Defect Formation in a Drying Paint Layer, J Colloid Interface Sci, 227 (2000) 191-205.

[7] M. Kadoura, The formation and drying of thin paint films sprayed on a solid surface, University of Toronto2011.

[8] T. Kajiya, E. Nishitani, T. Yamaue, M. Doi, Piling-to-buckling transition in the drying process of polymer solution drop on substrate having a large contact angle, Phys Rev E Stat Nonlin Soft Matter Phys, 73 (2006) 011601.

[9] F. Doumenc, T. Boeck, B. Guerrier, M. Rossi, Transient Rayleigh–Bénard–Marangoni convection due to evaporation: a linear non-normal stability analysis, Journal of Fluid Mechanics, 648 (2010) 521-539.

[10] H. Machrafi, A. Rednikov, P. Colinet, P. Dauby, Bénard instabilities in a binary-liquid layer evaporating into an inert gas, Journal of colloid and interface science, 349 (2010) 331-353.

[11] H. Machrafi, A. Rednikov, P. Colinet, P.C. Dauby, Time-dependent Marangoni-Bénard instability of an evaporating binary-liquid layer including gas transients, Physics of Fluids, 25 (2013).

[12] N. Bassou, Y. Rharbi, Role of Benard− Marangoni instabilities during solvent evaporation in polymer surface corrugations, Langmuir, 25 (2009) 624-632.

[13] https://www.brewers.co.uk/know-how/article/Painting-defects.

[14] D. Yin, N.R. Jiang, Y.F. Liu, X.L. Zhang, A.W. Li, J. Feng, H.B. Sun, Mechanically robust stretchable organic optoelectronic devices built using a simple and universal stencil-pattern transferring technology, Light Sci Appl, 7 (2018) 35.

[15] L. Guo, Gelation and micelle structure changes of aqueous polymer solutions, (2003).

[16] H.-W. Gao, R.-J. Yang, J.-Y. He, L. Yang, Rheological behaviors of PVA/H2O solutions of high-polymer concentration, Journal of Applied Polymer Science, (2009) NA-NA.

[17] M. Bercea, S. Morariu, D. Rusu, In situgelation of aqueous solutions of entangled poly(vinyl alcohol), Soft Matter, 9 (2013) 1244-1253.

[18] K.y. Ozawa, T. Okuzono, M. Doi, Diffusion Process during Drying to Cause the Skin Formation in Polymer Solutions, Japanese Journal of Applied Physics, 45 (2006) 8817-8822.

[19] K.y. Ozawa, E. Nishitani, M. Doi, Modeling of the Drying Process of Liquid Droplet to Form Thin Film, Japanese Journal of Applied Physics, 44 (2005) 4229-4234.

[20] C.J. Lawrence, Spin coating with slow evaporation, Physics of Fluids A: Fluid Dynamics, 2 (1990) 453-456.

[21] C.J. Lawrence, The mechanics of spin coating of polymer films, Physics of Fluids, 31 (1988).

[22] P.G. de Gennes, Solvent evaporation of spin cast films: “crust” effects, The European Physical Journal E, 7 (2002) 31-34.

[23] A. Münch, C.P. Please, B. Wagner, Spin coating of an evaporating polymer solution, Physics of Fluids, 23 (2011).

[24] M.G. Hennessy, G.L. Ferretti, J.T. Cabral, O.K. Matar, A minimal model for solvent evaporation and absorption in thin films, J Colloid Interface Sci, 488 (2017) 61-71.

[25] P. Colinet, J.C. Legros, M.G. Velarde, Nonlinear dynamics of surface-tension-driven instabilities, Wiley-vch Berlin2001.

[26] H. Bénard, Les tourbillons cellulaires dans une nappe liquide, Rev. Gen. Sci. Pures Appl., 11 (1900) 1261-1271.

[27] H. Bénard, Les tourbillons cellulaires dans une nappe liquide. - Méthodes optiques d'observation et d'enregistrement, Journal de Physique Théorique et Appliquée, 10 (1901) 254-266.

[28] L. Rayleigh, LIX. On convection currents in a horizontal layer of fluid, when the higher temperature is on the under side, The London, Edinburgh, and Dublin Philosophical Magazine and Journal of Science, 32 (1916) 529-546.

[29] M.J. Block, Surface tension as the cause of Bénard cells and surface deformation in a liquid film, Nature, 178 (1956) 650-651.

[30] J. Pearson, On convection cells induced by surface tension, Journal of fluid mechanics, 4 (1958) 489-500.

[31] J. Berg, M. Boudart, A. Acrivos, Natural convection in pools of evaporating liquids, Journal of Fluid Mechanics, 24 (1966) 721-735.

[32] J.P. Burelbach, S.G. Bankoff, S.H. Davis, Nonlinear stability of evaporating/condensing liquid films, Journal of Fluid Mechanics, 195 (1988) 463-494.

[33] E. Sultan, A. Boudaoud, M.B. Amar, Evaporation of a thin film: diffusion of the vapour and Marangoni instabilities, Journal of Fluid Mechanics, 543 (2005) 183-202.

[34] B. Haut, P. Colinet, Surface-tension-driven instabilities of a pure liquid layer evaporating into an inert gas, J Colloid Interface Sci, 285 (2005) 296-305.

[35] G. Toussaint, H. Bodiguel, F. Doumenc, B. Guerrier, C. Allain, Experimental characterization of buoyancy- and surface tension-driven convection during the drying of a polymer solution, International Journal of Heat and Mass Transfer, 51 (2008) 4228-4237.

[36] H. Machrafi, A. Rednikov, P. Colinet, P.C. Dauby, Bénard instabilities in a binary-liquid layer evaporating into an inert gas: Stability of quasi-stationary and time-dependent reference profiles, The European Physical Journal Special Topics, 192 (2011) 71-81.

[37] V.-M. Ha, C.-L. Lai, Onset of Marangoni instability of a two-component evaporating droplet, International journal of heat and mass transfer, 45 (2002) 5143-5158.

[38] S. Sakurai, C. Furukawa, A. Okutsu, A. Miyoshi, S. Nomura, Control of mesh pattern of surface corrugation via rate of solvent evaporation in solution casting of polymer film in the presence of convection, Polymer, 43 (2002) 3359-3364.

[39] P.G. De Gennes, Instabilities during the evaporation of a film: Non-glassy polymer+ volatile solvent, The European Physical Journal E, 6 (2001) 421-424.

[40] B. Trouette, E. Chénier, F. Doumenc, C. Delcarte, B. Guerrier, Transient Rayleigh-Bénard-Marangoni solutal convection, Physics of Fluids, 24 (2012) 074108.

[41] L.B. Smolka, T.P. Witelski, On the planar extensional motion of an inertially driven liquid sheet, Physics of Fluids, 21 (2009).

[42] K.H. Kang, C.K. Choi, A theoretical analysis of the onset of surface-tension-driven convection in a horizontal liquid layer cooled suddenly from above, Physics of Fluids, 9 (1997) 7-15.

[43] F. Doumenc, T. Boeck, B. Guerrier, M. Rossi, Transient Rayleigh-Bénard-Marangoni convection due to evaporation: a linear non-normal stability analysis, arXiv preprint arXiv:0911.2088, (2009).

[44] S. Shen, Some considerations on the laminar stability of time-dependent basic flows, Journal of the Aerospace Sciences, 28 (1961) 397-404.

[45] M.R.E. Warner, R.V. Craster, O.K. Matar, Unstable van der Waals driven line rupture in Marangoni driven thin viscous films, Physics of Fluids, 14 (2002) 1642-1654.

[46] T.D. Foster, Stability of a homogeneous fluid cooled uniformly from above, The Physics of Fluids, 8 (1965) 1249-1257.

[47] M. Souche, N. Clarke, Phase equilibria in polymer blend thin films: a Hamiltonian approach, J Chem Phys, 131 (2009) 244903.

[48] S.K. Serpetsi, S.G. Yiantsios, Stability characteristics of solutocapillary Marangoni motion in evaporating thin films, Physics of Fluids, 24 (2012).

[49] F. Doumenc, E. Chénier, B. Trouette, T. Boeck, C. Delcarte, B. Guerrier, M. Rossi, Free convection in drying binary mixtures: Solutal versus thermal instabilities, International Journal of Heat and Mass Transfer, 63 (2013) 336-350.

Chapter 2

Paper1: Effect of including a gas layer on the gel formation process during the drying of a polymer solution[1]

Abstract

In this paper, we study the influence of the upper gas layer on the drying and gelation of a polymer solution. The gel is formed due to the evaporation of the binary solution into (inert) air. A one-dimensional model is proposed, where the evaporation flux is more realistically described than in previous studies. The approach is based on general thermodynamic principles. A composition-dependent diffusion coefficient is used in the liquid phase and the local equilibrium hypothesis is introduced at the interface to describe the evaporation process. The results show that high thickness of the gas layer reduces evaporation, thus leading to longer drying times. Our model is also compared with more phenomenological descriptions of evaporation, for which the mass flux through the interface is described by the introduction of a Peclet number. A global agreement is found for appropriate values of the

[1] Ramin Rabani, Hatim Machrafi, Pierre Dauby, Effect of including a gas layer on the gel formation process during the drying of a polymer solution, Eur. Phys. J. E 40 (10) (2017) 89.

Peclet numbers and our model can thus be considered as a tool allowing to link the value of the empirical Peclet number to the physics of the gas phase. Finally, in contrast with other models, our approach emphasizes the possibility of very fast gelation at the interface, which could prevent all Marangoni convection during the drying process.

Keywords: Drying of polymer solution, Gel formation, Gas layer, Thermodynamic evaporation flux

2.1 Introduction

The drying of liquid films of polymer solutions by evaporation of the solvent is an important process which is considered in numerous industrial applications including painting [1-3], coating [4-6], ink-jet printing [7-9], production of electronic-devices [10] and so on. The building of a basis for these technologies necessitates understanding the underlying physics of drying phenomena, and especially requires quantitative analysis of solvent evaporation in thin films. Therefore, a number of theoretical studies have been performed to develop models of these processes [11]. In the case of film drying, Bornside et al. [12] have taken into account the diffusion process in their model of spin coating and predicted numerically the formation of a solid "skin" at the free surface. De Gennes [13] analyzed the concentration profiles and the skin (crust) formation, and estimated theoretically the lifetime of the skin. Although his qualitative argument gives some important features of the skin, it is not possible to obtain a detailed information about the whole process of the skin formation. Tsige and Grest [14] undertook the molecular dynamics simulations of the evaporation process in polymer films. They reported the formation of a polymer density gradient at the film/vapor interface and also expressed that the rate of solvent evaporation from the film depends on the magnitude of this density gradient. However, they did not

discuss the restriction for the skin formation related to practical experiments. Reyes and Duda [15] proposed a Monte Carlo simulation for predicting the evolution of particle volume fraction during the drying process. The results indicated that under a slow evaporation rate the particles are able to crystallize, while for a faster evaporation a random packing is predicted. Routh and Zimmerman [16] studied the drying steps by considering a diffusion equation for the particles. The results demonstrated that strong diffusion causes a uniform film profile, while weak diffusion leads to skinning. Konig et al. [17] analyzed the effect of additional salt and displayed that the higher salt concentrations result in high likelihood of the skin formation. A possible explanation was provided by Sarkar and Tirumkudulu [18] who demonstrated how the charge on colloidal particles increases the particle diffusivity and thus changes the volume fraction profile during drying. Another way to change the diffusion coefficient of colloidal particles is with free polymer (soluble polymer) [19]. It was shown how adding polymer to a silica water solution lowers the diffusion coefficient and effectively increases the Peclet number, enhancing non-uniform drying. Ozawa et al. [20] modeled a diffusion-type equation with regard to the gelation effect of the solution in polymer solution undergoing evaporation of the solvent at the free surface. The results implied that the drying dynamics of polymer solutions is strongly related to the gelation, which leads to a great enhancement in the diffusion coefficient of polymers. Hennessy et al. [21] presented a two-phase model for volatile solvent and a nonvolatile polymer in a thin-film. Accordingly, they formulated a two-phase model to describe an evaporating solvent-polymer mixture and then employed it to investigate the interplay between gravity, evaporation, and skin formation. They found that the shortest drying time occurs in the limit of strong gravitational effects due to the rapid formation of a bilayer with a polymer-rich lower layer and a

solvent-rich upper layer, while drag leads to the formation of a polymer-rich skin below the free surface and causes the drying time to increase significantly. In another study, Hennessy et al. [22] considered a model of solvent evaporation in a thin film comprised of volatile solvent and a nonvolatile solute which can be used to predict the dynamics of drying and film formation.

Undeniably, the numerous models proposed in previous studies to study the drying process have provided the opportunity to achieve a wealthy insight in this problem. However, the validity of some simplifying assumptions can still be questioned. For instance, many studies use a phenomenological law to describe the evaporation process, which amounts to introducing a Peclet number to quantify the importance of evaporation. However, the value of that number that can truly capture the drying process number for a given practical situation is not easy to determine. Another important question that has not been examined in the previous studies mentioned above is the possibility of a very fast gelation at the liquid-gas interface, which would prevent all Marangoni convection during the drying of the film.

To address these questions, the present study proposes a more realistic model of the evaporation flux, which is based on thermodynamic principles, as well as on the physics of the interaction between the gas phase and the liquid phase. A similar approach was already proposed in [23] for a binary liquid but here we consider the case of a polymer solution in order to include gelation phenomena. A composition dependent diffusion coefficient is introduced, which allows to describe gelation and the formation of a skin phase. In order to assess the importance of using a more realistic description of the evaporation flux, the present model is compared with other ones including linear and nonlinear models. In addition, the effect of various thickness of gas layer has been examined on the evaporation process.

2.2 Formulation of the problem

The studied system, shown in Fig. 2-1, is comprised of a mixture of a volatile solvent and a non-volatile polymer placed on a flat solid and non-permeable substrate, under a layer of inert air. Our model of the evaporation process introduces a thermodynamics-based expression for the evaporation flux and this approach will be compared with two models from the literature that express the evaporation flux, respectively, as a linear [20] and a non-linear [22] function of the mass fraction at the interface. In Fig. 2-1 and in the equations presented below, z is the vertical coordinate, whereas h is the total height of the solution and the possible skin, h_g is the thickness of the liquid part, while H is the total height of the liquid-skin-gas system. The gel thickness is thus given by h-h_g. The surface tension at the liquid-gas interface is assumed to be sufficiently strong for deformations of the film surface to be negligible. The time dependent thickness of the film can be depicted by a function of time $h(t)$. Diffusion is assumed to be the only mechanism of mass transport within the bulk and a Fick law is used, with a composition dependent diffusion coefficient. Any temperature variations, such as those resulting from evaporative cooling, are presumed to be sufficiently small so that the system can be treated as isothermal [22, 24]. We will also consider that the solvent and polymer densities are not too different, which allows to consider that during the drying process, the mixture keeps a constant density, equal to the initial density of the liquid mixture. Similarly, the density in the gas phase will also be assumed to be independent of the solvent concentration. We will also neglect the Stefan flow in the gas, but not at the liquid-gas interface. This is a reasonable assumption in case the solvent vapor content is low [25], which can safely be assumed when the solvent considered is water, whose saturation pressure is low with respect to the gas pressure. In situations for which the concentration of the vapor in the gas is

high due to a high vapor pressure (e.g. HFE -7100 [25]), the Stefan flow should of course be added in the description. Finally, we will not describe hydrodynamic instabilities and convection is thus not taken into account. In this context, and because the system is horizontally uniform, a one-dimensional description is proposed.

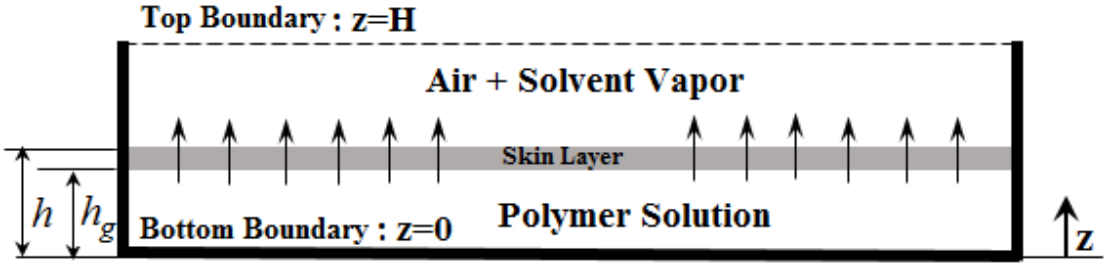

Fig. 2-1. Schematic of studied system

2.2.1 Thermodynamic model

A thermodynamic model of the evaporation process is built by considering the exchange of solvent with the gas phase. The evaporation process is described by a mass flux J that must balance the diffusive fluxes at the film surface. The total system with size H consists of two phases. The first phase is the gas layer, $h \leq z \leq H$, where the diffusion of solvent vapor takes place through the air and the gas mass fraction (of the solvent) C_g follows the diffusion equation

$$\frac{\partial C_g}{\partial t} = D_g \frac{\partial^2 C_g}{\partial z^2} \tag{1}$$

where D_g is the assumed constant diffusion coefficient in gas phase. The second part of the system is the liquid and gel layer, $0 \leq z \leq h$, where the conservation equation describing the solvent mass concentration (C_l) with variable diffusion coefficient in the drying process obeys

$$\frac{\partial C_l}{\partial t} = \frac{\partial}{\partial z}\left(D_l \frac{\partial C_l}{\partial z}\right) \tag{2}$$

where the composition dependent diffusion coefficient D_l for the polymer solution is given by [20]:

$$D_l = \begin{cases} D_0[C_l(1-C_l)^p] & C_l > C_{gel} \\ D_0\left[C_l(1-C_l)^p + dC_l(1-C_l)^p\left(C_{gel}-C_l\right)^p\right] & C_l \leq C_{gel} \end{cases} \quad (3)$$

where D_0 is the diffusion coefficient of pure solvent, while C_{gel} is the solvent mass fraction below which gelation takes place (here we will choose C_{gel} =0.5). As in [20], we take b=p=3 and we also take $d = 1000$ in order to have a clear gelation transition. It is important to stress here that a clear definition of a gel, and the corresponding modelling of this material, is a delicate subject, which remains somewhat controversial [26]. However, such interesting questions fall outside the scope of our work and together with [20], we will simply admit here that what we call a gel is described by Eq. (3). Note also that in Eqs. (1) and (2), we have used Fick's law. For the liquid phase, which is a polymer-solvent mixture, this law is not quantitatively precise for high polymer concentrations, and more complex descriptions of the thermodynamics of the non-ideal mixtures should be considered [27]. However, for the purpose of this paper, the qualitative description based on Fick's law is largely sufficient.

The boundary conditions for solving Eqs. (1) and (2) are the following. A no-flux boundary condition is applied at the non-permeable substrate (z=0):

$$\frac{\partial C_l}{\partial z} = 0 \quad (4)$$

A fixed constant value of the solvent mass fraction is imposed at the top boundary of the gas layer and, except otherwise stated, we will consider a zero humidity for the air far from the interface (i.e. z=H). One thus has:

$$C_g = 0 \tag{5}$$

The boundary conditions at the liquid-gas interface can be deduced from the principle of mass conservation. First, we assume that the polymer does not evaporate. Its flux across the moving boundary is thus zero and one has:

$$-\rho_l D_l \frac{\partial(1-C_l)}{\partial z}\Big|_{z=h} - \rho_l(1-C_l)\frac{dh}{\partial t} = 0 \tag{6}$$

where ρ_l is the (assumed constant) liquid density. The conservation of solvent then imposes

$$-\rho_l D_l \frac{\partial C_l}{\partial z}\Big|_{z=h} - \rho_l C_l \frac{dh}{\partial t} = J \tag{7}$$

Combining the previous two equations directly provides the following alternative expressions of the above boundary conditions at $z=h(t)$:

$$\frac{dh}{\partial t} = -\frac{J}{\rho_l} \tag{8}$$

$$-\rho_l D_l \frac{\partial C_l}{\partial z}\Big|_{z=h} = J(1-C_l)_{z=h} \tag{9}$$

Considering that air cannot be absorbed in the liquid and using a procedure similar to that used in the liquid, one can obtain the following additional boundary condition at $z=h(t)$:

$$-\rho_g D_g \frac{\partial C_g}{\partial z}\Big|_{z=h} = J(1-C_g)_{z=h} \tag{10}$$

where ρ_g is the gas density.

To describe local equilibrium at the liquid-gas interface, we will use Raoult's law [28]. This law is normally valid for ideal solutions and it is not sure that it is strictly correct in our case, especially when the concentration of the polymer becomes high. However, in our approach which is mainly qualitative and interested in general physical mechanisms, we will consider

this law as a sufficient approximation. Since only the solvent can cross the interface, Raoult's law takes the form:

$$y_g p_g = y_l p_{sat} \tag{11}$$

where y_g and $y_l$are the molar fractions of the solvent in the gas and liquid phases, respectively, p_g is the total pressure of gas at the interface, and p_{sat} is the saturation pressure of the pure solvent (at the temperature of the experiment). In terms of mass fraction, Raoult's law can be rewritten as follows:

$$\frac{C_g \delta as}{1+C_g(\delta as-1)} = \frac{C_l \delta pa}{1+C_l(\delta pa-1)} \frac{p_{sat}}{p_g} \tag{12}$$

where $\delta pa = \frac{M_p}{M_s}$ is the polymer to solvent molecular mass ratio, while $\delta as = \frac{M_a}{M_s}$ is the air to solvent molecular mass ratio.

2.2.2 Non-dimensionalization of the equations

It is convenient to rewrite the equations in a non-dimensional form. The initial film thickness of the liquid, h_0, is taken as the characteristic length and while the diffusion time scale in pure solvent, $\tau_l = {h_0}^2/D_0$, is chosen as time scale. In these new units, the equations take the form:

$$\frac{\partial C_l}{\partial t} = \frac{\partial}{\partial z}\left(\widetilde{D}_l \frac{\partial C_l}{\partial z}\right) \tag{13}$$

$$\frac{\partial C_g}{\partial t} = D \frac{\partial^2 C_g}{\partial z^2} \tag{14}$$

$$\widetilde{D}_l = \begin{cases} [C_l(1-C_l)^p] & C_l > C_{gel} \\ \left[C_l(1-C_l)^p + dC_l(1-C_l)^p\left(C_{gel}-C_l\right)^p\right] & C_l \le C_{gel} \end{cases} \tag{15}$$

$$\frac{\partial C_l}{\partial z} = 0\,, z = 0 \;\;\&\;\; C_g = 0\,, z = H \tag{16}$$

where z and H are now non-dimensional, with $D=Dg/D_0$. Note that the non-dimensional thickness h is now such that $h(0)=1$. The boundary conditions take the form:

$$-\widetilde{D}_l \frac{\partial C_l}{\partial z}\Big|_{z=h} = \zeta(1 - C_l)_{z=h} \tag{17}$$

$$-\frac{D}{\rho}\frac{\partial C_g}{\partial z}\Big|_{z=h} = \zeta\,(1 - C_g)_{z=h} \tag{18}$$

$$\left(\frac{dh}{\partial t}\right) = -\zeta \tag{19}$$

where $\rho = \frac{\rho_l}{\rho_g}$, while the dimensionless mass flux ζ is given by $\zeta = \frac{Jh_0}{\rho_l D_0}$. Raoult's law is already given by Eq. (12):

$$\frac{C_g \delta as}{1+C_g(\delta as-1)} = \frac{C_l \delta pa}{1+C_l(\delta pa-1)}\frac{p_{sat}}{p_g} \tag{20}$$

2.2.3 Linear and nonlinear models

Let us now briefly describe two other phenomenological models of evaporation to which ours will be compared [20, 22]. For these models, the behavior of the gas layer is no longer described and a simple phenomenological law is proposed to describe the evaporation flux. In both cases, the flux depends on the concentration of the evaporating component in the liquid along the interface. For solvent-polymer mixtures, linear and non-linear expressions were proposed by Ozawa et al. [20] and Hennessy et al. [22] respectively. The corresponding non-dimensional evaporation fluxes are denoted ζ_L and ζ_{nL} and take the form:

$$\zeta_L = PeC_l|_{z=h} \tag{21}$$

$$\zeta_{nL} = \left[PeC_l e^{1-C_l+\chi(1-C_l)^2}\right]_{z=h} \tag{22}$$

where Pe is the so-called Peclet number and χ is the interaction parameter. This non-dimensional number is the ratio of the diffusive time scale

$\tau_{diff} = \frac{h_0^2}{D_0}$ to the mass transfer time scale $\tau_{mt} = \frac{\rho_l h_0}{J_{ev}}$ where J_{ev} is a phenomenological constant. One thus has $P_e = \frac{J_{ev} h_0}{\rho_l D_0}$.

2.3 Results and discussion

The models presented above were solved using an explicit numerical method and applied to a binary mixture of PVA (polyvinyl-alcohol)–water system. The density of PVA (1270 kg/m^3) is a bit different from that of water but the effect of this difference will not be taken into account, as explained in Section 2.2. In the gas phase, the binary diffusion coefficient is fixed to 2.54×10^{-5} m^2/s [29]. Moreover, the total pressure of the gas is equal to the atmospheric pressure and the saturation pressure of water at a constant temperature of 300 K is P_{sat}=3.53×10^{-2} atm [29].

Before evaporation starts, it is assumed that the liquid film is well mixed, corresponding to spatially uniform distribution of solvent and solute in the liquid and the corresponding solvent concentration is C_{li}. Similarly, in the gas phase the solvent concentration is also assumed uniformed and equal to C_{gi}. Then suddenly at $t = 0$, the two phases are brought into contact and evaporation starts with the following initial conditions:

$$C_l(z,0) = C_{li} \quad , \quad 0 \le z \le h$$

$$C_g(z,0) = C_{gi} \quad , \quad h \le z \le H \tag{23}$$

$h(0)=1$

Table 2-1. Physical properties and parameters values of the problems

Physical property	Value	parameter	Value
ρ_{water}	1000 kg/m^3	C_{li}	0.7,0.51
ρ_{PVA}	1270 kg/m^3	C_{gi}	0
D_g	2.54×10^{-5} m^2/s	C_{gel}	0.5
p_{sat}	3.53×10^{-2} atm	Pe	$1<Pe<20$
p_g	1 atm	H	2,5,9,21,101

In the following, we present the general results of our study for which the physical properties of the fluids and the parameters corresponding to the simulations are summarized in Table 2-1. First, the time evolution of the system as predicted by our model is presented. Then these results are compared with those corresponding to the linear and nonlinear models.

2.3.1 General results

A typical numerical solution of Eqs. (13) and (14) is represented in Fig. 2-2. The uniform initial mass fractions of liquid and gas layers were set to C_{li}=0.7 and C_{gi}=0, respectively. The total thickness of the two-layer system was considered to be H=2. Fig. 2-2 (a) and (b) show the time evolution of the profile C_l and the contour plot of the binary liquid layer thickness in the drying process and gel formation, respectively. At the very beginning (small t), a polymer-rich region is formed near the free surface. Soon after, due to the high evaporation rate, $C_l(z,0)$ reaches C_{gel} and a gel layer in which $C_l(z,0) \leq C_{gel}$ is formed. As drying proceeds, the gel layer develops and get thicker, before the entire lower layer finally tends towards gelation. At this

moment, the evaporation rate considerably reduces, until only the polymer is present and evaporation ceases.

Fig. 2-3 shows the time evolution of the binary liquid layer thickness h for different values of H, which allows to emphasize the effect of the gas thickness on the evaporation process. As expected, thick gas layer corresponds to reduced evaporation rates, which leads to a longer drying time.

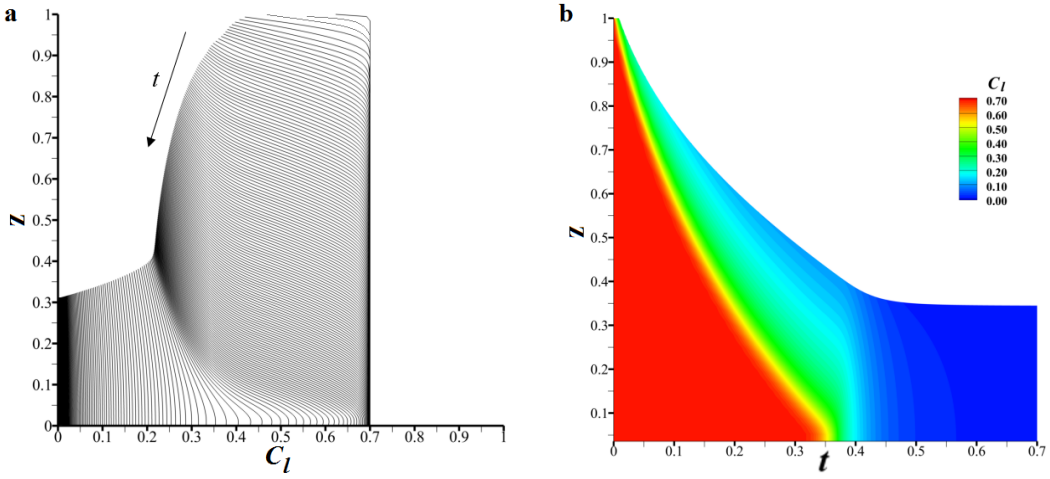

Fig. 2-2. (a) Time evolution of the solvent mass fraction profile $C_l(z,0)$ and (b) contour plot of the solvent mass fraction $C_l(z,0)$.

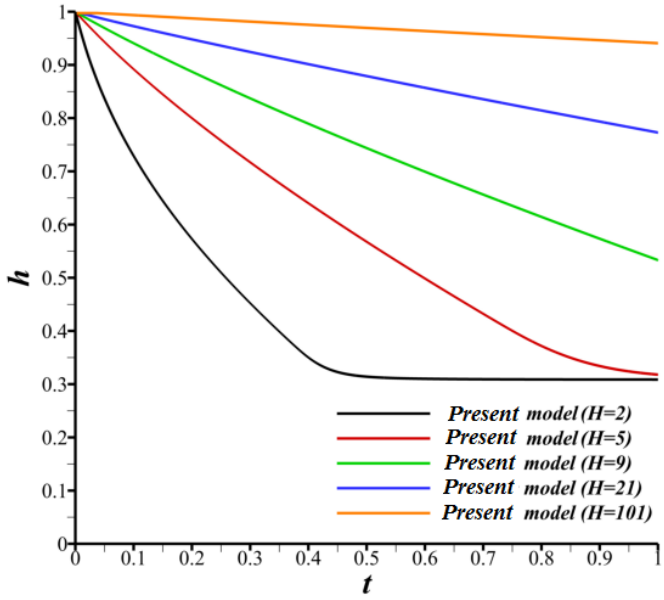

Fig. 2-3. Effect of the gas layer thickness on the time evolution of the mixture height h.

2.3.2 Immediate gelation

When the binary liquid and gas phase, which are not in equilibrium with respect to one another, are suddenly brought into contact at t=0, a very strong evaporation is expected in the very beginning. The resulting important decrease of the liquid solvent concentration at the interface could thus result in an immediate gelation. Of course, the detailed physics of the first instants after the discontinuity is difficult to describe precisely and a simplifying assumption must be introduced to study the system [29]. In order to examine the possibility of a direct gelation of the interface, we will assume that right after the two systems are brought into contact, an equilibrium between the liquid and gas phases is reached at $t = 0^+$, which means that a jump of the two interfacial concentrations occurs in order to satisfy the boundary conditions. This initial jump can be considered as a disturbance for the two phases, and the corresponding perturbations in the two phases will then propagate away from the interface and create two boundary layers. In the very beginning, the perturbations remain close to the interface, and the two phases can thus be considered as infinitely deep. We will now show that a self-similar model of the system can be developed, which will allow determining the values of the interfacial concentrations after the jump. As a first step to build the self-similar model, we consider a vertical axis that follows the moving interface. This amounts to considering the following change of variables: $\tau = t$ and $\xi = z - h(t)$, where $h(t)$ is the position (in the original z-coordinate) of the moving interface. Eqs. (13) and (14) then take the form:

$$\frac{\partial C_l}{\partial \tau} - \frac{\partial C_l}{\partial \xi}\frac{dh}{\partial \tau} = \frac{\partial}{\partial \xi}\left(\widetilde{D}_l \frac{\partial C_l}{\partial \xi}\right) \tag{24}$$

$$\frac{\partial C_g}{\partial \tau} - \frac{\partial C_g}{\partial \xi}\frac{dh}{\partial \tau} = D\frac{\partial^2 C_g}{\partial \xi^2} \tag{25}$$

Then a similarity parameter $\eta \in [0, +\infty]$ can be introduced, with $\eta = -\xi/\sqrt{\tau}$ in the liquid and with $\eta = \xi/\sqrt{\tau}$ in the gas. In terms of this parameter, one can easily check that the equations and boundary conditions become:

$$\widetilde{D}_l \frac{\partial^2 C_l}{\partial \eta^2} + 0.5\eta \frac{\partial C_l}{\partial \eta} + \frac{\partial \widetilde{D}_l}{\partial C_l}\left(\frac{\partial C_l}{\partial \eta}\right)^2 + \frac{\partial C_l}{\partial \eta}\frac{\left(\widetilde{D}_l \frac{\partial C_l}{\partial \eta}\right)_{\eta=0}}{1-C_l|_{\eta=0}} = 0 \tag{26}$$

$$\frac{\partial^2 C_g}{\partial \eta^2} + \frac{0.5}{D}\eta \frac{\partial C_g}{\partial \eta} + \frac{\partial C_g}{\partial \eta}\frac{\left(\frac{D}{\rho}\frac{\partial C_g}{\partial \eta}\right)_{\eta=0}}{1-C_g|_{\eta=0}} = 0 \tag{27}$$

$$\frac{D}{\rho(1-C_g)_{z=0}} \frac{\partial C_g}{\partial \eta}\Big|_{\eta=0} = -\frac{\widetilde{D}_l}{(1-C_l)_{z=0}} \frac{\partial C_l}{\partial \eta}\Big|_{\eta=0} \tag{28}$$

$$\left(\frac{C_g \delta as}{1+C_g(\delta as-1)}\right)_{\eta=0} = \left(\frac{C_l \delta pa}{1+C_l(\delta pa-1)} \frac{p_{sat}}{p_g}\right)_{\eta=0} \tag{29}$$

$$C_l|_{\eta=\infty} = C_{li} \tag{30}$$

$$C_g\big|_{\eta=\infty} = C_{gi} \tag{31}$$

This system of equations is a boundary value problem, but it is worth emphasizing that the values of the unknown fields and of their derivatives at the interface also appear in the differential equations. Defining unknown parameters equal to these quantities, the problem can be directly solved using the MATLAB bvp4c function. For evident numerical reasons, the boundary condition at infinity were expressed far from the interface, but at a finite distance which was chosen as $\eta = 10$.

The results of our analysis are summarized in Fig. 2-4, for which ambient pressure and temperature were assumed (T_{amb}= 300 K, $P_{amb} = 1\ atm$). The initial concentration in the liquid is fixed to C_{li} =0.51. We have then considered several initial concentrations in the gas phase, which were

equivalently expressed in terms of a relative humidity. To define precisely this quantity, we need to introduce first the saturated gas concentration (C_{gs}) at ambient conditions.

$$\frac{C_{gs}\delta as}{1+C_{gs}(\delta as-1)} = \frac{C_{li}\delta pa}{1+C_{li}(\delta pa-1)}\,\frac{p_{sat}}{p_g} \tag{32}$$

Then the initial relative humidity RH% of the gas is defined in terms of the initial concentration C_{gi} by RH%= $100\%\ \times C_{gi}\ /\ C_{gs}$. In Fig. 2-4, we have plotted the liquid interfacial solvent concentration $Cl_{\sum}$ at $t = 0^{+}$, i.e. the liquid interfacial concentration after the jump, for several initial relative humidities in the gas phase. The results show that for low initial humidity in the gas, immediate gelation can take place at the interface, as soon as the two liquid and gas layers are brought into contact. This immediate gelation is of course a consequence of the very strong evaporation that takes place in the system when the initial solvent concentration in the gas is very low. In these circumstances, the initial jump thus prevents all Marangoni instabilities and convection. Finally, let us mention that we have also checked that neglecting the motion of the liquid-gas interface, i.e. setting the term $dh\ /\ d\tau \equiv 0$ in Eqs. (24) and (25), changes the results of Fig. 2-4 by less than 0.1 % (in fact, the results with $dh\ /\ d\tau = 0$ were used as initial guess for the numerical procedure in bvp4c when $dh\ /\ d\tau \neq 0$).

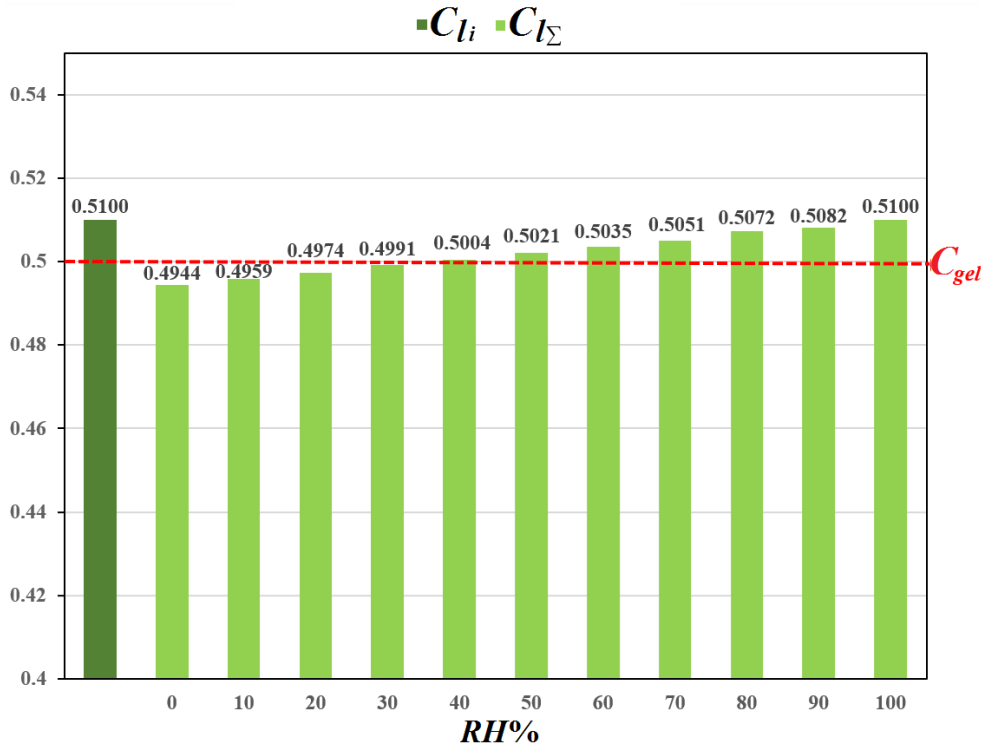

Fig. 2-4. Interfacial liquid mass fraction (Cl_{Σ}) after the jump for various initial humilities (RH%) in the gas phase (ambient pressure and temperature in the gas). The first bar (dark green) gives the value of the mass fraction in the liquid before the contact.

2.3.3 Comparison with other models

To compare our model with the phenomenological models described before, we have analyzed the time evolution of the thickness $h(t)$ as predicted in the different approaches. In Fig. 2-5 (a) and (b), we have plotted $h(t)$ respectively for the linear and nonlinear models and we have also considered several values of Pe and two values of H. In all figures, the results of our model are plotted using black full lines. Of course, we note that the final value of h, corresponding to $t \to \infty$, is independent of the model and also of H and of Pe. We also observe that increasing the Peclet number gives rise to a faster decrease of the thickness and that for a given Pe, evaporation is faster for the linear model that for the nonlinear one. Eventually, it is important to mention that is always possible to determine a value of the Peclet number

such that the evolutions predicted by our model and that coming from the linear or nonlinear model are quite similar (for the linear and nonlinear models, these values are respectively Pe=4 and Pe=11 for H=2 and at Pe=1.2 and Pe=3 for H=5). This is an important fact since it allows to relate the value of the purely empirical Peclet number to the true physical quantities that are considered in our approach (diffusion in the gas, condition at the top of the gas, etc.). However even if the general trends predicted by our model and by the phenomenological ones are the same for appropriate Pe, it is worth emphasizing important differences, especially in the very beginning of the drying process. Indeed, the phenomenological models do not allow jump to occur at the very beginning, because the evaporation flux, which is determined by the interfacial solvent concentration, remains always finite in these models, while it is theoretically infinite at $t = 0$ in our approach. As an illustration of this difference, Fig. 2-6 is a plot of the time evolution of the interfacial solvent concentration in the liquid for our model and also for the linear model with Pe=14. We have considered a zero initial humidity in the gas and an initial concentration in the liquid equal to C_{li}=0.51. After the jump, the interfacial concentration becomes 0.4944 in our model (see Fig. 2-4). Fig. 2-6 then clearly emphasizes that even if the long-time behavior predicted by the two models are quite similar, the evolutions for small times are clearly different. In particular, immediate gelation takes places for our model, while this phenomenon is always impossible for the phenomenological models. Note also that the sudden slope change around t=0.29 is due to the fact that the bottom of the gel layer reaches the substrate (z=0) at that time.

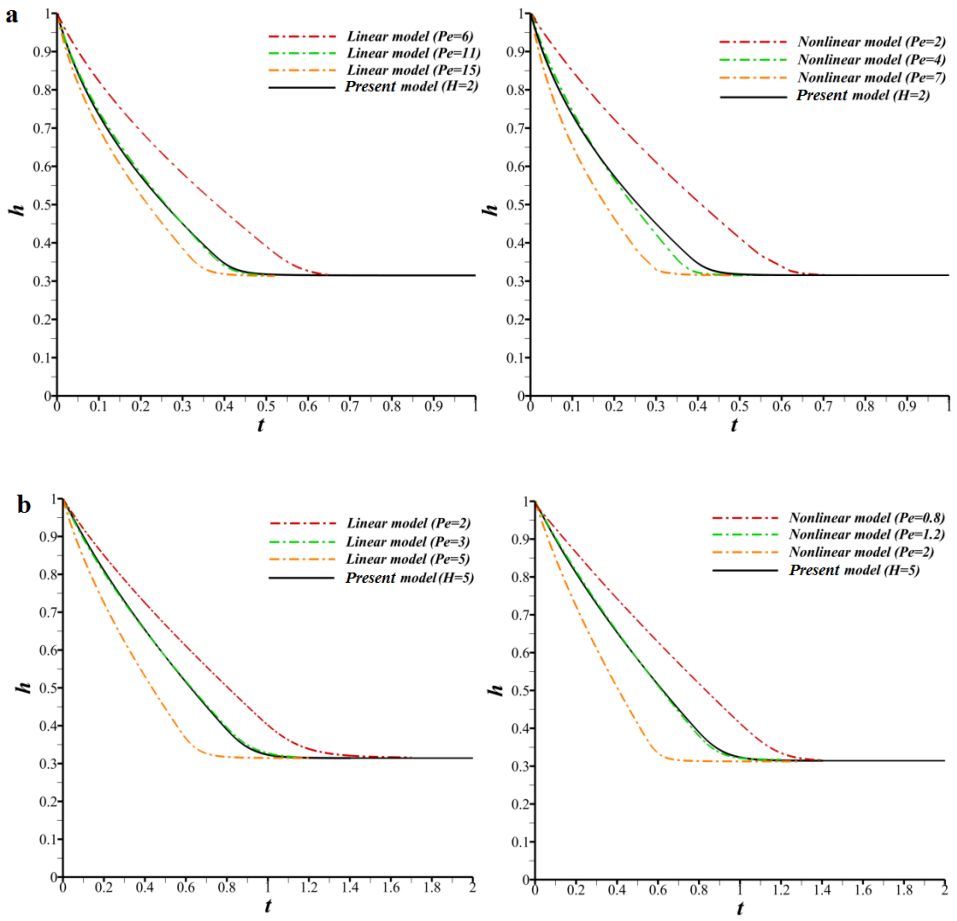

Fig. 2-5.Time evolution of the thickness: comparison between our model and the linear and nonlinear models (left and right panels respectively) for different Peclet numbers; (a) H=2 and (b) H=5.

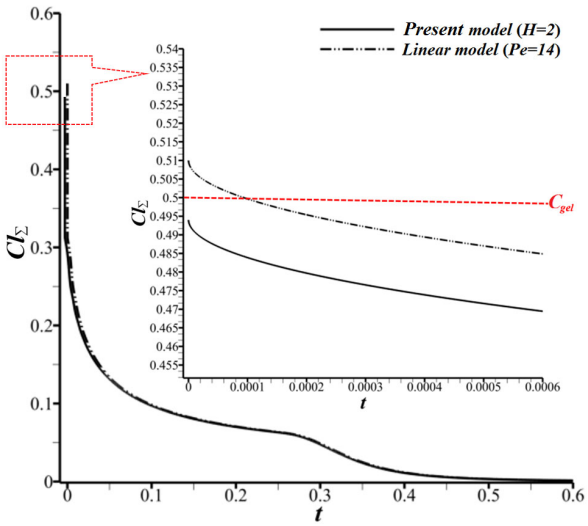

Fig. 2-6. Liquid mass fraction (Cl_Σ) at interface as a function of time for the linear (with $Pe = 14$) and present models (RH%=0 and C_{li} =0.51).

2.4 Other initial conditions

From an experimental point of view, bringing suddenly the 2 phases into contact at $t = 0$ is not quite realistic, rendering comparisons with experiments virtually impossible. For this reason, we have also examined the possibility of different initial conditions and a different start of the drying process, which could more easily be considered in experiments. For $t < 0$, we now consider an equilibrium situation for which the gas and liquid are in contact and for which the humidity of the gas is such that no evaporation takes place. The system is supposed at ambient pressure and temperature $(300\ \mathrm{K}, 1\ \mathrm{atm})$, which corresponds for a water-PVA mixture to a saturation pressure 3.53×10^{-2} atm. For a given water concentration in the liquid, Raoult's law allows then to determine the corresponding concentration in the gas. Then a sudden Joule expansion of the gas is allowed to take place at $t = 0$, which keeps the temperature constant and decreases the (total) pressure P_t. Since the propagation of pressure perturbations is very fast, one can consider an immediate pressure decrease in the gas, which initiates evaporation, with a jump at the interface, similar to that described earlier. Fig. 2-7 is a plot of the concentration at the interface after the jump as a function of the post-expansion pressure Pt_{after} and for different initial concentrations in the liquid phase. As expected, the jump in the interfacial concentration increases with the imposed pressure drop and for sufficiently low post-expansion pressures and sufficiently low initial water concentrations in the mixture, immediate gelation can take place, preventing Marangoni convection.

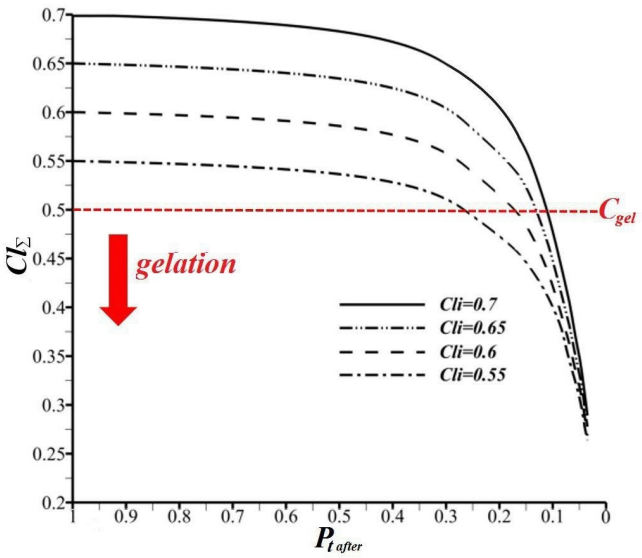

Fig. 2-7. Interfacial liquid mass fraction (Cl_Σ) after the jump as a function of the post-expansion pressure Pt_{after} (in atm).

2.5 Conclusion

In this paper, we have built a model for the drying process of a polymer solution taking into account the physics of the upper gas layer and its interactions with the liquid. During the drying process, the solvent evaporates, which results in a decrease of C_l and of the thickness of the binary mixture. When the mass fraction of liquid reaches the so-called gelation mass fraction, a phase-change takes place near the free surface and the upper part of the mixture is not a liquid anymore. Then, as drying proceeds, the whole binary liquid layer tends towards gelation and a dryer and dryer gel layer progressively invades the whole system, until evaporation finally ceases. A large thickness of the gas layer leads to a slower drying process, because the evaporation rates is smaller in that situation. Our model has also been compared with previous approaches [20, 22] for which a phenomenological law was introduced to describe the evaporation flux. In those works, the importance of the evaporation flux is described by a Peclet number and we proved that for appropriate values of this number, a good

global agreement between our model and the other ones can be found. Otherwise stated, our model allows to relate the value of the purely empirical Peclet number to true physical quantities such as diffusion in the gas, condition at the top of the gas, etc., and thus to determine theoretically the value of the Peclet number corresponding to a given practical situation. Another important result of our work is the description of possible immediate gelation at the liquid-gas interface when evaporation is induced in a rather sudden way. This immediate gelation is related to the very high (theoretically infinite) evaporation flux predicted by our approach and impossible with the other models. This immediate gelation could thus prevent Marangoni convection in the system, which could clearly be of interested in some practical situations.

Acknowledgements

We thank P. Colinet, B. Haut and B. Sobac (TIPs, University of Brussels) for interesting discussions. Financial support from F.R.S.-FNRS ("DITRASOL" PDR T.0123.16) and from BELSPO ("EVAPORATION" MAP-PRODEX project) is also acknowledged.

2.6 Reference

[1] P. Evans, L. Schwartz, R. Roy, A mathematical model for crater defect formation in a drying paint layer, Journal of colloid and interface science, 227 (2000) 191-205.

[2] S. Howison, J. Moriarty, J. Ockendon, E. Terrill, S. Wilson, A mathematical model for drying paint layers, Journal of Engineering Mathematics, 32 (1997) 377-394.

[3] P. Mokarian-Tabari, M. Geoghegan, J. Howse, S. Heriot, R. Thompson, R. Jones, Quantitative evaluation of evaporation rate during spin-coating of polymer blend films: Control of film structure through defined-atmosphere solvent-casting, The European Physical Journal E, 33 (2010) 283-289.

[4] S. Walheim, E. Schäffer, J. Mlynek, U. Steiner, Nanophase-separated polymer films as high-performance antireflection coatings, Science, 283 (1999) 520-522.

[5] A. Münch, C.P. Please, B. Wagner, Spin coating of an evaporating polymer solution, Physics of Fluids, 23 (2011) 102101.

[6] B. Guerrier, C. Bouchard, C. Allain, C. Bénard, Drying kinetics of polymer films, AIChE Journal, 44 (1998) 791-798.

[7] B.-J. de Gans, U.S. Schubert, Inkjet printing of well-defined polymer dots and arrays, Langmuir, 20 (2004) 7789-7793.

[8] T. Kawase, T. Shimoda, C. Newsome, H. Sirringhaus, R.H. Friend, Inkjet printing of polymer thin film transistors, Thin solid films, 438 (2003) 279-287.

[9] B.J. De Gans, P.C. Duineveld, U.S. Schubert, Inkjet printing of polymers: state of the art and future developments, Advanced materials, 16 (2004) 203-213.

[10] B. Li, Y.-P. Cao, X.-Q. Feng, H. Gao, Mechanics of morphological instabilities and surface wrinkling in soft materials: a review, Soft Matter, 8 (2012) 5728-5745.

[11] A.F. Routh, Drying of thin colloidal films, Reports on Progress in Physics, 76 (2013) 046603.

[12] D. Bornside, C. Macosko, L. Scriven, Spin coating: One-dimensional model, Journal of Applied Physics, 66 (1989) 5185-5193.

[13] P.G. De Gennes, Solvent evaporation of spin cast films:“crust” effects, The European Physical Journal E, 7 (2002) 31-34.

[14] M. Tsige, G.S. Grest, Molecular dynamics study of the evaporation process in polymer films, Macromolecules, 37 (2004) 4333-4335.

[15] Y. Reyes, Y. Duda, Modeling of drying in films of colloidal particles, Langmuir, 21 (2005) 7057-7060.

[16] A.F. Routh, W.B. Zimmerman, Distribution of particles during solvent evaporation from films, Chemical Engineering Science, 59 (2004) 2961-2968.

[17] A.M. König, T.G. Weerakkody, J.L. Keddie, D. Johannsmann, Heterogeneous drying of colloidal polymer films: Dependence on added salt, Langmuir, 24 (2008) 7580-7589.

[18] A. Sarkar, M.S. Tirumkudulu, Consolidation of charged colloids during drying, Langmuir, 25 (2009) 4945-4953.

[19] F. Buss, C.C. Roberts, K.S. Crawford, K. Peters, L.F. Francis, Effect of soluble polymer binder on particle distribution in a drying particulate coating, Journal of colloid and interface science, 359 (2011) 112-120.

[20] K.y. Ozawa, T. Okuzono, M. Doi, Diffusion process during drying to cause the skin formation in polymer solutions, Japanese journal of applied physics, 45 (2006) 8817.

[21] M.G. Hennessy, C.J. Breward, C.P. Please, A two-phase model for evaporating solvent-polymer mixtures, SIAM Journal on Applied Mathematics, 76 (2016) 1711-1736.

[22] M.G. Hennessy, G.L. Ferretti, J.T. Cabral, O.K. Matar, A minimal model for solvent evaporation and absorption in thin films, Journal of colloid and interface science, 488 (2017) 61-71.

[23] H. Machrafi, A. Rednikov, P. Colinet, P.C. Dauby, Bénard instabilities in a binary-liquid layer evaporating into an inert gas: Stability of quasi-stationary and time-dependent reference profiles, The European Physical Journal Special Topics, 192 (2011) 71-81.

[24] T. Okuzono, M. Doi, Effects of elasticity on drying processes of polymer solutions, Physical Review E, 77 (2008) 030501.

[25] H. Machrafi, A. Rednikov, P. Colinet, P. Dauby, Importance of wave-number dependence of Biot numbers in one-sided models of evaporative Marangoni instability: Horizontal layer and spherical droplet, Physical Review E, 91 (2015) 053018.

[26] W.B. Russel, W. Russel, D.A. Saville, W.R. Schowalter, Colloidal dispersions, Cambridge university press1991.

[27] A.E. Nesterov, Y.S. Lipatov, Thermodynamics of polymer blends, CRC Press1998.

[28] P. Atkins, Physical Chemistry: Chapter Simple Mixtures, Oxford University Press, Oxford, 2001.

[29] H. Machrafi, A. Rednikov, P. Colinet, P.C. Dauby, Time-dependent Marangoni-Bénard instability of an evaporating binary-liquid layer including gas transients, Physics of Fluids, 25 (2013) 084106.

Chapter 3

Paper2: Influence of Composition Dependent Diffusion Coefficient, Viscosity and Relaxation Time on Evaporative Rayleigh-Bénard-Marangoni Instabilities Induced by Solvent Evaporation in a Polymer Solution[1]

Abstract

In this study, a linear stability analysis is performed for both monotonic and oscillatory modes within a horizontal polymer solution layer, which solely the solvent evaporates into air. The approach is based on general thermodynamic principles and also on the physics of the gas phase and its interactions with the liquid phase. Due to evaporation, the solvent mass fraction changes and cooling occurs at the liquid-gas interface. This can trigger solutal and thermal Rayleigh-Bénard-Marangoni instabilities in the system. For the monotonic mode, the effects of composition dependent diffusion coefficient and dynamic viscosity on the onset of Rayleigh-Bénard-Marangoni convection are studied. Moreover, the effect of different total

[1] Ramin Rabani, Hatim Machrafi, Pierre Dauby, Influence of composition dependent diffusion coefficient, viscosity and relaxation time on evaporative Rayleigh–Bénard–Marangoni instabilities induced by solvent evaporation in a polymer solution, Microgravity Sci. Technol. 31, 615–628 (2019).

heights of the liquid-gas system on the behavior of convection onset is considered. The results show that a variable diffusion coefficient and a variable viscosity can notably change the onset of instability for a polyisobutylene (PIB)/toluene solution. Our model for the monotonic mode is also satisfactorily compared with an experimental study. For the oscillatory mode, where the relaxation time is also composition dependent, we observe that very thin layers will be susceptible to an oscillatory instability when drying occurs in the system. Finally, an approximate model is derived exploiting the fact that the solutal Marangoni is by far the most dominant instability mechanism here. A negligible difference with respect to the full model confirms the predominance of the solutal Marangoni mechanism.

Keywords: Drying of polymer solution, Variable viscosity, Variable diffusion coefficient, Variable relaxation time, Transient gas layer, Rayleigh-Bénard-Marangoni instabilities, Monotonic and oscillatory modes

3.1 Introduction

Convection in multilayer systems [1-3] is a widespread phenomenon that is of particular interest in numerous branches of drying technology. The drying of liquid films of polymer solutions including one volatile component appears in many industrial and natural processes such as drying of paint films [4-6] , ink-jet printing [7-9], packaging [10-12], and so on. In these evaporative phenomena, which are generally of transient nature, the prediction of critical conditions for the onset of convection necessitates the understanding of the underlying physics of drying phenomena, and especially requires a quantitative analysis of solvent evaporation in thin films. Evaporation of a volatile component at the upper free surface of a solution generates a temperature gradient in the liquid due to the latent heat

absorption [13-17]. In the case of binary mixtures, this evaporation also generates a concentration gradient due to the volatility difference between components [18, 19]. Therefore, both thermal and solutal gradients can generate thermo-solutal instabilities in fluid mixtures.

The thermal instability problem has been analyzed theoretically, numerically and experimentally for many years. In most studies, a steady basic state is considered for stability analyses [13, 20]. However, in evaporative systems, convection often appears before the system reaches a steady state. To study the instability threshold in the case of transient basic profiles, the so-called frozen-time approach is often used [21, 22]. This method consists of applying a classical normal mode stability analysis to the transient basic profile, frozen at each given time. Machrafi et al. [23] have used this method to analyze the thermal Marangoni instability in two different evaporative configurations, a horizontal layer and a spherical droplet of a pure liquid, both evaporating into ambient air. Vidal and Acrivos [24] have analyzed the evaporation of a liquid layer to determine the time of thermal Bénard-Marangoni convection onset. Note that methods different from the frozen-time approach have also been introduced in the literature. The amplification method that takes into account the time dependence of the basic state has been developed by Foster [25, 26] to determine the onset time of thermal Rayleigh-Bénard convection. Doumenc et al. [27] have performed a linear analysis based on a non-normal approach and an amplification method, to determine the stability conditions of the thermal Rayleigh-Bénard-Marangoni problem in drying polymer solutions. These methods will however not be considered in the present paper.

When the fluid is a polymer solution or a binary mixture, Rayleigh-Bénard-Marangoni convection can also be induced due to concentration gradients, evoking solutal mechanisms. Machrafi et al. [28, 29] have performed a linear

stability of a binary mixture using the frozen-time approach taking into account buoyancy and surface tension effects, of thermal and solutal origin, as well as the Soret effect. De Gennes [30] used scaling arguments to estimate the critical thickness for the onset of convection in a dilute polymer solution. It was concluded that the solutal critical thickness is much smaller than the thermal one, so the concentration effects should dominate the thermal effects. Trouette et al. [31] undertook numerically the analysis of the transient solutal Rayleigh-Bénard-Marangoni for a polymer solution. They described the onset of solutal convection for a transient drying problem with a constant evaporative flux and also considered a model, which took into account the variation of viscosity with solute concentration. Bormashenko et al. [32] have analyzed experimentally the evaporation of a thin layer of polymer solutions including amorphous polymers and chlorinated solvents. They reported that temperature-gradient-driven Marangoni instability is hardly responsible for the large-scale patterning in rapidly evaporating polymer solutions comprising amorphous polymers and chlorinated solvents and they finally related the observed patterning to the effects induced by gradients of polymer concentration. This implies Marangoni instability due to concentration gradients.

Undeniably, the numerous instability analyses proposed in the previous research studies to study the onset of convection have provided the opportunity to achieve a wealthy insight in this problem. However, the validity of some simplifying assumptions can still be questioned. When a thin layer of a polymer solution and a neighboring gas phase, which are initially not in equilibrium with respect to one another, are suddenly brought into contact, a strong evaporation is expected in the very beginning. This results in an important decrease of the liquid solvent concentration at the interface. Many studies use a constant diffusion coefficient and a constant

dynamic viscosity in the liquid layer, but the importance of the dependence with respect to concentration of properties like diffusion coefficient or viscosity has been emphasized for instance in [33-35]. The variations of such liquid properties with the change of concentration during the evaporation, especially at the liquid-gas interface due to the high concentration gradient, can truly change the stability threshold. To address this question, the present study proposes a model for a horizontal layer of a fluid in the case of a binary mixture consisting of a polymer solution, of which solely the solvent evaporates into (inert) air. Our model is based on thermodynamic principles and the physics of the gas phase and its interactions with the liquid phase is also taken into account. In order to assess the importance of the variable diffusion coefficient and the variable dynamic viscosity on monotonic instabilities, four cases are considered, with combinations of constant/variable diffusion coefficients and constant/variable dynamic viscosities. Since our model does not neglect the interaction of the polymer solution with the gas layer above it, the effect of the gas layer thickness on the onset of convection is examined as well. Another interesting new issue that has not been well studied in the literature is to analyze the possibility of an oscillatory mode of instability during the drying of a polymer solution. Indeed, it is well known that polymer solutions can actually be viscoelastic, which allows oscillatory modes of instability. Accordingly, we will consider a constant value of dimensional relaxation time as well as a relaxation time depending on the polymer concentration and analyze the possible associated oscillatory instability.

The general organization of the present study is the following. First, sections 3.2 and 3.3 provide a mathematical description of our model with the boundary conditions, followed by the physical properties in section 3.4. Second, the results about the transient reference solution behavior as

described by our model are presented in section 3.5. Subsequently, section 3.6 is concerned with the linear stability analysis for the monotonic and oscillatory solutions and then the results of the monotonic solution of the linear stability analysis are compared with an experimental result. Finally, an approximate model of our stability analysis is carried out in section 3.7 making use of various simplifications possible within the full model.

3.2 Model formulation

The physical system, of which we will study the instability threshold, is sketched in Fig. 3-1. It consists of a horizontal layer of a polymer solution (thickness d_l), with a volatile solvent and a non-volatile polymer, placed on a horizontal flat solid and non-permeable substrate, and under a layer of inert air. The gas layer thickness is here given by $H^d - d_l$ (H^d is the total height of the liquid-gas system). The subscript d denotes the dimensional character of the symbol in view of its later use in dimensionless form. The gas layer thickness can be described in the sense of an effective transfer distance, above which the bulk of the gas phase is perfectly mixed, allowing to present a formal upper virtual boundary (see [36, 37] for more details on this approach). A thermodynamic model of the evaporation process is built by considering the exchange of solvent with the gas phase. The surface tension of the polymer solution is assumed to be sufficiently strong so that deformations in the liquid-gas interface from the flat state can be neglected (for the interested reader, we refer to [37] for a more detailed discussion about the assumption of an undeformable interface, and also about the possibility of a long wave-length mode of deformation in the case of very thin layers). The density in the gas phase will be assumed to be independent of the solvent concentration, due to the relatively low value of this concentration.

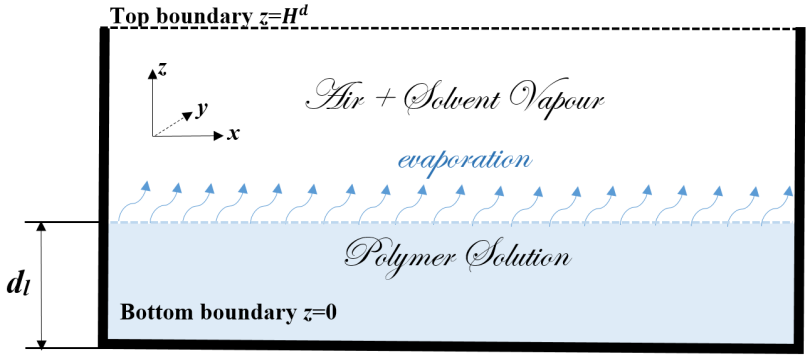

Fig. 3-1. Schematic of the studied configuration.

3.3 Mathematical model

3.3.1 Bulk equation

The densities of the liquid and gas phases are assumed to depend linearly on temperature and concentration of the solvent. The corresponding state equations are written under the following form:

$$\rho_l = \rho_{l,0}\left(1 - \alpha_l\left(T_l^d - T_{l,0}^d\right) - \beta_l\left(c_l - c_{l,0}\right)\right)$$
$$\rho_g = \rho_{g,0}\left(1 - \alpha_g\left(T_g^d - T_{g,0}^d\right) - \beta_g\left(c_g - c_{g,0}\right)\right) \quad (1)$$

In these relations, ρ is the density, T is the temperature, c is the mass fraction of the solvent, α and β are the thermal and the solutal expansion coefficients, respectively. The subscripts "l" and "g" stand for the liquid and gas phases respectively. The subscript "0" refers to a state with certain reference values of the temperatures and mass fractions, here taken to be $T_{l,0}^d = T_{g,0}^d = T_{amb}$, where symbol "$amb$" denotes the ambient conditions, $c_{l,0} = c_{li}$, where c_{li} is the initial solvent concentration in the liquid phase (see later), and $c_{g,0} = c_{amb}$, with c_{amb} an imposed concentration above the aforementioned gas transfer distance, which is assumed to be fixed at the top of the gas layer. The quantities $\rho_{l,0}$ and $\rho_{g,0}$ are the liquid and gas densities corresponding to these temperatures and mass fractions. If the temperature and mass fractions

variations with respect to the reference values remain small -and we have checked that it is always the case, both in the liquid and in the gas, in the situations analyzed later on-, the density changes are also small and the Boussinesq approximation can be used to describe the two phases of the system [17] In this context, the densities of the liquid and gas layers can be replaced by their (constant) reference values $\rho_{l,0}$ and $\rho_{g,0}$ everywhere in the equations, except in the buoyancy terms, where they must keep the expressions given by Eq. (1). In the following, we will actually do this simplification and, to keep the notations as simple as possible, we will definitely replace symbols $\rho_{l,0}$ and $\rho_{g,0}$ by ρ_l and ρ_g in all future equations.

During the drying process, the solvent evaporates, which results in a decrease of the solvent mass fraction. The decrease of solvent mass fraction leads to an increase of the variable diffusion coefficient and of the dynamic viscosity, especially close to the liquid-gas interface. When the mass fraction of the liquid reaches the so-called "gel point", the diffusion coefficient strongly increases and the dynamic viscosity diverges. The composition dependent diffusion coefficient $D_l(c_l)$ for the polymer solution is given by the phenomenological expression [38]

$$D_l(c_l) = \begin{cases} D_0[\emptyset(c_l)(1-\emptyset(c_l))^p] & c_l > c_{gel} \\ D_0\left[\emptyset(c_l)(1-\emptyset(c_l))^p + d\emptyset(c_l)(1-\emptyset(c_l))^p\left(\emptyset_{gel}-\emptyset(c_l)\right)^p\right] & c_l \le c_{gel} \end{cases} \quad (2)$$

$$\emptyset(c_l) = \frac{c_l}{c_l+(1-c_l)\frac{\rho_s}{\rho_p}} \quad (3)$$

where D_0 is a phenomenological coefficient, ρ_s and ρ_p are respectively the density of solvent and polymer, $\emptyset(c_l)$ is the solvent volume fraction, while $\emptyset_{gel}$ is the solvent volume fraction below which gelation takes place (here we will choose $c_{gel} = 0.5012$). Based on [38], we consider b=p=3 and we also take $d = 1000$ in order to have a clear gelation transition. It is worth

emphasizing that the original composition dependent diffusion coefficient provided by [38] is a function of volume fraction and we modified it as a function of concentration for the present study. For the variable viscosity as a function of concentration, we have used an empirical relation [35]. We have also assumed that a similar relation can also be used to describe the variable relaxation time that will be introduced in section 3.4

As mentioned in the Introduction, we will describe the liquid polymer solution as a viscoelastic medium. Constitutive equations for such fluids have been described in details in the literature and we can refer the interested reader for example to [39, 40]. In our approach, we will consider the so-called Maxwell model, which has already been used in other stability analyses [41]. This model introduces a relaxation time λ^d, which allows to describe the delay that a viscoelastic fluid needs to adapt stress and strain rate tensors. Below, the nondimensionalized Maxwell constitutive equation is given by Eq. (6).

We introduce now a Cartesian coordinates system and all the equations are non-dimensionalised by appropriate scales. The length scale is taken to be d_l. The liquid diffusion time $d_l{}^2/D_0$ is used as the time scale. It is important to stress that the liquid thickness (d_l) is assumed to remain effectively constant on the relevant time scales of the problem and we will explain the validity of this assumption in section 3.5. The dimensionless temperatures T_l and T_g in the liquid and gas are respectively defined by $(T_l^d\text{-}T_{l,0}^d)/\theta$ and $(T_g^d\text{-}T_{g,0}^d)/\theta$, where $\theta = \frac{L}{Cp_l}$ is the temperature scale, where, L and Cp_l are the latent heat and heat capacity of the pure solvent, respectively. The velocity, pressure, and stress tensor $\boldsymbol{\tau}$ scales are respectively chosen as $D_0/\, d_l$, $\mu_0\, D_0/\, d_l{}^2$, and $\mu_0\, D_0/\, d_l{}^2$ where $\mu_0 = \mu_l(c_l = 1)$.

$$\nabla.\vec{v}_l = 0 \tag{4}$$

$$\frac{\partial \vec{v}_l}{\partial t} = -\left(\vec{v}_l.\vec{\nabla}\right)\vec{v}_l + Sc_l\left\{-\vec{\nabla}p_l - Ga_l 1_z + Ra_l {Le_l}^{-1} T_l 1_z + Rs_l(c_l - c_{li})1_z + \nabla.\boldsymbol{\tau}\right\} \tag{5}$$

$$\boldsymbol{\tau} + \lambda\frac{\partial \vec{\tau}}{\partial t} = \frac{\mu_l}{\mu_0}\nabla^2(\nabla\vec{v}_l + (\nabla\vec{v}_l)^T) \tag{6}$$

$$\frac{\partial c_l}{\partial t} = -\left(\vec{v}_l.\vec{\nabla}\right)c_l + \left\{\nabla.(\widetilde{D}_l(c_l)\nabla c_l)\right\}$$
$$\widetilde{D}_l(c_l) = D_l(c_l)/D_0 \tag{7}$$

$$\frac{\partial T_l}{\partial t} = -\left(\vec{v}_l.\vec{\nabla}\right)T_l + {Le_l}^{-1}\nabla^2 T_l \tag{8}$$

$$\nabla.\vec{v}_g = 0 \tag{9}$$

$$\frac{\partial \vec{v}_g}{\partial t} = -\left(\vec{v}_g.\vec{\nabla}\right)\vec{v}_g + Sc_l\left\{-\rho^{-1}\vec{\nabla}p_g - Ga_l 1_z + \nu\nabla^2\vec{v}_g + \alpha Ra_l {Le_l}^{-1} T_g 1_z + \beta Rs_l\left(c_g - c_{amb}\right)1_z\right\} \tag{10}$$

$$\frac{\partial c_g}{\partial t} = -\left(\vec{v}_g.\vec{\nabla}\right)c_g + D\nabla^2 c_g \tag{11}$$

$$\frac{\partial T_g}{\partial t} = -\left(\vec{v}_g.\vec{\nabla}\right)T_g + {Le_l}^{-1}\kappa\nabla^2 T_g \tag{12}$$

The symbols u, v and w stand for the x, y and z velocity field components, respectively. Eqs. (4) - (12) contain the following dimensionless numbers:

$$Sc_l = \frac{\nu_l}{D_0},\ Le_l = \frac{D_0}{\kappa_l},\ Ga_l = \frac{g{\mathrm{d}_l}^3}{D_0\nu_l},\ Ra_l = \frac{\alpha_l g\theta{\mathrm{d}_l}^3}{\kappa_l\nu_l},\ Rs_l = \frac{\beta_l g{\mathrm{d}_l}^3}{D_0\nu_l},\ \rho = \frac{\rho_g}{\rho_l},$$
$$\nu = \frac{\nu_g}{\nu_l}, \alpha = \frac{\alpha_g}{\alpha_l},\ \beta = \frac{\beta_g}{\beta_l}, \kappa = \frac{\kappa_g}{\kappa_l}, D = \frac{D_g}{D_0}, \mu = \frac{\mu_g}{\mu_0},\ \lambda = \frac{\lambda^d D_0}{{d_l}^2}$$

where $\nu_l = \frac{\mu_0}{\rho_l}$ and $\nu_g = \frac{\mu_g}{\rho_g}$ respectively refer to the kinematic viscosity in liquid and gas, and Sc_l, Le_l, λ, Ga_l, Ra_l, and Rs_l are respectively the Schmidt, Lewis, dimensionless relaxation time, Galileo, thermal Rayleigh, and solutal

Rayleigh numbers in the liquid phase. The symbols ρ,ν, α, β, κ, and D denote the ratios of the corresponding material properties in the gas to those in the liquid.

3.3.2 Boundary and initial conditions

The boundary conditions for the liquid layer at the bottom of the liquid (z=0) are the following. No slip and a no-flux boundary condition are applied at the non-permeable and adiabatic substrate:

$$\vec{v}_l = 0, \quad \vec{\nabla} c_l = 0, \quad \vec{\nabla} T_l = 0, \tag{13}$$

Concentration and temperature are assumed to be fixed at what we called ambient conditions at the top boundary of the gas layer, with soft hydrodynamic conditions, i.e. the normal stress being equal to a certain value p_t, with zero tangential stress. In dimensionless notation, the boundary conditions at the top of the gas, i.e. at $z = H$, where $H = H_d/d_l$ is the total dimensionless height of the liquid-gas system, are then

$$c_g = c_{amb} \ , \ T_g = 0 \tag{14}$$

$$w_g = \frac{\partial u_g}{\partial z} + \frac{\partial w_g}{\partial x} = \frac{\partial v_g}{\partial z} + \frac{\partial w_g}{\partial y} = 0 \tag{15}$$

$$-p_g + 2\mu \frac{\partial w_g}{\partial z} = -p_t \tag{16}$$

At the liquid-gas interface, the following conditions are considered. The continuity of the temperature and of the tangential velocity components are given by:

$$T_g = T_l \ , \quad u_g = u_l \ , \quad v_g = v_l \tag{17}$$

The energy conservation at the interface implies a balance between the heat fluxes arriving from both phases and the latent heat of evaporation [29]

$$J = \frac{1}{Le_l}\left(-\frac{\partial T_l}{\partial z} + K\frac{\partial T_g}{\partial z}\right) \tag{18}$$

where $K = \frac{K_g}{K_l}$, with K_g and K_l the thermal conductivities of gas and liquid, respectively. Considering the tangential stress balance at the interface, it is assumed that the dimensional surface tension γ between the liquid and the gas depends linearly on the temperature and on the solvent mass fraction in the liquid:

$$\begin{aligned} \gamma =& \gamma_0 - \gamma_T\left(T_l^d - T_{l,0}^d\right) - \gamma_c\left(c_l - c_{l,0}\right), \quad \gamma_T = -\left(\frac{\partial \gamma}{\partial T}\right) \\ & \gamma_c = -\left(\frac{\partial \gamma}{\partial c}\right) \end{aligned} \tag{19}$$

Then, the dimensionless conditions expressing the tangential stress balance [29] at the liquid-gas interface are:

$$-\mu\left(\frac{\partial w_g}{\partial x} + \frac{\partial u_g}{\partial z}\right) + \tau_{xz} + Ma\ {Le_l}^{-1}\frac{\partial T_l}{\partial x} + Ms\frac{\partial c_l}{\partial x} = 0 \tag{20}$$

$$-\mu\left(\frac{\partial w_g}{\partial y} + \frac{\partial v_g}{\partial z}\right) + \tau_{yz} + Ma\ {Le_l}^{-1}\frac{\partial T_l}{\partial y} + Ms\frac{\partial c_l}{\partial y} = 0 \tag{21}$$

where τ_{xz} and τ_{yz} refer to the components of stress tensor $\boldsymbol{\tau}$ and $Ma = \frac{\gamma_T \theta \mathrm{d}_l}{\kappa_l \mu_0}$, $Ms = \frac{\gamma_c \mathrm{d}_l}{D_0 \mu_0}$ are the thermal and solutal Marangoni numbers, respectively.

Considering that the inert gas adsorption in the liquid is negligible, the mass flux J calculated in both phases at the interface takes the following forms [29]

$$J = -\frac{\widetilde{D}_l(c_l)}{1-c_l}\left\{\frac{\partial c_l}{\partial z}\right\} \tag{22}$$

$$J = -\frac{\rho D}{1-c_g}\frac{\partial c_g}{\partial z} \tag{23}$$

To describe the local equilibrium at the liquid-gas interface, we use a modified Raoult's law [42]. It is worth emphasizing that the standard Raoult's law [29] is not valid here for polymer solutions due to the fact that the polymer molecules are large and have a large molecular weight. Therefore we apply a Flory-Huggins adaptation using an exponential factor [42]. In terms of the mass fraction, the modified Raoult's law can be rewritten as follows:

$$\frac{c_g}{c_g+(1-c_g)\delta sa} = \frac{c_l}{c_l+(1-c_l)\frac{\rho_s}{\rho_p}}\left(e^{(1-(\frac{1}{m}))(1-\frac{c_l}{c_l+(1-c_l)\frac{\rho_s}{\rho_p}})}\right)\frac{p_{sat}|_{T_\Sigma}}{p_g}$$

$$p_{sat}|_{T_\Sigma} = p_{sat}|_{T_{amb}} e^{\left(-\frac{L\times MW_{solvent}}{R}\left(\frac{1}{T_\Sigma}-\frac{1}{T_{amb}}\right)\right)} \tag{24}$$

$$\delta sa = \frac{MW_{solvent}}{MW_{air}}\ , \qquad m = \left(\frac{MW_{polymer}}{MW_{solvent}}\right)$$

where p_g is the total pressure of the gas at the interface, $p_{sat}|_{T_\Sigma}$ is the saturation pressure at the interface temperature, $p_{sat}|_{T_{amb}}$is the saturation pressure of the pure solvent (at ambient temperature), T_{amb} is the ambient temperature, $R \approx 8.31\frac{\text{J}}{\text{mol K}}$ is the universal gas constant, L=$3.61\times10^5\,\frac{\text{J}}{\text{kg}}$ is the latent heat of toluene evaporation at T_{amb}, and the symbol "Σ" denotes the liquid-gas interface. $MW_{solvent}, MW_{polymer},$ and MW_{air} are the molecular weights of the solvent, the polymer, and air, respectively.

Before evaporation starts, it is assumed that the liquid film is well mixed, corresponding to spatially uniform distribution of solvent and polymer in the liquid and the corresponding solvent concentration is c_{li}. The liquid film temperature is also initially uniform and fixed at the ambient temperature, with $T_l(\vec{z},0) = 0$. Similarly, in the gas phase, the concentration of the solvent and the temperature are also assumed uniform and equal to c_{amb}

and $T_g(\vec{z},0)=0$, respectively. Then, suddenly at $t=0$, the two phases are brought into contact and evaporation starts with the following initial conditions:

$$\begin{aligned} &c_l(\vec{z},0)=c_{li} \quad , \ 0\le z\le 1 \\ &T_l(\vec{z},0)=0 \quad , \ 0\le z\le 1 \\ &c_g(\vec{z},0)=c_{amb} \quad , 1\le z\le H \\ &T_g(\vec{z},0)=0 \quad , 1\le z\le H \end{aligned} \tag{25}$$

3.4 Physical properties

The model presented above will be solved for the particular case of a 5% polyisobutylene (PIB)/95% toluene solution system ($c_{li}=0.95$) evaporating into air and $c_{amb}=0$. The density of toluene and PIB are respectively $\rho_s = 867\frac{kg}{m^3}$ and $\rho_p = 917\frac{kg}{m^3}$, the total pressure of the gas is equal to the atmospheric pressure, the saturation pressure of toluene at the ambient temperature (T_{amb} =298K) is $p_{sat}|_{T_{amb}} = 3.95\times10^{-2}$ atm [43] and $MW_{solvent} = 92.14\times10^{-3}\frac{kg}{mol}$, $MW_{polymer} = 500\frac{kg}{mol}$, $MW_{air} = 28.97\times10^{-3}\frac{kg}{mol}$. The physical properties of the corresponding fluids are given in Table 3-1 [43].

For the variable viscosity, we have used an empirical relation [35] that we have modified and fitted on experimental data for a 5% polyisobutylene (PIB)/95% toluene solution [44]. This empirical relation [35] depicts that the viscosity diverges when the concentration of polymer reaches the gelation concentration. The result of the fitting is shown in Fig. 3-2 and the modified expression that we used is given by:

$$\mu_l = \mu_0\left((1-\frac{1-c_l}{1-c_{gel}})^{-4}{c_l}^{0.01}e^{62(1-c_l)}\right) \tag{26}$$

where μ_l and μ_0 are the dynamic viscosity of liquid phase and pure solvent ($c_l = 1$), respectively.

Table 3-1. Physical properties and parameters values of the liquid for a 5 % polyisobutylene (PIB)/95% toluene solution ($c_l = 0.95$) and for the gas layer. The ambient conditions are defined by T_{amb} =298K and $c_{amb} = 0$.

Physical property in the liquid	**Value**	**Physical property in the gas**	**Value**
ρ_l	$870\,\frac{kg}{m^3}$	ρ_g	$1.18\,\frac{kg}{m^3}$
K_l	$0.142\,\frac{W}{m.K}$	K_g	$2.62 \times 10^{-2}\,\frac{W}{m.K}$
κ_l	$0.97 \times 10^{-7}\,\frac{m^2}{s}$	κ_g	$2.22 \times 10^{-5}\,\frac{m^2}{s}$
ν_l	$6.3 \times 10^{-7}\,\frac{m^2}{s}$	ν_g	$1.58 \times 10^{-5}\,\frac{m^2}{s}$
α_l	$1.07 \times 10^{-3}\mathrm{K}^{-1}$	α_g	$3.35 \times 10^{-3}\mathrm{K}^{-1}$
μ_l	$20.8 \times 10^{-3} Pa.s$	μ_g	$1.85 \times 10^{-5} Pa.s$
D_l	$10^{-10}\,\frac{m^2}{s}$	D_g	$8.11 \times 10^{-6}\,\frac{m^2}{s}$
β_l	5.82×10^{-2}	β_g	-6.86×10^{-1}
γ_c	$5.4 \times 10^{-3}\,\frac{N}{m}$		
γ_T	$1.19 \times 10^{-4}\,\frac{N}{m.K}$		
D_0	$0.2 \times 10^{-9}\,\frac{m^2}{s}$ [45]		

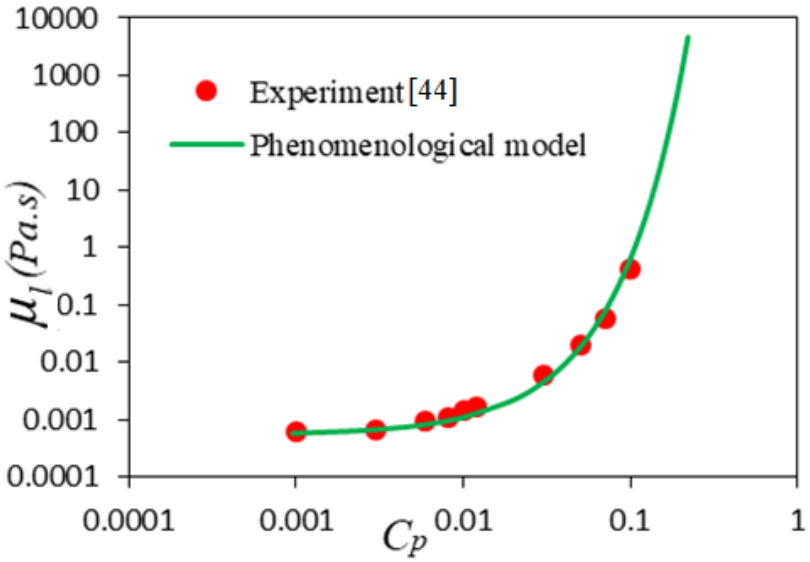

Fig. 3-2. Dynamic viscosity of liquid phase (μ_l) as a function of polymer concentration ($c_p = 1 - c_l$).

As other quantities [46], the relaxation time also diverges at the gelation point. Moreover, the relaxation time vanishes for pure solvent, since the latter is assumed Newtonian. In other words, the relaxation time is very short in normal fluids but increases strongly in polymeric solutions. To take this into account, we have introduced the following phenomenological expression with exponent 4 to describe the strong variation of dimensional relation time λ_d with concentration:

$$\lambda^d = \tilde{\lambda}^d \left(\frac{1-c_l}{1-\tilde{c}_l}\right)\left(\frac{c_{gel}-(1-\tilde{c}_l)}{c_{gel}-(1-c_l)}\right)^4 \tag{27}$$

In this relation $\tilde{\lambda}^d = 0.5\,(s)$ is a typical value of the relaxation time, corresponding to a solvent concentration $c_l = \tilde{c}_l = 0.95$ [47]. Fig. 3-3 shows the increase of the dimensional relaxation time as a function of polymer solution. The relaxation time increases fast with increase of polymer concentration and eventually becomes infinite.

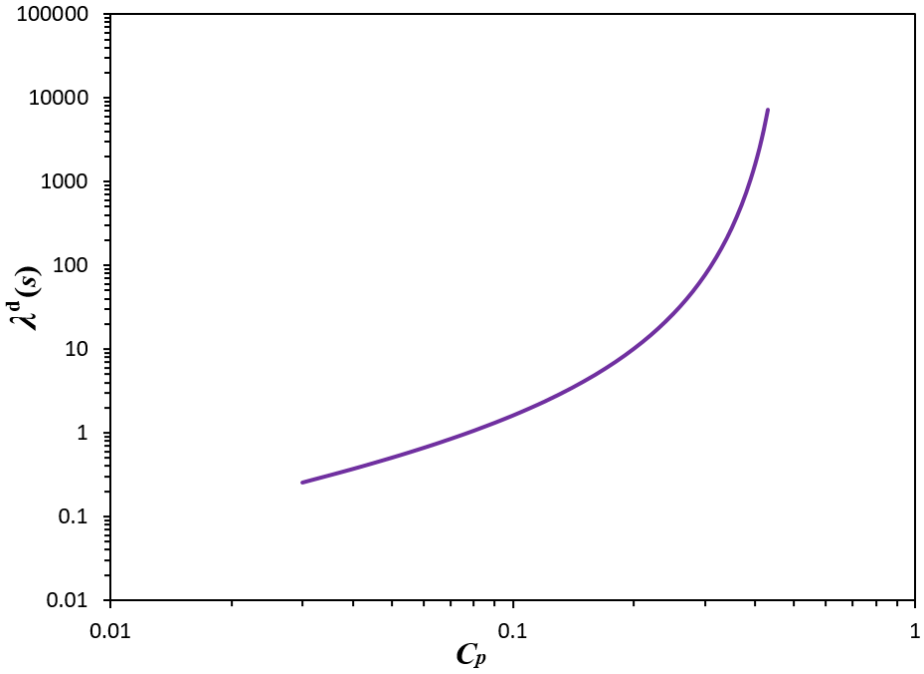

Fig. 3-3. Dimensional relaxation time of liquid phase (λ^d) as a function of polymer concentration ($c_p = 1 - c_l$).

3.5 Transient reference solution

The reference solution whose stability will be examined is a horizontally homogeneous solution with a zero velocity in the liquid. This solution is time dependent in our model and consists of diffusive boundary layers that develop in the spatially uniform liquid and gas layers. These boundary layers correspond to the evolution of the temperature T_l and the solvent mass fraction c_l in the liquid phase and to the evolution of the temperature T_g and solvent mass fraction c_g in the gas phase, respectively. In the gas, the horizontal components of the velocity also vanish, while the vertical one is imposed by evaporation (Stefan flow). In the present study, these solutions will be obtained numerically as in [48]. For the physical system described in section 3.3, the time evolutions of the solvent concentration profile in the liquid are presented in Fig. 3-4 for H equal to 2, 11, and 101 (let us remind that H is the total dimensionless height of the liquid-gas system). As we

already mentioned before, a solutal boundary layer grows into the liquid layer as time passes in the beginning. For high H values, the slope of the profile is less steep, which means that, as expected, the evaporation rate reduces as the gas thickness increases. Note that we have also calculated the corresponding results for a constant diffusion coefficient and we have observed that the corresponding solutal boundary layer grows slower into the liquid layer. In fact, the composition dependent diffusion coefficient increases as the solvent concentration decreases during the evaporation process, and this explains why the solutal boundary layers grow faster than in the case of a constant diffusion coefficient. It is also important to mention that due to evaporation, the thickness of the liquid layer decreases in the course of time. However, our calculation for the case in which the evaporation is the fastest (H=2) revealed that this variation remains very small even for the longest time (t=0.015(s)) that will be considered later for linear stability analysis, with $\delta d_l = 0.5\%$ of the liquid thickness d_l. Therefore, the thickness can safely be assumed to remain effectively constant. We had also observed the same behavior in [48] for very small times.

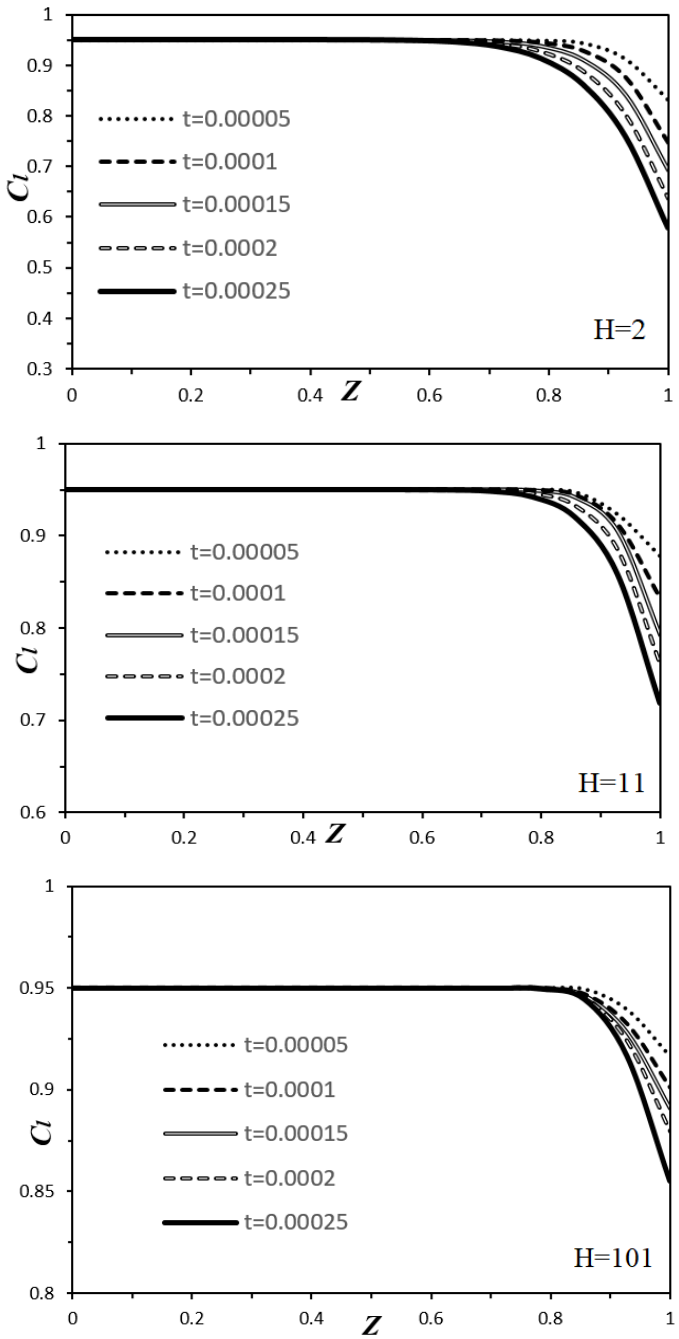

Fig. 3-4. The reference solution for the solvent mass fraction in the liquid layer for different total thicknesses (H = 2 (up), 11 (middle), and 101 (down)) and for several values of the dimensionless time. The variable Z on the horizontal axis is the non-dimensional vertical coordinate in the liquid layer.

3.6 Linear stability analysis

To study the linear stability of the reference solution (denoted by the subscript "*ref*"), the time evolution of infinitesimal perturbations with

respect to this solution must be analyzed. It should be underlined that we have neglected the temporal dependency of the liquid thickness and thus it is consistent to neglect the perturbation of the liquid thickness as well. The stability analysis is performed in the framework of the so-called "frozen-time" assumption, also called the quasi-steady state approximation (QSSA [49]). This means that the stability analysis of the reference solution is performed by assuming that the nonlinear reference profile can be frozen at each specified instant before analyzing the time evolution of infinitesimal perturbations. This approach has already been used by many studies in the context of linear stability analyses (see for instance [29, 43]) and it is worth mentioning that it is strictly valid only when the growth rate of the perturbations is much larger than the rate of change of the base state whose stability is analyzed. Since our base state consists essentially in the propagation of diffusive boundary layers from the liquid-gas interface, and since this propagation is fast in the first instants after the layers are brought into contact, the frozen time assumption is only valid for not too small times. This point will be commented in further detail in Section 3.6.3.

The small perturbations are introduced, both in the liquid and gas phases, by writing:

$$\begin{aligned} c_l &= c_{l_{ref}} + c_l',\ T_l = T_{l_{ref}} + T_l' \\ c_g &= c_{g_{ref}} + c_g',\ T_g = T_{g_{ref}} + T_g' \\ \vec{v}_l &= \vec{v}_{l_{ref}} + \vec{v}_l',\ p_l = p_{l_{ref}} + p_l' \\ \vec{v}_g &= \vec{v}_{g_{ref}} + \vec{v}_g',\ p_g = p_{g_{ref}} + p_g' \end{aligned} \tag{28}$$

where the primed quantities represent the perturbed variables. These decompositions (Eq. (28)) can be introduced in the bulk equations and boundary conditions, which are then linearized with respect to the

infinitesimal perturbations. The horizontal components of the velocity (u and v) can be eliminated from the equations (by applying $\nabla \times \nabla \times$ to the momentum equation). Then, a normal mode expansion of the dependent variables is introduced as follows:

$$\left\{c_l^{'}, T_l^{'}, w_l^{'}, p_l^{'}\right\} = \{C_l(z), \theta_l(z), W_l(z), P_l(z)\} e^{[st+i(k_x x+k_y y)]} \quad (29)$$

$$\left\{c_g^{'}, T_g^{'}, w_g^{'}, p_g^{'}\right\} = \{C_g(z), \theta_g(z), W_g(z), P_g(z)\} e^{[st+i(k_x x+k_y y)]} \quad (30)$$

where $s = \sigma + i\,\omega$ is the complex growth rate of the perturbations and k_x and k_y are the components of the horizontal wave vector $\vec{k}$ (with the wavenumber $k \equiv \sqrt{k_x^2 + k_y^2}$), whereas C, θ, W, P are the complex amplitudes of respectively the mass fraction, temperature, vertical velocity, and pressure. This eigenvalue problem is solved using a MATLAB code which is based on the general code package developed by [50].

3.6.1 Monotonic mode

For monotonic solution of the linear stability problem, the frequency ω is considered zero and the marginal stability curves are defined by $s = \sigma = 0$. Before proceeding to the results, let us stress that the liquid thickness d_l will be considered as the control parameter. Remind also that this quantity enters into the dimensionless formulation through the dimensionless numbers Ma, Ms, Ra_l, and Rs_l [28, 29]. In this context, for a fixed H and at a given instant of dimensionless time t (corresponding to a given frozen reference profile), the stability analysis consists in determining the function $d_l(k)$ corresponding to a zero-growth rate and to minimize this function with respect to the wavenumber k. This procedure provides the critical thickness $d_l^c(t)$ (and critical wavenumber k^c) corresponding to the chosen time t. This function $d_l^c(t)$ can also be inverted, which allows determining the critical time $t^c(d_l)$ at which a layer of thickness d_l becomes unstable. This critical

time makes up our main result and is presented in Fig. 3-5 for $H = 2$ (note the logarithmic scales used in the figure). Let us mention that about 40 points have been calculated to draw the curves presented in Fig. 3-5 (or in other figures presenting similar results below). It is important to stress that the curves are not single-valued since quite often two critical times are associated with a given thickness. This point has already been observed and discussed in [29], and we refer the interested reader to our previous paper [29] on this question. In order to examine the importance of concentration dependent diffusion coefficient and viscosity, we have also represented in Fig. 3-5 the results corresponding to constant diffusion and/or constant viscosity. It is important to note that the constant values of μ_l and D_l used in the calculations are those corresponding to the initial uniform composition of the mixture ($\mu_l = \mu_l(c_{li} = 0.95) = 20.8 \times 10^{-3} Pa.s$ and $D_l(c_{li} = 0.95) = 10^{-10} \frac{m^2}{s}$).

The solid line in Fig. 3-5 corresponds to a constant diffusion coefficient and a constant dynamic viscosity and is strictly equivalent to the results obtained in [29] for a different binary mixture. It is worth emphasizing that there is a certain critical liquid thickness (turning point in the curve), below which no instability ever occurs (no growing perturbations occur) and for thicknesses larger than this critical value, the first unstable state with growing perturbation is located on the lower part of the curve. When we consider a variable viscosity (Eq. (26)) in comparison with the constant viscosity case (solid curve), the fluid layer becomes globally more viscous since evaporation increases the concentration of polymer and the critical curve is shifted upwards and to the right (dashed curve). For the variable diffusion coefficient (empty dashed curve), or when both the viscosity and diffusion dependences on concentration are taken into account (dotted curve), similar displacements of the stability curve are observed in Fig. 3-5. Increased mean

viscosity and/or mean diffusion induced by the evaporation of the solvent are thus stabilizing in the sense that for a given fluid thickness, the critical time for instability is larger when variable viscosity and diffusion are considered. This critical time can even disappear, with an always stable layer, when the turning point of the stability curves is displaced to value of d_l larger than that corresponding to the studied system.

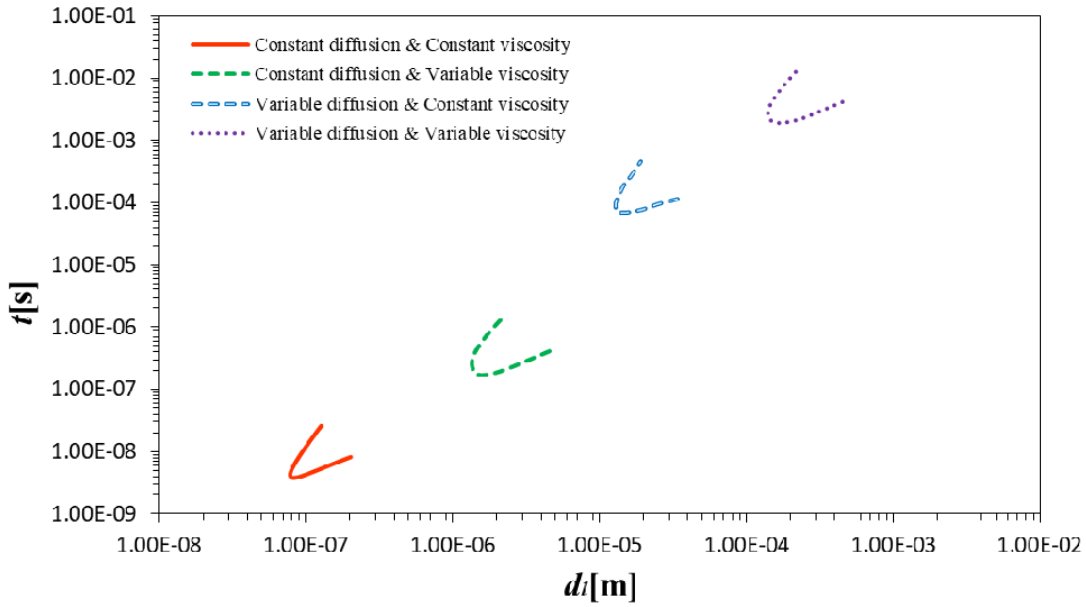

Fig. 3-5. The critical curves for $H = 2$ for the four cases.

In the following figures, we have considered only composition dependent diffusion coefficient and viscosity and Fig. 3-6 depicts the results corresponding to different values of the total height of the liquid-gas system, with $H = 2$, 11, 51, 61, and 101. We observe that an increased H makes the system more stable since the stability curves are shifted upwards and to the right. This is due to the fact that evaporation is reduced and the mass fraction gradients at the liquid-gas interface thus decrease. Note also in Fig. 3-6 that the turning point on the curves is present for all H.

Our results were also compared with the experimental data obtained by Doumenc et al. [43]. In this experimental study, polyisobutylene (PIB)/toluene solutions were poured in a dish evaporating into air and one

aim of the study was to find out the unstable configurations, i.e. to determine which sets of liquid thickness, initial PIB mass fraction, and dimensional time are associated with the onset of convection. Moreover, the authors also emphasized that the convective patterns, when observed, always appear at the very beginning of the drying process. The critical liquid thickness and time of convection onset corresponding to the case of a 5% PIB/95% toluene solution ($c_{li} = 0.95$) are reproduced in Table 3-2. Since evaporation takes place in ambient air, we can consider that the value of parameter H is large in experiments. Considering our Fig. 3-6, we note that the critical time for the onset of convection of a thickness of 8 mm is given by t =2.23 (s) for all $H \geq 51$, which is quite in the range measured in the experiments of Doumenc et al. This agreement is an important validation of our model. Note that we have also calculated the critical time for H=101 and the same liquid thickness of 8 mm, but considering (a) constant viscosity and diffusion coefficient, (b) variable viscosity and constant diffusion coefficient, and (c) constant viscosity and variable diffusion coefficient. The results we found for these three situations are respectively $t = 3.84 \times 10^{-6}$ (s), $t = 2.26 \times 10^{-4}$ (s), and $t = 5.36 \times 10^{-2}$ (s), which are really much smaller than the value given above. This clearly shows the importance of taking into account both the viscosity and the diffusion dependences with respect to the polymer concentration in order to have an agreement between theory and experiments.

Table 3-2. Data corresponding to an experimental case described in [43].

Critical liquid thickness	d_l=8mm
Initial PIB mass fraction	5% PIB (c_{li}=0.95)
Dimensional time (in seconds) corresponding to the onset of convection	t[s]≲10

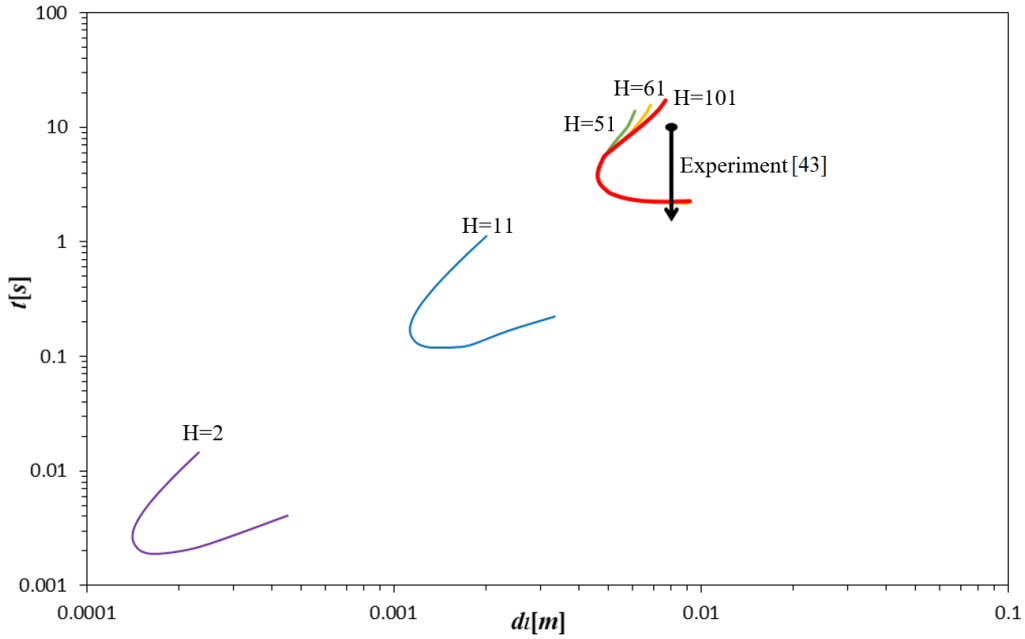

Fig. 3-6. The dimensional critical times as a function of the liquid thickness for $H = 2$, 11, 51, 61, and 101 in the case of variable diffusion coefficient and the variable viscosity. The axes are on logarithmic scale.

Another interesting comparison with the experimental results presented by Doumenc et al. in [43] can be obtained by considering the turning points that appear in our stability curves. These turning points determine a limit for the thicknesses under which no instability ever takes place. In Fig. 3-7, we have represented these limit thicknesses in terms of the initial concentration of the mixture (note that only the 3 red circles correspond to calculated results, while the dotted line is just the link between these points). In the same picture, we have also reproduced some information extracted from [43]. More precisely, the square dots represent situations provided in [43] for which no instability was observed experimentally. Since the dashed line in the figure represents the boundary between stable and unstable domains, it is worth emphasizing that all the square dots should be located on the left of this line, which is indeed the case. Our model thus provides a good description of the limit of fluid thickness under which instability is not possible.

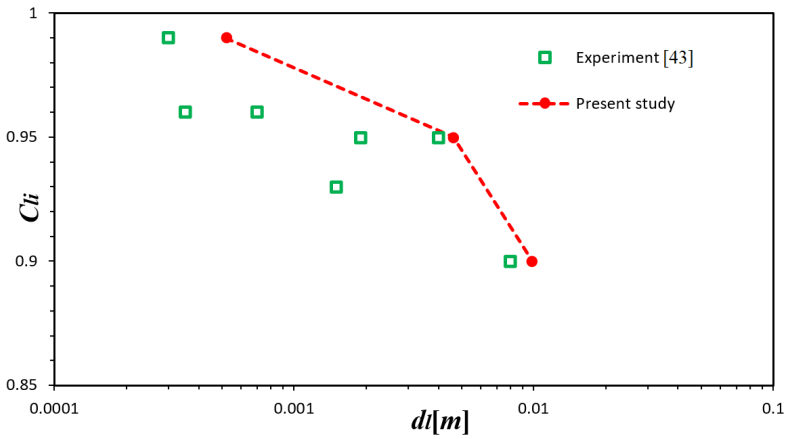

Fig. 3-7. Comparison of theoretical and experimental results in the plane (c_{li}, d_l) for the transition between the ‘‘stable” and ‘‘unstable” domains. Symbol d_l stands for the liquid thickness while c_{li} is the initial liquid mass fraction. For our results, only the red dots represent calculated data.

3.6.2 Oscillatory mode

When non-Newtonian fluids are submitted to temperature and/or solutal gradients, non-monotonic instabilities can occur, as already studied and discussed in several papers [41, 51]. Since we consider here a viscoelastic Maxwell fluid, this option must also be examined and the possibility of oscillatory modes of convection must be analyzed. The marginal state for this situation is defined by $s = 0$ with $\omega \neq 0$. It is worth recalling that the liquid thickness d_l is considered here as the control parameter, in terms of which our results are presented. Note also that this thickness was used to define the time scale needed to deduce the dimensionless equations of the problem. Therefore, since the physical dimensional relaxation time λ^d given by (Eq. (27)) depends only on the nature of the fluid, the value of the dimensionless relaxation time λ changes with d_l in our results. Fig. 3-8 corresponds to H=101 and shows the critical dimensional time at which the oscillatory instability occurs in terms of the thickness of the liquid layer. The associated frequency $\omega(Hz)$ is also represented. To assess the importance of considering a composition dependent relaxation time, we have also plotted

in Fig. 3-8 the results for a constant relaxation time, whose value is taken as that of the initial uniform mixture ($\lambda^d = \lambda^d(c_{il} = 0.95) = 0.5$). We observe that the two curves are indeed different, even if the effect of a composition dependent relaxation time is a bit less important than the corresponding effect for viscosity or diffusion coefficient. Then it is important to emphasize the appearance of a turning point in the stability curve, as in the case of monotonic convection, but this turning point defines here a maximal thickness above which no oscillatory instability is possible. Note also that this maximal thickness is in the micrometer range, which means that oscillatory instabilities are possible only in very thin layers.

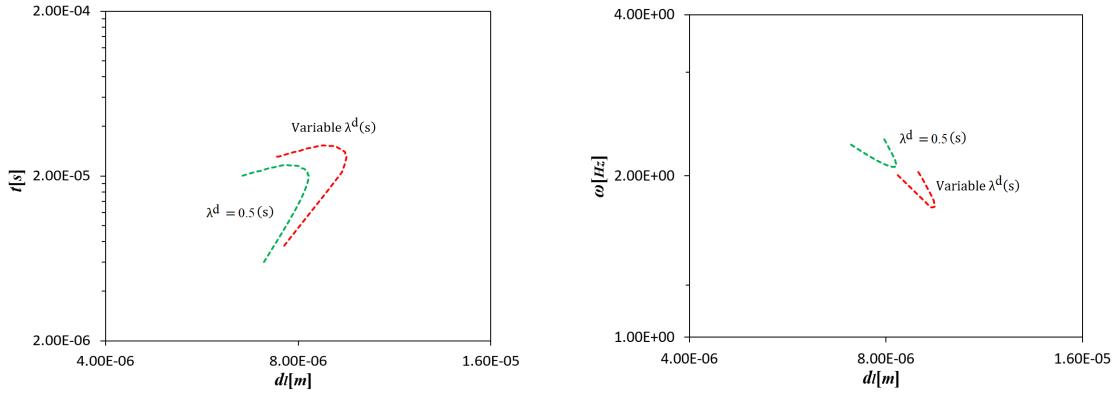

Fig. 3-8. The critical curves and corresponding frequencies ω for the oscillatory motions, $H = 101$. Both a constant (dimensional) relaxation time and a concentration dependent (dimensional) relaxation time are considered.

3.6.3 Comparison of monotonic and oscillatory modes

Fig. 3-9 is a summary of the stability analysis and presents the critical curves for both monotonic and oscillatory modes, considering variable viscosity, diffusion coefficient, and relaxation time. The solid curve represents the monotonic neutral curve (ω=0) while the dashed curve corresponds to the oscillatory instability ($\omega \neq 0$). As already mentioned above, oscillatory instability is possible only in very thin layers (micrometer range), while monotonic modes appear in thicker systems (millimeter range). We also

observe a window in the values of fluid thickness, determined by the two turning points, within which the layer of fluid is always stable. Note also that to our knowledge, no experimental results are available regarding the oscillatory instability in very thin layer. Finally, let us emphasize that as far as the validity of the frozen time assumption is concerned, the smallest critical times considered in Fig. 3-9 are of the order of $\sim 10^{-5}$ s. We can then check from Fig. 3-4 that for such values of the time, the thicknesses of the boundary layers are already rather large and the change of the base state is thus not too fast any more.

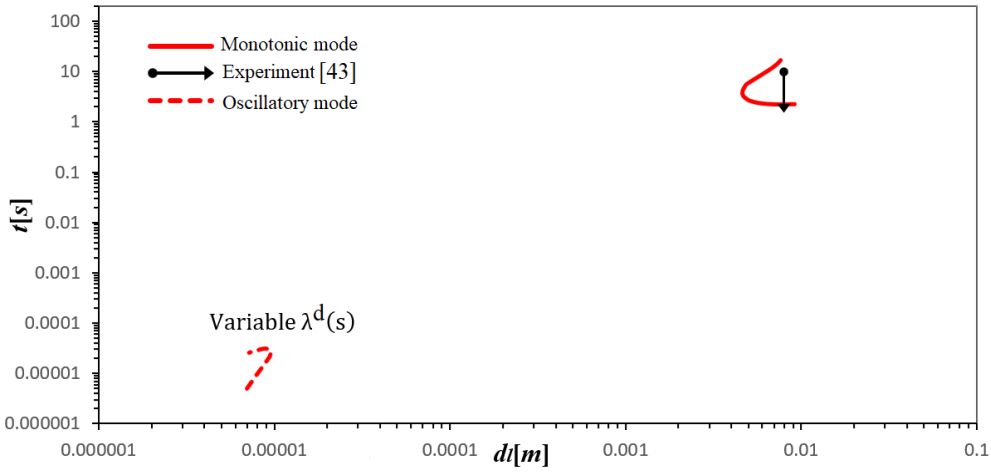

Fig. 3-9. The dimensional critical times as a function of the liquid thickness for the monotonic and oscillatory modes for $H = 101$.

3.7 Approximate model

In the current section, an approximate model of the system is considered, which is derived from the complete model mentioned in section 3.3. The approximate model is constructed by keeping only the most important physical phenomena (from the instability threshold point of view). First, it is only the solutal Marangoni mechanism of instability, considered to be the predominant one here, that is retained ($Ms \neq 0$, $Ma = Ra_l = Rs_l = 0$). Second, we end up with a totally isothermal formulation (the problem for the concentration field is decoupled from the thermal one). Third, it is assumed

that the gas mass fraction of the solvent is small, $c_g \ll 1$, and thus the convective effect of the Stefan flow can be neglected in the gas phase. The gas phase is thus considered as a purely diffusive medium. The result of the approximate model is compared in Fig. 3-10 with the corresponding result of the full approach for both monotonic and oscillatory modes, and the agreement is seen to be good indeed. From this comparison, it can be concluded that the thermal and Rayleigh effects can indeed be neglected and the gas phase can actually be considered as a purely diffusive medium for the solvent vapor. This also proves that the solutal Marangoni effect is much stronger than thermal and Rayleigh effects and is the actual main physical mechanism generating the instability. The same conclusion was also observed in [29] in the case of evaporation of a binary mixture and in [30] in the case of evaporation of a dilute polymer solution.

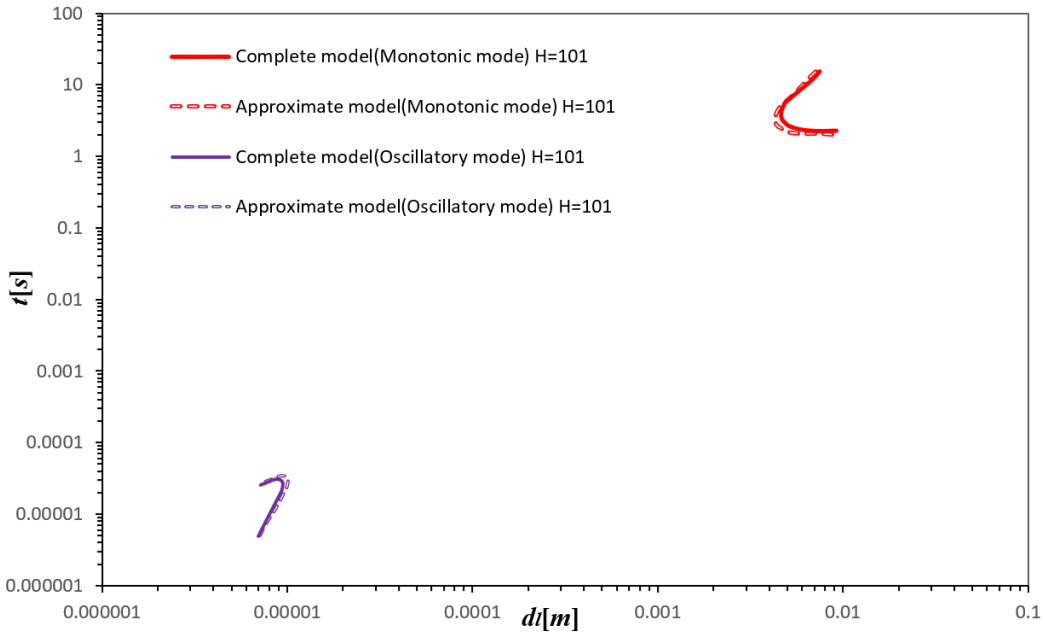

Fig. 3-10. The critical curves for both monotonic and oscillatory modes for $H = 101$ comparing the complete and approximate models in the case of variable diffusion coefficient and the variable viscosity.

3.8 Conclusion

Evaporation is a very common phenomenon that takes place everywhere in nature and in many industrial processes. Due to the cooling effect, the surface of an evaporating fluid induces temperature gradients in the liquid. Moreover, when the fluid is a binary mixture of a polymer solution, evaporation also induces concentration gradients. Therefore, evaporation can actually generate thermo-solutal instabilities in fluid mixtures. In this study, we presented a detailed analysis of the onset of convection for a transient drying problem for both monotonic and oscillatory solutions.

When a thin layer of polymer solution and a gas phase, which are not in equilibrium with respect to one another, are suddenly brought into contact, a very strong evaporation is expected in the very beginning. The resulting important decrease of the liquid solvent concentration at the interface could thus result in the variation of the viscosity, diffusion and relaxation time with the change of concentration, especially close to the liquid-gas interface due to the high concentration gradients. We have built a model for the drying process of a polymer solution taking into account the physics of the upper gas layer and its interactions with the liquid layer and the variation of the viscosity, diffusion and relaxation time with the solvent mass fraction.

For the monotonic mode, we have shown that the concentration dependent diffusion and viscosity makes the system more stable, in the sense that the critical time for the appearance of convection is larger than the value that would correspond to constant properties of the fluid. We have also shown that increasing the gas thickness makes the system more stable and, for thick gas layers, we have obtained a good agreement between our stability results and the experimental work of Doumenc et al. [43]. More precisely, our predicted critical time for instability is of the same order as that observed in

these experiments. In addition, our description on the limit of fluid thicknesses under which no instability ever occurs, which is linked to the appearance of a turning point in the stability curves, is also in good agreement with observations.

We have also confirmed that the viscoelastic effect can lead to an oscillatory instability, while just a monotonic one would take place in its absence. For the oscillatory mode, a turning point also appears in the stability curve, but this turning point defines a maximal thickness above which no oscillatory instability is possible. This maximal thickness is in the micrometer range, which means that oscillatory instabilities are possible only in very thin layers. Because of this condition on the thickness, the oscillatory instabilities should probably be rather difficult to observe in experiments and have not been reported to date. Remind also that the two turning points define a window in fluid thicknesses, within which the layer remains always stable.

Another important result of our analysis is the need to consider concentration dependent physical properties for polymer solutions in evaporative instabilities. Indeed, strong evaporation induced gradients close to the interface importantly modify the viscosity, diffusion coefficient and relaxation time of the fluid, which in turn changes notably the instability threshold. Finally, the use of an “approximate model” has also enabled to demonstrate that the solutal Marangoni mechanism is by far the most dominant instability mechanism here and that other small effects (convection in the gas, temperature effects, …) can also be safely neglected in the description.

Acknowledgements

Financial support from F.R.S.-FNRS ("DITRASOL" PDR T.0123.16) and from BELSPO ("EVAPORATION" MAP-PRODEX project) is also acknowledged.

3.9 Reference

[1] V. Bekezhanova, I. Shefer, Influence of gravity on the stability of evaporative convection regimes, Microgravity Science and Technology, 30 (2018) 543-560.

[2] I.B. Simanovskii, A. Viviani, F. Dubois, J.-C. Legros, Symmetric and asymmetric convective oscillations in a multilayer system, Microgravity Science and Technology, 22 (2010) 257-263.

[3] I.B. Simanovskii, A. Viviani, F. Dubois, J.C. Legros, The influence of the horizontal component of the temperature gradient on nonlinear oscillatory convective regimes in multilayer system, Microgravity Science and Technology, 23 (2011) 25.

[4] P. Evans, L. Schwartz, R. Roy, A mathematical model for crater defect formation in a drying paint layer, Journal of colloid and interface science, 227 (2000) 191-205.

[5] S. Howison, J. Moriarty, J. Ockendon, E. Terrill, S. Wilson, A mathematical model for drying paint layers, Journal of Engineering Mathematics, 32 (1997) 377-394.

[6] P. Mokarian-Tabari, M. Geoghegan, J. Howse, S. Heriot, R. Thompson, R. Jones, Quantitative evaluation of evaporation rate during spin-coating of polymer blend films: Control of film structure through defined-atmosphere solvent-casting, The European Physical Journal E, 33 (2010) 283-289.

[7] B.-J. de Gans, U.S. Schubert, Inkjet printing of well-defined polymer dots and arrays, Langmuir, 20 (2004) 7789-7793.

[8] T. Kawase, T. Shimoda, C. Newsome, H. Sirringhaus, R.H. Friend, Inkjet printing of polymer thin film transistors, Thin solid films, 438 (2003) 279-287.

[9] B.J. De Gans, P.C. Duineveld, U.S. Schubert, Inkjet printing of polymers: state of the art and future developments, Advanced materials, 16 (2004) 203-213.

[10] S. Walheim, E. Schäffer, J. Mlynek, U. Steiner, Nanophase-separated polymer films as high-performance antireflection coatings, Science, 283 (1999) 520-522.

[11] A. Münch, C.P. Please, B. Wagner, Spin coating of an evaporating polymer solution, Physics of Fluids, 23 (2011) 102101.

[12] B. Guerrier, C. Bouchard, C. Allain, C. Bénard, Drying kinetics of polymer films, AIChE Journal, 44 (1998) 791-798.

[13] J. Pearson, On convection cells induced by surface tension, Journal of fluid mechanics, 4 (1958) 489-500.

[14] C.S. Iorio, O.A. Kabov, J.-C. Legros, Thermal patterns in evaporating liquid, Microgravity Science and Technology, 19 (2007) 27-29.

[15] J. Reichenbach, H. Linde, Linear perturbation analysis of surface-tension-driven convection at a plane interface (Marangoni instability), Journal of Colloid and Interface Science, 84 (1981) 433-443.

[16] D. Goussis, R. Kelly, On the thermocapillary instabilities in a liquid layer heated from below, International journal of heat and mass transfer, 33 (1990) 2237-2245.

[17] P. Colinet, J.C. Legros, M.G. Velarde, Nonlinear dynamics of surface-tension-driven instabilities, Wiley-vch Berlin2001.

[18] S. Sakurai, C. Furukawa, A. Okutsu, A. Miyoshi, S. Nomura, Control of mesh pattern of surface corrugation via rate of solvent evaporation in solution casting of polymer film in the presence of convection, Polymer, 43 (2002) 3359-3364.

[19] N. Bassou, Y. Rharbi, Role of Benard− Marangoni instabilities during solvent evaporation in polymer surface corrugations, Langmuir, 25 (2009) 624-632.

[20] D. Nield, Surface tension and buoyancy effects in cellular convection, Journal of Fluid Mechanics, 19 (1964) 341-352.

[21] M. Dondlinger, P. Colinet, P.C. Dauby, Influence of a nonlinear reference temperature profile on oscillatory Bénard-Marangoni convection, Physical Review E, 68 (2003) 066310.

[22] K.H. Kang, C.K. Choi, A theoretical analysis of the onset of surface-tension-driven convection in a horizontal liquid layer cooled suddenly from above, Physics of Fluids, 9 (1997) 7-15.

[23] H. Machrafi, A. Rednikov, P. Colinet, P. Dauby, Importance of wave-number dependence of Biot numbers in one-sided models of evaporative Marangoni instability: Horizontal layer and spherical droplet, Physical Review E, 91 (2015) 053018.

[24] A. Vidal, A. Acrivos, Effect of nonlinear temperature profiles on onset of convection driven by surface tension gradients, Industrial & Engineering Chemistry Fundamentals, 7 (1968) 53-58.

[25] T.D. Foster, Onset of convection in a layer of fluid cooled from above, The Physics of Fluids, 8 (1965) 1770-1774.

[26] T.D. Foster, Stability of a homogeneous fluid cooled uniformly from above, The Physics of Fluids, 8 (1965) 1249-1257.

[27] F. Doumenc, T. Boeck, B. Guerrier, M. Rossi, Transient Rayleigh-Bénard-Marangoni convection due to evaporation: a linear non-normal stability analysis, arXiv preprint arXiv:0911.2088, (2009).

[28] H. Machrafi, A. Rednikov, P. Colinet, P.C. Dauby, Bénard instabilities in a binary-liquid layer evaporating into an inert gas: Stability of quasi-stationary and time-dependent reference profiles, The European Physical Journal Special Topics, 192 (2011) 71-81.

[29] H. Machrafi, A. Rednikov, P. Colinet, P.C. Dauby, Time-dependent Marangoni-Bénard instability of an evaporating binary-liquid layer including gas transients, Physics of Fluids, 25 (2013) 084106.

[30] P.G. De Gennes, Instabilities during the evaporation of a film: Non-glassy polymer+ volatile solvent, The European Physical Journal E, 6 (2001) 421-424.

[31] B. Trouette, E. Chénier, F. Doumenc, C. Delcarte, B. Guerrier, Transient Rayleigh-Bénard-Marangoni solutal convection, Physics of Fluids, 24 (2012) 074108.

[32] E. Bormashenko, S. Balter, R. Pogreb, Y. Bormashenko, O. Gendelman, D. Aurbach, On the mechanism of patterning in rapidly evaporated polymer solutions: Is temperature-gradient-driven Marangoni instability responsible for the large-scale patterning?, Journal of colloid and interface science, 343 (2010) 602-607.

[33] D. Bratsun, K. Kostarev, A. Mizev, E. Mosheva, Concentration-dependent diffusion instability in reactive miscible fluids, Physical Review E, 92 (2015) 011003.

[34] D.A. Bratsun, O.S. Stepkina, K.G. Kostarev, A.I. Mizev, E.A. Mosheva, Development of concentration-dependent diffusion instability in reactive miscible fluids under influence of constant or variable inertia, Microgravity Science and Technology, 28 (2016) 575-585.

[35] B.K. Chatterjee, S. Roy, Viscosity divergence and gelation, Radiation Physics and Chemistry, 74 (2005) 419-425.

[36] B. Haut, P. Colinet, Surface-tension-driven instabilities of a pure liquid layer evaporating into an inert gas, J Colloid Interface Sci, 285 (2005) 296-305.

[37] H. Machrafi, A. Rednikov, P. Colinet, P.C. Dauby, Benard instabilities in a binary-liquid layer evaporating into an inert gas, J Colloid Interface Sci, 349 (2010) 331-353.

[38] K.y. Ozawa, T. Okuzono, M. Doi, Diffusion Process during Drying to Cause the Skin Formation in Polymer Solutions, Japanese Journal of Applied Physics, 45 (2006) 8817-8822.

[39] R.B. Bird, R.C. Armstrong, O. Hassager, Dynamics of polymeric liquids. Vol. 1: Fluid mechanics, (1987).

[40] R.I. Tanner, Engineering rheology, OUP Oxford2000.

[41] P. Dauby, P. Parmentier, G. Lebon, M. Grmela, Coupled buoyancy and thermocapillary convection in a viscoelastic Maxwell fluid, Journal of Physics: Condensed Matter, 5 (1993) 4343.

[42] A.A. Cantú, A study of the evaporation of a solvent from a solution—application to writing ink aging, Forensic science international, 219 (2012) 119-128.

[43] F. Doumenc, E. Chénier, B. Trouette, T. Boeck, C. Delcarte, B. Guerrier, M. Rossi, Free convection in drying binary mixtures: solutal versus thermal instabilities, International Journal of Heat and Mass Transfer, 63 (2013) 336-350.

[44] G. Toussaint, H. Bodiguel, F. Doumenc, B. Guerrier, C. Allain, Experimental characterization of buoyancy- and surface tension-driven convection during the drying of a polymer solution, International Journal of Heat and Mass Transfer, 51 (2008) 4228-4237.

[45] V.M. Litvinov, P.P. De, Spectroscopy of rubbers and rubbery materials, iSmithers Rapra Publishing2002.

[46] L. Guo, Gelation and micelle structure changes of aqueous polymer solutions, (2003).

[47] D. Getachew, S. Rosenblat, Thermocapillary instability of a viscoelastic liquid layer, Acta mechanica, 55 (1985) 137-149.

[48] R. Rabani, H. Machrafi, P. Dauby, Effect of including a gas layer on the gel formation process during the drying of a polymer solution, Eur Phys J E Soft Matter, 40 (2017) 89.

[49] C. Tan, G. Homsy, Stability of miscible displacements in porous media: Rectilinear flow, The Physics of fluids, 29 (1986) 3549-3556.

[50] H.-Y. Ye, L.-J. Yang, Q.-F. Fu, Spatial instability of viscous double-layer liquid sheets, Physics of Fluids, 28 (2016) 102101.

[51] G. Lebon, P. Parmentier, O. Teller, P. Dauby, Bénard-Marangoni instability in a viscoelastic Jeffreys' fluid layer, Rheologica acta, 33 (1994) 257-266.

II Phase separation in thin evaporating film of a partially miscible binary mixture

Chapter 4

Introduction to papers 3 and 4

4.1 General context

Phase separation or demixing often takes place in condensed matter and has many applications in metallurgy or other industrial processes related to semiconductors, polymers, emulsions, ceramics, biological materials, *etc*. (see for instance the references in [1-3]). As an example, we can mention image inpainting, which is the filling in of damaged or missing areas of an image with the use of information from surrounding areas [4-6] (Fig. 4-1). Its applications include the restoration of old paintings in museums, or the removal of scratches from photographs. It is also interesting to mention that the growth of cancer cells can also be described as a phase separation phenomenon (Fig. 4-2) [7].

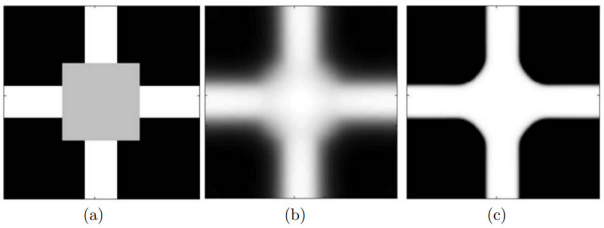

Fig. 4-1. Damaged binary image and the solution of Cahn–Hilliard inpainting [4].

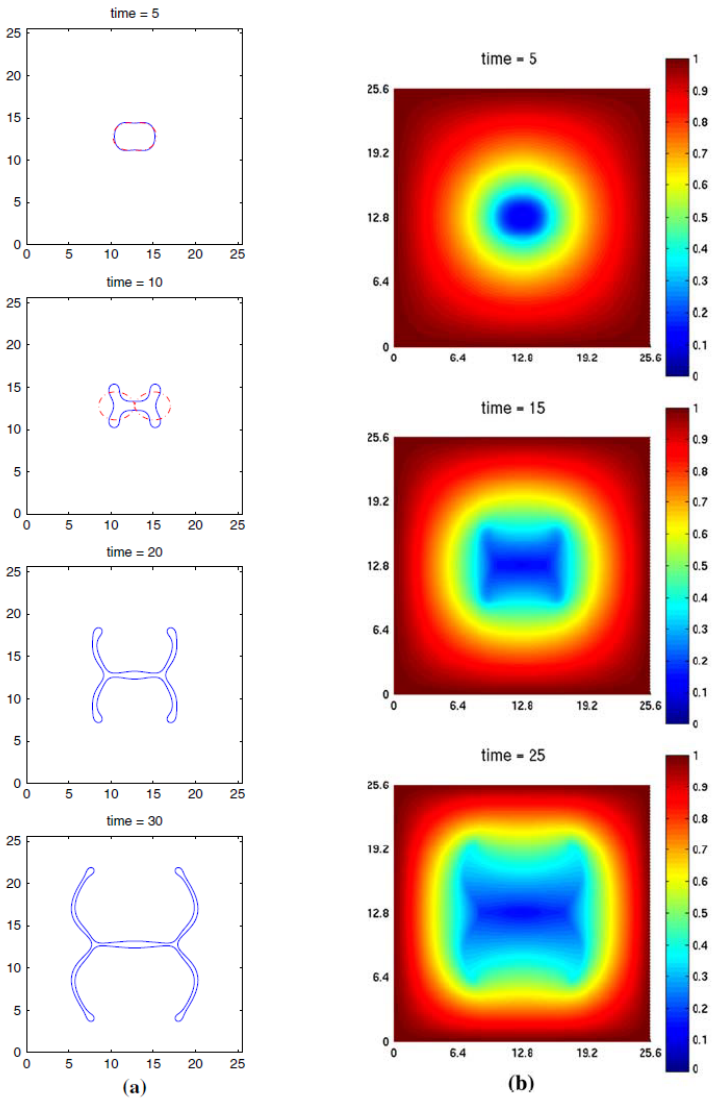

Fig. 4-2. a) Evolution of the tumor surface [7], b) Contour plots of nutrient concentration evolution [7].

One can furthermore cite the fabrication of organic solar cells [8-10], during which evaporation removes a solvent from an active layer of a polymer solution (Fig. 4-3). This results in concentration changes in the active layer that can lead to the phase separation playing directly an significant role in determining the final efficiency of the organic solar cell [11].

From a physical point of view, it is therefore highly desirable to understand and have control over how the phase separation occurs in aforementioned applications and subsequently evolve.

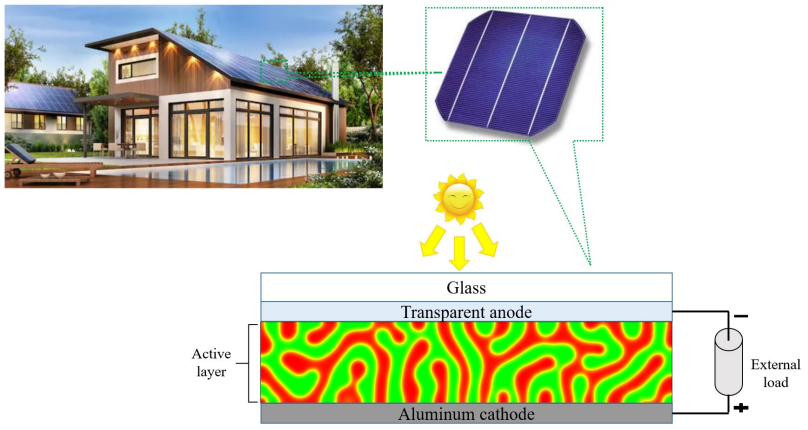

Fig. 4-3. Schematic of the organic solar cell.

4.2 Thermodynamics of phase separation

4.2.1 Free energy and phase diagram

In the context of classical thermodynamic, phase separation of a binary mixture is an example of phase transition in multicomponent fluids. This phase separation depends on the free energy between the mixed and demixed states. Therefore, the free energy function (the potential function) is a starting point to describe the mechanism of phase separation. A fourth order polynomial potential function and a logarithmic potential function are two common types of potential functions [12-15]. A fourth order polynomial form is used for a simple binary mixture, in which we have a symmetric potential function with two minima giving the same value for the potential. In contrast, a logarithmic form is used for a binary polymer blend, in which we have an asymmetric potential function, where the two minima correspond to different values and describe different degrees of polymerization in the polymer blend (see [16] for more details). In this thesis, we used a fourth order polynomial form of potential function for our binary mixture. Two typical forms of such a potential function, which depends on temperature and concentration, are represented schematically in Fig. 4-4-a. An explicit expression will be provided in Chapter 6. It is important to emphasize that if

the temperature exceeds a critical value T_c (see the case of T_2 in Fig. 4-4-a), the potential function f_0 gives rise to a convex function, with only one minimum. Thus, the composition of the mixture tends to this unique value, i.e. the mixture becomes homogeneous. But if the temperature is lowered below T_c (see the case of T_1 in Fig. 4-4-a), the potential function f_0 gets a double-well structure, allowing the separation of the mixture into two distinct phases. In that situation, when the mean concentration of the mixture is between the two concentrations $\emptyset_1^b$ and $\emptyset_2^b$ corresponding to the minima of function f_0, separation occurs in the fluid and two equilibrium phases appear, with concentrations $\emptyset_1^b$ and $\emptyset_2^b$, in order to decrease the total free energy towards its minimum possible value.

The behavior of a partially miscible binary mixture in terms of temperature and composition can be summarized in a phase diagram, an example of which is shown in Fig. 4-4-b. The solid curve is called the "binodal" or the "co-existence" curve and it describes the minima of potential function f_0 for a given temperature. The dotted line represents the "spinodal" curve, which bounds the region where the mixture is unstable, and it denotes, for a given temperature, the compositions at which the potential function f_0 has a vanishing second derivative with respect to the composition ($\frac{d^2 f_0}{d\emptyset^2} = 0$). When the temperature is above the binodal curve, the homogeneous solution is stable and no phase separation occurs. If the composition and temperature lie in the region above the spinodal curve, but below the binodal curve, the homogeneous state is meta-stable. Fig. 4-4-c illustrates the behavior of the system in the meta-stable and unstable regions. In the meta-stable region, the infinitesimal fluctuations in composition decrease over time and a finite amplitude fluctuation is required for the separated phases to form (in Fig. 4-4-c, descending the stairs actually needs energy). Therefore, phase

separation occurs via nucleation and growth mechanism [17, 18]. Domain nucleation requires an energy barrier to be overcome and hence phase separation does not occur spontaneously. If the temperature and mean composition are below the spinodal curve, the amplification of even very small fluctuations will cause the solution to demix spontaneously into two phases, with compositions that lie on the co-existence curve [19, 20]. Since there is no thermodynamic barrier to phase growth, the phase separation occurs spontaneously (in Fig. 4-4-c, falling down the stairs does not need to use energy). This process is known as spinodal decomposition.

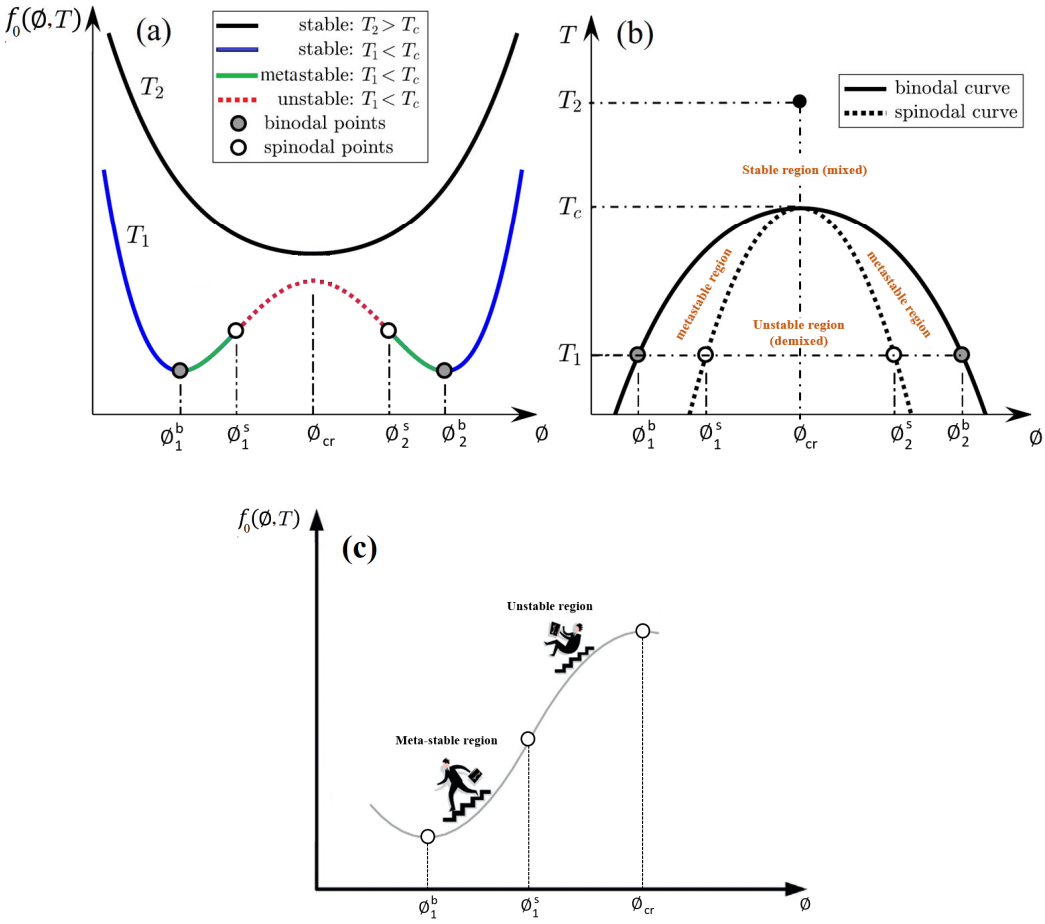

Fig. 4-4. a) Potential function f_0 in terms of concentration, for two values of temperature ($\emptyset_1^b$ and $\emptyset_2^b$ represent the equilibrium phase compositions at temperature T_1; $\emptyset_1^s$ and $\emptyset_2^s$ represent the bounds of the unstable spinodal region at temperature T_1). b) Phase diagram c) Illustration of meta-stable and unstable regions [21].

4.2.2 Cahn-Hilliard equation and dynamics of phase separation mechanism

The phase diagram in Fig. 4-4-b only gives information on the conditions of existence of the possible phases, but provides no direct indication on the dynamics of phase transitions and their evolution in time when some thermodynamic parameters of a system are changed (the temperature and the concentration). We know that phase separation is not instantaneous and that it is a dynamic phenomenon. In fact, phase separation is a transient and non-equilibrium process by which an initially mixed state changes to an unmixed state. In this subsection, the dynamics of phase separation and coarsening phenomena will be described using the Cahn-Hilliard equation, which was originally proposed by Cahn and Hilliard in 1958 to investigate phase separations in binary alloys [22, 23]. This equation captures how the phase or domain will change over time. From a thermodynamic point of view, the total free energy of mixture of two fluids can be written in the Ginzburg-Landau form [3, 14, 24-29]:

$$F(\emptyset, \nabla\emptyset, T) = f_0(\emptyset, T) + \frac{1}{2}\varepsilon^2|\nabla\emptyset|^2 \quad (1)$$

where T is the local liquid phase temperature and $\emptyset$ is the concentration of a component within a binary mixture. The first term in Eq. (1) is the potential function and it depends on the local concentration and temperature. The second term in Eq. (1), depends on the concentration gradient, defines the diffuse interface between two phases. ε is the capillary width characterizing the thickness of the diffuse interface between the two phases.

The Cahn-Hilliard equation has been proved to allow the description of different phenomena, ranging from nano/microscale precipitation [30, 31] to planet formation [32]. Formally, the Cahn-Hilliard equation is a fourth-order

partial differential equation. We start by defining the chemical potential of the system. Based on Eq. (1), a generalized chemical potential for a binary mixture can be introduced: $\mu = \frac{\delta F}{\delta \emptyset} = \frac{\partial F}{\partial \emptyset} - \nabla . \frac{\partial F}{\partial (\nabla \emptyset)}$ [33-35], where $\delta / \delta \emptyset$ is the functional derivative. In fact, in the presence of a gradient, if we make a local change in the composition we also change the local gradient. Therefore, we must consider the functional derivative of the total free energy with respect to composition. Using Fick's First Law for the mass flux $\vec{J} = -M\vec{\nabla}\mu$, where M is the mobility, which is assumed constant, and the continuity equation $\frac{\partial \emptyset}{\partial t} = -\vec{\nabla} \cdot \vec{J}$, the Cahn–Hilliard equation is given by:

$$\begin{aligned} \frac{\partial \emptyset}{\partial t} &= M\nabla^2 \mu \\ &= M\nabla^2 \left(\frac{\partial f_0}{\partial \emptyset} - \varepsilon^2 \nabla^2 \emptyset \right) \end{aligned} \tag{2}$$

When the mixture is suddenly quenched below the spinodal curve, the spinodal decomposition occurs in the system. During this process, matter diffuses up toward higher concentrations from lower concentration. In fact, this is the opposite of the typical situation, where matter flows from regions of high concentration to regions of low concentration. For this reason, this process is called ‘‘up-hill’’ diffusion. The phase separation mechanism for the spinodal decomposition may be classified into the following three regimes: (a) early stage, (b) intermediate stage, and (c) late stage [36-39]. These stages are schematically represented in Fig. 4-5. During the early stage of spinodal decomposition, the wavelength of the spatial concentration fluctuations remains constant and corresponds to the fastest growing wavenumber of the unstable domain; however, the wave amplitude of the spatial concentration fluctuations (the concentration difference of two phases) increases with time. In this stage, the phase separation can be described by the linearized Cahn–Hilliard theory [36-40]. The linearization

of Eq. (2) with respect the infinitesimal perturbations around the mean concentration $\emptyset_0$ within the miscibility gap gives:

$$\frac{\partial \emptyset}{\partial t} = M\left(\left(\frac{\partial^2 f_0}{\partial \emptyset^2}\right)_{\emptyset_0} \nabla^2 \emptyset - \varepsilon^2 \nabla^4 \emptyset\right) \tag{3}$$

with growth rate:

$$\omega(k) = -Mk^2\left(\left(\frac{\partial^2 f_0}{\partial \emptyset^2}\right)_{\emptyset_0} + \varepsilon^2 k^2\right) \tag{4}$$

where $k = \frac{2\pi}{\lambda}$ is the wavenumber and λ is wavelength of the perturbation. The growth of perturbations, which requires $\omega(k) > 0$, is obtained for:

$$k < k_c = \sqrt{\frac{-\left(\frac{\partial^2 f_0}{\partial \emptyset^2}\right)_{\emptyset_0}}{\varepsilon^2}} \tag{5}$$

and has a maximum (dominant wavenumber) at:

$$k_m = \frac{1}{2}k_c^2 \tag{6}$$

The corresponding maximum growth rate is then:

$$\omega_m = \frac{M\varepsilon^2}{4}k_c^4 \tag{7}$$

Note that the early stage of spinodal decomposition is usually the most difficult to visualize experimentally because it occurs at such a fast rate. When the peak compositions approach the coexisting compositions (see middle picture in Fig. 4-5), the system enters in the intermediate stage of phase separation, during which both the wavelength and the wave amplitude of the concentration fluctuations increase with time. Finally, in the late stage, the wave amplitude is at its equilibrium composition values and remains constant, while the wavelength increases with time due to coarsening.

In the absence of external surface effects, when a homogeneous binary mixture is abruptly cooled to a lower temperature in the unstable region,

phase separation can lead to two types of morphology according to the average initial concentration. For an off-critical concentration, where the average concentration of the binary mixture is not the same as the critical concentration ($\emptyset_{cr}$ in Fig. 4-4-b), a droplet-type morphology (Fig. 4-6-a) forms. On the contrary, the interconnected structure (Fig. 4-6-b) forms when the average concentration of the binary mixture is the critical concentration [20, 37, 41-43]. In fact, the interconnected type of morphology is dominant when there is a symmetry between the two phases. In contrast, the droplet-type morphology is observed when there is an asymmetry in the two phases. It means that the minority/majority phase separates from the majority/minority phase.

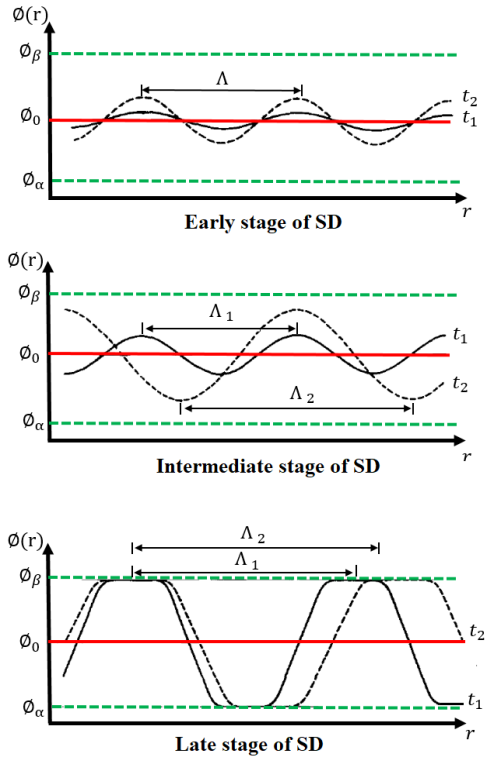

Fig. 4-5. Schematic representation of spatial concentration fluctuation of one component in the critical mixture at three different stages of demixing: early stage of SD, intermediate stage of SD, and late stage of SD. Time evolution of the fluctuation within each stage is shown by solid (t_1) and dashed (t_2) lines ($t_1 < t_2$). $\emptyset_\alpha$ and $\emptyset_\beta$ are the equilibrium concentrations of one component in the coexisting two liquid phases [44].

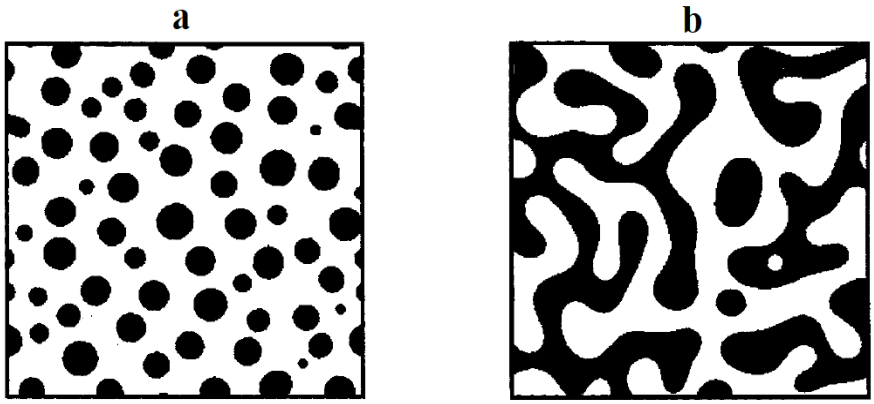

Fig. 4-6. a) Droplet-type morphology, b) Interconnected type of morphology [20].

4.3 Phase separation in confined geometries

The presence of external surfaces which act to confine a binary mixture can importantly influence the dynamics of phase separation and, as a consequence, the long-term morphology of system. Introducing a confining surface into the system can lead to new interactions that occur between the components of the mixture and the external surface. This can cause one of the 2 separating components to be preferentially attracted to or repelled from the surface. This mode of phase separation has been termed surface-directed spinodal decomposition and it was first observed experimentally by Jones et al. [45]. Further experiments were performed by Krausch et al. [46] in order to quantify the growth of the wetting layer during the process of spinodal decomposition of a binary polymer mixture. The first theoretical study of surface-directed spinodal decomposition using a coarse-grained and continuous model was conducted by Puri and Binder [47]. They were able to capture the propagation of composition waves but their model predicted linear growth of the layers in time. Detailed summaries of the experimental aspects of phase separation in confined geometries can be found in the review papers by Geoghegan and Krausch [48] and Krausch [49]. The

theoretical aspects of this topic are comprehensively reviewed by Puri [50] and Binder et al. [51].

4.3.1 Phase separation in a thin film

Thin layer of mixtures is an example of confined geometries commonly involved in a number of industrial contexts ranging from semiconductor, inkjet printing, and the fabrication of the photoactive layers of polymeric organic solar cells devices [9, 52, 53]. In all of these applications, the quality of the resulting thin film is directly related to its morphology and composition. Consequently, these applications often seek films with specific pattern of morphologies that are optimal in some sense. For instance, In the case of organic solar cells, the efficiency of the device is directly associated with the shape of the interfaces between the polymer structures [11]. Thus, the polymers that constitute the photoactive component of the device should interpenetrate on nanometer scales to minimize exciton recombination [54]. From a practical point of view, it is therefore highly desirable to understand and have control over how these structures form and subsequently evolve.

4.3.2 Evaporation-induced phase separation

Both temperature and concentration can be changed to move the system in the phase space and to induce demixing or phase separation. Phase separation induced by a decrease in temperature is known as temperature-induced phase separation and is usually performed by cooling down the binary mixture. Phase separation can also be induced by a change in the concentrations of the different components of a mixture which is known as concentration-induced phase separation. The effect of temperature or concentration gradients on the phase separation of a binary mixture in a thin film has been analyzed numerically by Jaiswal et al. [55-57]. They showed that these gradients in a thin film result in the creation of a lateral structure (a periodic

array of stripes) or a lamellar structure (a bilayer). Evaporation induces both concentration and temperature changes in the system simultaneously. Several researchers have tried to probe and understand the mechanism of phase separation in polymer mixtures (ternary mixtures with two polymers and one solvent, or binary mixtures consisting a single polymer and solvent) resulting from solvent evaporation. The scientific and industrial relevance of the thin evaporating thin film of a mixture motivated a number of recent experimental studies. Typically, these experiments involve spin coating of a ternary mixture consisting of two polymers that have been blended in a common solvent. Dunbar et al. [58] investigated the relationship between the initial polymer concentration and the film morphology. Mokarian-Tabari et al. [59] showed how different morphologies could be achieved by a quantitative control of the evaporation rate. Jaczewska et al. [60] changed the solubility parameters through the use of different solvents and polymers to exhibit different types of morphology. The results from these experiments, along with those of Heriot & Jones [61] indicated that the polymer films often take one of two morphologies: either the constituent polymers demix and form a bilayer (see Fig. 4-7-a), or they demix to form laterally separated domains (see Fig. 4-7-b). The formation of a polymer bilayer is thought to be the result of energetic interactions between the substrate and the polymers. The bilayer is then a result of one of the polymers being preferentially attracted by the substrate, and is also related to a slow evaporation rate that suppresses the Marangoni instability, and allows vertical phase separation to proceed [59, 61]. As far as the laterally separated or columnar topology shown in Fig. 4-7-b is concerned, the proposed interpretation goes as follows. The columns are ultimately the result of an initial Marangoni instability at the interface between the two separating components [58-60]. This instability deforms this interface and causes it to become corrugated.

These corrugations then grow in amplitude, until they hit the substrate and the free surface of the layer, and thus forms the columns that are observed experimentally. Another explanation, related to the lateral structure, is that an initial Marangoni instability takes place at the free surface of the layer [62, 63]. This instability is believed to trigger the phase separation that moves from the free surface of layer towards the substrate. Thus, the columns are basically enlarged from the top to the bottom.

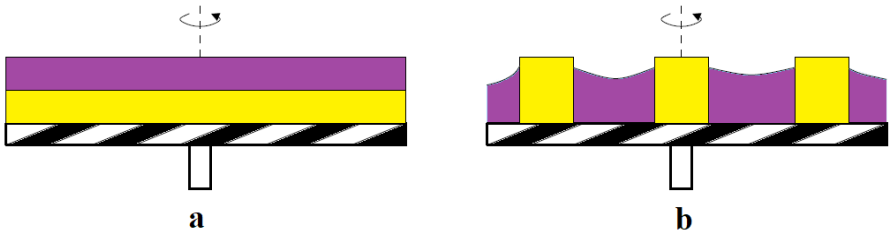

Fig. 4-7. Typical cross sections of polymer films that are created by spin coating a mixture of two polymers, A and B, and a common solvent [59]. The two colors represent A-rich and B-rich regions. As the solvent evaporates, the polymers undergo phase separation to either form a bilayer (a) or a laterally separated structure (b).

Numerical investigation of the phase separation in an evaporative film of a ternary mixture has been considered by many researchers. Wodo & Ganapathysubramanian [64] developped three-dimensional simulations of an evaporating blend consisting of two polymers and a solvent that sits on a substrate. They examined the effect of different variables such as evaporation rate, blend ratio, and solvent type on the morphology evaluation. Zoumpouli et al. [65] examined hydrodynamic effects on phase separation morphologies developed during solvent evaporation of a three-component thin film containing two dissolved polymers and a volatile solvent. They explored that the Marangoni hydrodynamic instabilities tend to break the lamellar configurations into laterally separated phases. Recently, Negi et al. [66] used a numerical model to investigate the microstructure evolution during spin-coating by the evaporation of solvent in a ternary mixture. Their

simulations showed that depending on the evaporation rate, phase separation begins either in the top layers of the thin film or uniformly across the thickness of the drying film. In the case of evaporative thin film of a binary mixture, Schaefer et al. [67] have made significant findings regarding the phase separation of a binary mixture consisting of a single polymer and solvent using two-dimensional (2D) phase field simulations. However, their strategy was to investigate the system by solvent removal uniformly from the entire simulation domain (in the limit of small Biot numbers). In another similar kind of work, Dayal and Kyu [68] analyzed the interplay between the dynamics of the phase separation and the evaporation rate and its impact on the morphology of a single polymer and solvent in a cylindrical geometry.

4.4 Research aims of the second part of the thesis

The evaporation and phase separation phenomena can be further examined, in the framework of the thin evaporating film of a binary mixture, by computer simulations and different experimental set-ups. The aim of the second part of this thesis is to address the two main questions: “How does solvent evaporation in a sessile drop of a binary mixture lead to the demixing of two phases?” and “How does the competition between evaporation and phase separation give rise to the different morphology types in a thin evaporating film of a binary mixture?”.

In Chapter 5, which is a paper published in Colloids and Surfaces A: Physicochemical and Engineering Aspects, we present the experimental results which have been obtained in a collaboration with the TIPs research group in ULB regarding the demixing in the sessile drop. In this experiment, we describe different stages of the phase separation during the evaporation process. In this work, our aim is to explore how the removal of solvent in sessile drop consisting of two partially miscible liquids, maintained initially

at room temperature, can give rise to the phase separation of the binary mixture. In order to determine the onset of the phase separation, a diffusive model for evaporating solvent-solute mixture is developed, taking into account the physics of the upper gas layer and its interactions with the liquid. Note that we examine the system without considering the phase separation between components of the binary mixture. Our model predicts the initial conditions for which phase separation will happen in the system as well as for which no phase separation will ever take place.

As discussed in subsection 4.3.2, there are several different mechanisms for a ternary mixture that can lead to the different types of morphology (lamellar and lateral structures). In Chapter 6, which is a paper submitted in Colloids and Surfaces A: Physicochemical and Engineering Aspects, we present a detailed analysis regarding the competition between the evaporation and phase separation for creating lamellar and lateral structures, which has not been examined in the literature. Therefore, we focus on the phase separation induced by the evaporation of a binary mixture of partially miscible liquids consisting of a solvent and a solute in a two-dimensional thin film of infinite horizontal extent. To simplify our study, the hydrodynamic effects and convective flow are not modeled and each component of the binary mixture is assumed to be equally attracted by the surfaces (substrate and liquid-gas interface) with the same strength, leading to a diffuse interface perpendicular to the surface upon phase separation. A non-isothermal phase field model that describes the dynamics of phase separation is used and, in particular, we focus exclusively on the morphology evolution in the system. Having established this model, we then examine how the interplay between the evaporation rate and the phase separation forms different types of morphology (bulk, lateral, and lamellar structures). Finally, we present an

experimental set-up to display that our simulated morphologies closely resemble experimental trends.

4.5 References

[1] H. Tanaka, Viscoelastic phase separation, Journal of Physics: Condensed Matter, 12 (2000) R207.

[2] J. Berry, C.P. Brangwynne, M. Haataja, Physical principles of intracellular organization via active and passive phase transitions, Rep Prog Phys, 81 (2018) 046601.

[3] M. Dehghan, V. Mohammadi, The numerical solution of Cahn–Hilliard (CH) equation in one, two and three-dimensions via globally radial basis functions (GRBFs) and RBFs-differential quadrature (RBFs-DQ) methods, Engineering Analysis with Boundary Elements, 51 (2015) 74-100.

[4] A. Bertozzi, S. Esedolu, A. Gillette, Analysis of a Two-Scale Cahn–Hilliard Model for Binary Image Inpainting, Multiscale Modeling & Simulation, 6 (2007) 913-936.

[5] M. Burger, L. He, C.-B. Schönlieb, Cahn–Hilliard Inpainting and a Generalization for Grayvalue Images, SIAM Journal on Imaging Sciences, 2 (2009) 1129-1167.

[6] I. Capuzzo Dolcetta, S. Finzi Vita, R. March, Area-preserving curve-shortening flows: from phase separation to image processing, Interfaces and Free Boundaries, 4 (2002) 325-343.

[7] V. Cristini, X. Li, J.S. Lowengrub, S.M. Wise, Nonlinear simulations of solid tumor growth using a mixture model: invasion and branching, J Math Biol, 58 (2009) 723-763.

[8] G. Dennler, M.C. Scharber, C.J. Brabec, Polymer-Fullerene Bulk-Heterojunction Solar Cells, Advanced Materials, 21 (2009) 1323-1338.

[9] S. Günes, H. Neugebauer, N.S. Sariciftci, Conjugated polymer-based organic solar cells, Chemical reviews, 107 (2007) 1324-1338.

[10] F.-C. Chen, Spontaneous phase separation for efficient polymer solar cells, transportation, 1 (2008) 2.

[11] P. Peumans, S. Uchida, S.R. Forrest, Efficient bulk heterojunction photovoltaic cells using small-molecular-weight organic thin films, Materials for Sustainable Energy: A Collection of Peer-Reviewed Research

and Review Articles from Nature Publishing Group, World Scientific2011, pp. 94-98.

[12] M. Copetti, C.M. Elliott, Numerical analysis of the Cahn-Hilliard equation with a logarithmic free energy, Numerische Mathematik, 63 (1992) 39-65.

[13] J. Lowengrub, L. Truskinovsky, Quasi–incompressible Cahn–Hilliard fluids and topological transitions, Proceedings of the Royal Society of London. Series A: Mathematical, Physical and Engineering Sciences, 454 (1998) 2617-2654.

[14] J. Kim, A numerical method for the Cahn–Hilliard equation with a variable mobility, Communications in Nonlinear Science and Numerical Simulation, 12 (2007) 1560-1571.

[15] J. Shin, S. Kim, D. Lee, J. Kim, A parallel multigrid method of the Cahn–Hilliard equation, Computational materials science, 71 (2013) 89-96.

[16] J. Zhu, X. Lu, R. Balieu, N. Kringos, Modelling and numerical simulation of phase separation in polymer modified bitumen by phase-field method, Materials & design, 107 (2016) 322-332.

[17] R.A.L. Jones, Polymers at surfaces and interfaces, Cambridge University Press1999.

[18] A. Novick-Cohen, Chapter 4 The Cahn–Hilliard Equation, 2008, pp. 201-228.

[19] T.L. Tran, P.K. Chan, D. Rousseau, Morphology control in symmetric polymer blends using spinodal decomposition, Chemical Engineering Science, 60 (2005) 7153-7159.

[20] K. Binder, P. Fratzl, Spinodal decomposition, Phase transformations in materials, (2001) 409-480.

[21] H. Firoozmand, 2009. Microstructure and rheology of phase-separating solutions of gelatin and starch. , Ph.D. Thesis. University of Leeds.

[22] J.W. Cahn, J.E. Hilliard, Free energy of a nonuniform system. I. Interfacial free energy, The Journal of chemical physics, 28 (1958) 258-267.

[23] J.W. Cahn, Free energy of a nonuniform system. II. Thermodynamic basis, The Journal of chemical physics, 30 (1959) 1121-1124.

[24] R. Ball, R. Essery, Spinodal decomposition and pattern formation near surfaces, Journal of Physics: Condensed Matter, 2 (1990) 10303.

[25] J.F. Blowey, C.M. Elliott, The Cahn–Hilliard gradient theory for phase separation with non-smooth free energy Part I: Mathematical analysis, European Journal of Applied Mathematics, 2 (2009) 233-280.

[26] O. Wodo, B. Ganapathysubramanian, Computationally efficient solution to the Cahn–Hilliard equation: Adaptive implicit time schemes, mesh sensitivity analysis and the 3D isoperimetric problem, Journal of Computational Physics, 230 (2011) 6037-6060.

[27] P. Gera, D. Salac, The cahn-hilliard-cook equation on curved surfaces in three-dimensional space, arXiv preprint arXiv:1605.07108, (2016).

[28] D. Anders, K. Weinberg, Thermophoresis in binary blends, Mechanics of Materials, 47 (2012) 33-50.

[29] A. Khodadadian, M. Parvizi, M. Abbaszadeh, M. Dehghan, C. Heitzinger, A multilevel Monte Carlo finite element method for the stochastic Cahn–Hilliard–Cook equation, Computational Mechanics, 64 (2019) 937-949.

[30] R. Saxena, G.T. Caneba, Studies of spinodal decomposition in a ternary polymer-solvent-nonsolvent system, Polymer Engineering & Science, 42 (2002) 1019-1031.

[31] B. Zhou, A.C. Powell, Phase field simulations of early stage structure formation during immersion precipitation of polymeric membranes in 2D and 3D, Journal of Membrane Science, 268 (2006) 150-164.

[32] S. Tremaine, On the origin of irregular structure in Saturn's rings, The Astronomical Journal, 125 (2003) 894.

[33] E.B. Nauman, D.Q. He, Nonlinear diffusion and phase separation, Chemical Engineering Science, 56 (2001) 1999-2018.

[34] E. Petrishcheva, R. Abart, Exsolution by spinodal decomposition I: Evolution equation for binary mineral solutions with anisotropic interfacial energy, American Journal of Science, 309 (2009) 431-449.

[35] A. Novick-Cohen, L.A. Segel, Nonlinear aspects of the Cahn-Hilliard equation, Physica D: Nonlinear Phenomena, 10 (1984) 277-298.

[36] L.M. Robeson, Polymer blends, A Comprehensive Review, (2007).

[37] P.K. Chan, A.D. Rey, Computational analysis of spinodal decomposition dynamics in polymer solutions, Macromolecular theory and simulations, 4 (1995) 873-899.

[38] P.K. Chan, A.D. Rey, A numerical method for the nonlinear Cahn-Hilliard equation with nonperiodic boundary conditions, Computational materials science, 3 (1995) 377-392.

[39] T. Hashimoto, Dynamics in spinodal decomposition of polymer mixtures, Phase Transitions: A Multinational Journal, 12 (1988) 47-119.

[40] S. Asai, S. Majumdar, A. Gupta, K. Kargupta, S. Ganguly, Dynamics and pattern formation in thermally induced phase separation of polymer–solvent system, Computational Materials Science, 47 (2009) 193-205.

[41] J.T. Cabral, J.S. Higgins, N.A. Yerina, S.N. Magonov, Topography of phase-separated critical and off-critical polymer mixtures, Macromolecules, 35 (2002) 1941-1950.

[42] P.K. Chan, Effect of concentration gradient on the thermal-induced phase separation phenomenon in polymer solutions, Modelling and Simulation in Materials Science and Engineering, 14 (2006) 41.

[43] T.L. Tran, P.K. Chan, D. Rousseau, Morphology control in symmetric polymer blends using two-step phase separation, Computational Materials Science, 37 (2006) 328-335.

[44] T. Hashimoto, M. Itakura, H. Hasegawa, Late stage spinodal decomposition of a binary polymer mixture. I. Critical test of dynamical scaling on scattering function, The Journal of Chemical Physics, 85 (1986) 6118-6128.

[45] R.A. Jones, L.J. Norton, E.J. Kramer, F.S. Bates, P. Wiltzius, Surface-directed spinodal decomposition, Phys Rev Lett, 66 (1991) 1326-1329.

[46] G. Krausch, C.A. Dai, E.J. Kramer, F.S. Bates, Real space observation of dynamic scaling in a critical polymer mixture, Phys Rev Lett, 71 (1993) 3669-3672.

[47] S. Puri, K. Binder, Surface-directed spinodal decomposition: Phenomenology and numerical results, Phys Rev A, 46 (1992) R4487-R4489.

[48] M. Geoghegan, G. Krausch, Wetting at polymer surfaces and interfaces, Progress in Polymer Science, 28 (2003) 261-302.

[49] G. Krausch, Surface induced self assembly in thin polymer films, Materials Science and Engineering: R: Reports, 14 (1995) v-94.

[50] S. Puri, Surface-directed spinodal decomposition, Journal of Physics: Condensed Matter, 17 (2005) R101.

[51] K. Binder, S. Puri, S.K. Das, J. Horbach, Phase separation in confined geometries, Journal of Statistical Physics, 138 (2010) 51-84.

[52] J. Weng, W. Xia, J. Zhang, W. Chen, Q. Chen, Y. Jiang, Q. Cheng, G. Zhu, Dissipative particle dynamics simulation of phase separation in semiconducting/ferroelectric blend resistive films, Polymer, 116 (2017) 233-239.

[53] Y. Xia, R.H. Friend, Controlled phase separation of polyfluorene blends via inkjet printing, Macromolecules, 38 (2005) 6466-6471.

[54] E. Moons, Conjugated polymer blends: linking film morphology to performance of light emitting diodes and photodiodes, Journal of Physics: Condensed Matter, 14 (2002) 12235.

[55] P.K. Jaiswal, S. Puri, K. Binder, Phase separation in thin films: Effect of temperature gradients, EPL (Europhysics Letters), 103 (2013).

[56] P.K. Jaiswal, K. Binder, S. Puri, Formation of metastable structures by phase separation triggered by initial composition gradients in thin films, J Chem Phys, 137 (2012) 064704.

[57] P.K. Jaiswal, K. Binder, S. Puri, Phase separation of binary mixtures in thin films: Effects of an initial concentration gradient across the film, Phys Rev E Stat Nonlin Soft Matter Phys, 85 (2012) 041602.

[58] A.D. Dunbar, P. Mokarian-Tabari, A.J. Parnell, S.J. Martin, M.W. Skoda, R.A. Jones, A solution concentration dependent transition from self-stratification to lateral phase separation in spin-cast PS:d-PMMA thin films, Eur Phys J E Soft Matter, 31 (2010) 369-375.

[59] P. Mokarian-Tabari, M. Geoghegan, J.R. Howse, S.Y. Heriot, R.L. Thompson, R.A. Jones, Quantitative evaluation of evaporation rate during spin-coating of polymer blend films: Control of film structure through defined-atmosphere solvent-casting, Eur Phys J E Soft Matter, 33 (2010) 283-289.

[60] J. Jaczewska, A. Budkowski, A. Bernasik, E. Moons, J. Rysz, Polymer vs solvent diagram of film structures formed in spin-cast poly (3-alkylthiophene) blends, Macromolecules, 41 (2008) 4802-4810.

[61] S.Y. Heriot, R.A. Jones, An interfacial instability in a transient wetting layer leads to lateral phase separation in thin spin-cast polymer-blend films, Nat Mater, 4 (2005) 782-786.

[62] S. Ebbens, R. Hodgkinson, A.J. Parnell, A. Dunbar, S.J. Martin, P.D. Topham, N. Clarke, J.R. Howse, In situ imaging and height reconstruction

of phase separation processes in polymer blends during spin coating, ACS nano, 5 (2011) 5124-5131.

[63] K.-H. Wu, S.-Y. Lu, H.-L. Chen, Formation of parallel strips in thin films of polystyrene/poly (vinyl pyrrolidone) blends via spin coating on unpatterned substrates, Langmuir, 22 (2006) 8029-8035.

[64] O. Wodo, B. Ganapathysubramanian, Modeling morphology evolution during solvent-based fabrication of organic solar cells, Computational Materials Science, 55 (2012) 113-126.

[65] G.A. Zoumpouli, S.G. Yiantsios, Hydrodynamic effects on phase separation morphologies in evaporating thin films of polymer solutions, Physics of Fluids, 28 (2016).

[66] V. Negi, O. Wodo, J.J. van Franeker, R.A.J. Janssen, P.A. Bobbert, Simulating Phase Separation during Spin Coating of a Polymer–Fullerene Blend: A Joint Computational and Experimental Investigation, ACS Applied Energy Materials, 1 (2018) 725-735.

[67] C. Schaefer, P. van der Schoot, J.J. Michels, Structuring of polymer solutions upon solvent evaporation, Physical Review E, 91 (2015).

[68] P. Dayal, T. Kyu, Porous fiber formation in polymer-solvent system undergoing solvent evaporation, Journal of Applied Physics, 100 (2006).

Chapter 5

Paper3: Evaporation induced demixing in binary sessile drops [1]

Abstract

The interplay between evaporation and liquid–liquid phase separation (demixing) in binary sessile drops of partially miscible liquids is investigated. To determine the onset of the demixing phenomenon, a simple model is developed, which predicts a considerable temperature reduction (~20 °C) in the mixture due to evaporative cooling. Temperature reduction alongside with the change of composition lead to demixing in the mixtures. The model explains why a mixture at room temperature is able to demix, whilst the demixing upper critical temperature is at 6.3 °C. Five stages of the process are identified and explained. For the cases studied here, once the demixing begins through nucleation, a growing fingering pattern is formed at the contact line. The length of the fingers and the final area of deposition

[1] Hosein Sadafi, Ramin Rabani, Sam Dehaeck, Hatim Machrafi, Benoit Haut, Pierre Dauby, Pierre Colinet, Evaporation induced demixing in binary sessile drops, Colloids and Surfaces A: Physicochemical and Engineering Aspects, (2020) 125052.

increase with the initial concentration. Experimental tests were performed using a double telecentric setup.

Keywords: Phase separation, two-phase, demixing, sessile drop, evaporation

5.1 Introduction

Evaporation of droplets is an attractive topic due to its applications in industries such as coating [1], ink jet printing and colloidal particle synthesis [2, 3], food production and spray drying [4, 5], DNA sampling [6] and heat exchanger technologies [7, 8]. When a drop is not made of a pure liquid, the composition change induced by the evaporation can lead to other phase change processes. More generally, composition and/or temperature variations can indeed trigger transformation of liquid to gel [9, 10], glassy state [11, 12] or rigid solid [13, 14]. In certain conditions, the evaporation of solution drops is thus coupled with liquid–liquid phase separation (demixing phenomenon), a poorly investigated situation, which can be expected to result in a complex dynamics.

For a binary mixture of partially miscible liquids, the “concentration-temperature” phase diagram has two regions: a single homogeneous phase (stable), which is typically at high temperature and high/low concentration, and an unstable zone with phase separation, where at equilibrium, two liquid phases eventually coexist. The latter zone usually is located at low temperature and intermediate concentrations in the phase diagram. The curve separating the two regions is called the coexistence curve [15]. Demixing starts by nucleation and growth mechanism or by spinodal decomposition. As such, isolated droplets of solute-rich phase with a composition close to equilibrium initially appear, and then grow to yield an irregular two-phase structure [16]. Liquid-liquid phase separation within an initially stable sessile

drop of a binary mixture of partially miscible components may take place via two different routes: concentration change to reach a critical value (depending on temperature), or a decrease in temperature and consequently crossing the coexistence curve. Quenching polymer solutions into the two-phase region is a well-known mechanism, and is performed by cooling down thin films while the concentration of the solute is kept constant. This process leads to a spinodal decomposition [17, 18]. As a result, solute-rich droplets nucleate, grow and coalesce continuously to reduce the interfacial free energy [19]. During the evaporation of ternary Ouzo drops (water+oil+ethanol), the local concentration of the volatile component diminishes, and oil particles nucleate near the interface [20]. By tracking the oil microdroplets using a confocal microscope, Diddens et al. [21] concluded that the coalescence of oil microdrops creates a ring around the drop. As the density of oil is lower than water, the oil content covers the surface and delays the evaporation of water. While focusing on the dynamics of phase separation, there is limited information in literature on the onset of demixing phenomenon as well as the path to the unstable zone in the phase diagram.

On the other hand, mixing of two liquids with different surface tension, can generate solutal Marangoni effect, which might lead to self contraction [22, 23] or spreading [24]. Solutal Marangoni flow may also lead to segregation at the contact line. Li et al. [25] observed phase segregation at the contact line of sessile drops of an aqueous surfactant. Due to the small difference between the surface tensions of the two components in the mixture, the Marangoni flow was not strong enough to mix liquids and maintain a homogeneous state. Thus, the accumulated solute separated from the inner liquid, and formed a uniform ring at the contact line. In the presence of a thin extrinsic layer of water on the substrate, Troian et al. [26] observed outflow of liquid via multiple fingers from the drops of an aqueous solution of

surfactant. As the water film around the sessile drop had larger surface tension than the solution, the droplet was pulled outwards, yielding a fingering pattern at the contact line. Cachile et al. [27] studied the influence of concentration and relative humidity on the spreading of sessile drops of the binary mixture of Anapoe (surfactant) and ethylene glycol. While normal spreading was observed in dry air, above a certain relative humidity a dendritic pattern around a main drop was reported. In another study, they deposited the binary drops on a thin layer of the solvent spin coated on the substrate [28]. They showed that as the thickness of the layer increased, the fingering instability was weakened.

In order to rationalize the interesting observations during evaporation of binary mixtures, much effort was devoted over the last decade. Very recently, Rabani et al. [29] have presented a thermodynamic 1-D model of the evaporation process for a polymer solution in a thin film taking into account the physics of the upper gas layer and its interactions with the liquid phase. In another work, Mikishev et al. [30] have studied the effect of an insoluble surfactant on the thresholds of an evaporative Bénard-Marangoni instability in a liquid layer evaporating into air using one-sided model formulation, which means that only the lower liquid layer was modelled, while the upper gas layer is not described in detail and its influence on the liquid is introduced in a phenomenological way, by appropriate boundary conditions at the common interface. Rabani et al. [31] performed a linear stability analysis within a horizontal polymer solution layer, which evaporates into air. Due to the cooling effect, the surface of an evaporating fluid induces temperature gradients in the liquid. Moreover, when the liquid is a binary mixture of a polymer solution, evaporation also induces concentration gradients. Therefore, they showed that evaporation can generate thermo-solutal instabilities in liquid mixtures. In another work,

Doumenc et al. [32] carried out a linear analysis to determine the stability conditions of the thermal Rayleigh-Bénard-Marangoni problem in the drying a polymer solutions. In the case of evaporation and phase separation, Zoumpouli et al. [33] examined numerically the effects of hydrodynamics on phase separation morphologies developed during the evaporation of a thin film containing a mixture of two polymers and a solvent. Another analysis of an evaporating and demixing fluid layer is presented by Cummings et al. [34]. In their study, a thermodynamic derivation of the equations is proposed for a mixture of two polymers and a solvent.

The main objective of this article is to investigate the demixing phenomenon induced by the evaporation of sessile drops of binary mixtures of partially miscible liquids. While ternary mixtures have attracted many researchers [20, 21, 33, 34], to our knowledge, literature lacks fundamental studies on sessile drops of binary mixtures. This article tackles the physical process during evaporation and demixing of such droplets, and explains the conditions under which demixing may take place in them. The focus is on the case when a volatile liquid is mixed with another liquid of negligible volatility. In contrast to several studies that considered the phenomenon to be isothermal [35, 36], we take the change of temperature into account and its importance is investigated. The possibility of demixing via simultaneous change in temperature and concentration induced by evaporation is analyzed both experimentally and theoretically. Moreover, the complex interplay between the two phase change mechanisms (evaporation and demixing) at the gas-liquid interface is studied. Different stages of demixing and the role of initial concentration of the less volatile component on the spreading are investigated. The experimental results alongside with a theoretical model contribute to a better understanding of demixing phenomenon in evaporating sessile drops.

5.2 Method and materials

The spreading and evaporation of sessile drops of a binary mixture is studied. The components are partially miscible and there is a considerable gap between their volatility. The liquids studied in this work are n-hexane and 2-(2-Ethoxyethoxy)ethanol, also known as Diethylene Glycol Monoethyl Ether (DGME), used as purchased from Sigma–Aldrich company. Table 5-1 lists the physical properties of the liquids. The studied mixtures are insoluble in water, thus hygroscopicity effects are neglected in this research.

For partially miscible mixture of DGME and n-hexane, the mixed (stable) and demixed (unstable) zones are separated by the coexistence curve shown in Fig. 5-1-a [37]. This curve is a relationship between temperature and composition. The horizontal axis is the volumetric concentration of DGME, and the vertical axis is the temperature of the mixture. In Fig. 5-1-a, any state of hypothetically on the dotted line is at an equilibrium between points A (DGME-rich phase) and B (n-hexane-rich phase).

The droplets were deposited on 500 μm thick glass substrates. To observe the demixing induced by evaporation of the binary drops, a double telecentric system is used (Fig. 5-1-b). The advantage of this method is its sensitivity to the gradients of refractive index, which is useful here as the studied liquids have different refractive indices. The indices measured in this study are 1.375 and 1.427 for n-hexane and DGME, respectively. The setup contains two telecentric lenses with pinholes, a digital camera, two mirrors, a light source and a sample holder. In addition, to further investigate processes occurring inside the mixtures, an inverted manual microscope from Leica was used (not shown in Fig. 5-1-b).

Table 5-1. Physical properties of studied liquids.

Physical property	n-Hexane	DGME
Chemical formula	C_6H_{14}	$C_6H_{14}O_3$
Surface tension, (mN/m)	18.40	31.70
Molar mass, (g/mol)	86.18	134.17
Saturation pressure, (kPa)	15	0.02
Heat capacity, (J/(kgK))	2260	2168
Density, (kg/m^3)	659	1000
Kinematic viscosity, (m^2/s)	4.56e-7	3.85e-6
Latent heat of evaporation, (kJ/kg)	365	51
Thermal conductivity, (W/(mK))	0.124	0.173

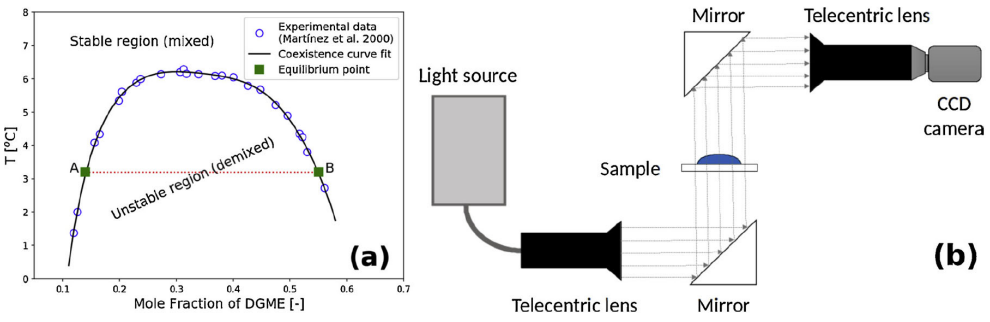

Fig. 5-1. a) Experimental coexistence curve of binary mixture of DGME and n-hexane [37], b) schematic of double telecentric system in the test rig; light source, telecentric lens, two mirrors, sample and sample holder, telecentric lens and CCD camera.

Surface cleaning significantly affects spreading and final pattern of the drops. Therefore, a plasma cleaner was used to remove all unwanted organic material from the substrates. To obtain a repeatable behavior, first the glass substrates were washed with ethanol and wiped using optical tissues. Next, a plasma cleaner was used for 1 min, and finally, the substrate was left to rest for 3 min. The tests were performed in different days with room temperature between 20 °C and 22 °C, relative humidity between 38% and 44%, and at atmospheric pressure. Each test was repeated at least four times.

5.3 Theoretical modeling

The purpose of the present section is to use numerical simulations to characterize qualitatively how the evaporation of a sessile drop of two partially miscible liquids, initially at room temperature (T_{amb}=294K), can lead to the demixing of the binary mixture. Because the contact angle of the sessile droplets considered in our experiments are small (measured value is approximately 6.5^{o}), the curvature of the interface remains small. Therefore, in a first modelling approach, it is a reasonable assumption to consider that the interface remains flat and the system can be described as a thin flat film. We do not either consider the pinning of the fluid at the contact line or the non-uniform evaporative flux across the drop surface and our model is assumed to describe the regions close to the center of the drop. The initial thickness of the DGME and n-hexane mixture is estimated by dividing a sessile drop volume by its initial wetting area, which gives 0.17 mm.

Our model considers a 1-D situation for which heat and mass transports are purely diffusive in the liquid phase and in the upper gas layer. We will also assume that only the “solvent” evaporates into air, while the total amount of “solute” in the liquid layer remains unchanged.

Table 5-1 shows that the density, heat capacity and heat conductivity of the 2 components of our mixture are not too different. For this reason, we will consider in our approach that the values of these properties are not substantially modified by the evaporation induced concentration changes in the mixture and can thus be considered as concentration independent during the time evolution of the system. We will also assume that the cooling effect of evaporation does not modify the thermophysical properties of the mixture. Under these hypotheses, the dimensional form of the temperature and concentration equations in the substrate, liquid and gas phases are given by [29, 38]:

$$\frac{\partial C}{\partial t} = D\frac{\partial^2 C}{\partial z^2} \tag{1}$$

and for temperature in the substrate, gas and liquid phases by [38]:

$$\frac{\partial T}{\partial t} = \kappa\frac{\partial^2 T}{\partial z^2} \tag{2}$$

where *T, c, D* and *κ* are the temperature, concentration, diffusion coefficient and the thermal diffusivity, respectively. The diffusion coefficient in the liquid binary mixture and in the upper gas (n-hexane vapor and air) are $4\times10^{-9}\frac{m^2}{s}$ (self diffusion) [39] and $2\times10^{-5}\frac{m^2}{s}$ (calculated using the procedure given by [40]), respectively. Due to the small amount of n-hexane in the upper gas, thermal diffusivity in this phase is assumed to be equal to that of air ($2.22\times10^{-5}\frac{m^2}{s}$) [15].

5.3.1 Boundary and initial conditions

At the bottom of the substrate where z=0 (see Fig. 5-2), that heat transfer through the impermeable wall is described by Newton's law of cooling. The corresponding boundary conditions can thus be written as [38]:

$$-\beta_s \frac{\partial T_s}{\partial z}\Big|_{z=0} = h_{amb}(T_{amb} - T_s|_{z=0}) \quad (3)$$

where β and h are the thermal conductivity and the heat transfer coefficient, and the subscripts "s" and "amb" stand for the substrate and ambient, respectively.

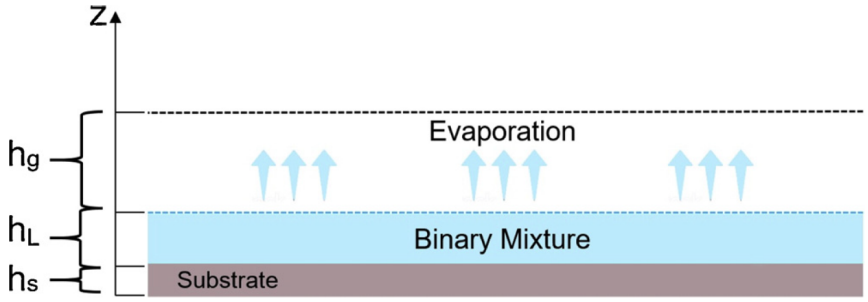

Fig. 5-2.Thin film assumption for the model; the binary solution is initially fully mixed. z direction is perpendicular to the substrate and solution.

At the substrate–liquid interface ($z=h_s$), the following conditions are considered for an impermeable substrate-liquid interface [38]:

$$T_s = T_l \quad , \beta_s \frac{\partial T_s}{\partial z} = \beta_l \frac{\partial T_l}{\partial z} \quad , \quad \frac{\partial c_l}{\partial z}=0 \quad (4)$$

where subscript "l" stands for the liquid phase. At the liquid-gas interface ($z=h_s+h_l$), the continuity of temperature imposes that $T_g=T_l$, where the subscript "g" corresponds to the gas phase. The energy conservation imposes also that [38]

$$JL = -\beta_l \frac{\partial T_l}{\partial z} + \beta_g \frac{\partial T_g}{\partial z} \quad (5)$$

where J and L are the evaporation rate and the latent heat of the solvent, respectively. Considering that the inert gas adsorption in the liquid is negligible, the mass flux J calculated for each phase at the interface will be [29]:

$$J = -\frac{\rho D}{1-c}\frac{\partial c}{\partial z} \quad (6)$$

where ρ is density. Subsequently, the decrease of the fluid layer thickness due to evaporation is described by [29]:

$$\frac{dh_l}{dt} = -\frac{J}{\rho_l} \tag{7}$$

To describe the local equilibrium at the liquid-gas interface, the Raoult's law [41] coupled with the Clausius-Clapeyron's law are used, which gives the following relations:

$$\frac{c_g}{c_g+(1-c_g)\delta sa} = \frac{c_l}{c_l+(1-c_l)\delta sst}\frac{p_{sat}|_{T_\Sigma}}{p_g}$$

$$p_{sat}|_{T_\Sigma} = p_{sat}|_{T_{amb}} e^{\left(-\frac{LM_{solvent}}{R}\left(\frac{1}{T_\Sigma}-\frac{1}{T_{amb}}\right)\right)} \tag{8}$$

$$\delta sa = \frac{M_{solvent}}{M_{air}} \qquad \delta ss = \frac{M_{solvent}}{M_{solute}}$$

where p_g is the total pressure of the gas at the interface, $p_{sat}\big|_{T_\Sigma}$, is the saturation pressure at the interface temperature, $p_{sat}|_{T_{amb}}$ is the saturation pressure of the pure solvent (at ambient temperature), $R \approx 8.31\frac{\mathrm{J}}{\mathrm{mol\,K}}$ is the universal gas constant, and the symbol Σ denotes the liquid-gas interface. $M_{solvent}, M_{solute}$, and M_{air} are the molecular weights of the solvent, the solute, and air, respectively.

At the top of the gas layer, the concentration and temperature are assumed to be constant. The associated boundary conditions take then the form:

$$c_g = c_{amb} \ , \ T_g = T_{amb} \tag{9}$$

Before evaporation starts, it is assumed that the liquid film is well mixed, corresponding to a spatially uniform distribution of solvent and solute in the liquid. The liquid film temperature is also initially uniform and fixed at then ambient temperature. Similarly, in the gas phase, the concentration of the

solvent and the temperature are also assumed uniform and equal to c_{amb} and T_{amb}, respectively. Then suddenly at t=0, the two phases are brought into contact and evaporation starts.

5.4 Results and discussion

5.4.1 Onset of demixing

The model presented in Section 5.3 has been solved using an explicit numerical method on a one-dimensional lattice. It should be noted that for each case computed, a mesh convergence test is performed, in which the number of points is gradually increased until the solution remains unchanged. Thus, 200 nodes in the substrate, 100 nodes in the liquid and 400 nodes in the gas and a fixed time increment $\Delta t = 10^{-5}$ s are used. The heat transfer coefficient between the liquid and the ambient is taken as 5 W/(m^2.K) [42]. The physical properties of liquid and gas phases and the substrate are given in Table 5-2.

Table 5-2. Physical properties of liquid and gas phases and substrate.

Physical property	**Mixture**	**Gas**	**Substrate**
$\rho(\frac{kg}{m^3})$	689	1.2	3000
$\beta(\frac{W}{m.K})$	0.124	2.6×10^{-2}	1
$\kappa(\frac{m^2}{s})$	8.23×10^{-8}	2.22×10^{-5}	4.16×10^{-7}
$D(\frac{m^2}{s})$	4×10^{-9}	2×10^{-5}	-
$L(\frac{j}{mol})$	31390	-	-

Evaporation is the key phenomenon driving phase separation and affects the region in the bulk where phase separation is initiated. When the liquid is placed on a glass substrate with a thickness 0.5 mm, the system is at ambient temperature. Because this temperature is above the upper critical temperature (6.3 °C [37]) of the coexistence curve, the binary liquid is initially perfectly mixed. However, the rapid evaporation induces a temperature decrease at the liquid–gas interface, together with a decrease of the solvent concentration in the upper part of the liquid layer. As a consequence, the representative point of the mixture at the interface rapidly approaches the coexistence curve, while the bottom of the layer remains at some distance from the miscibility gap. Thus, the phase separation occurs first in the upper part of the system. As time increases, phase separation subsequently propagates into the depth of the film. It is worth mentioning that we observe the same physical behavior in the experiment, where the phase separation is initiated at liquid–gas interface (see Section 5.4.2). The time evolution of the DGME mass fraction and liquid temperature at the liquid–gas interface are presented in Fig. 5-3-a for the particular case of a 7.5% DGME in n-hexane solution system evaporating into air, c_{amb}=0, and for T_{amb}=21 °C, 28 °C, and 35 °C. Eliminating the time between the evolution of temperature and concentration in Fig. 5-3-a gives the path in the phase-space of the interfacial temperature and the mass fraction. The paths corresponding to the 3 temperatures given above are described by the colored solid curves in Fig. 5-3-b. The square symbols indicate the initial state of the mixture while the circle symbols correspond to the crossing of the coexistence curve, i.e. to the onset of demixing close to the interface. Due to evaporation, the solvent mass fraction changes and a strong cooling occurs at the liquid–gas interface resulting in a fast temperature reduction. The two curves corresponding to the initial temperatures T_{amb}=21 °C and 28 °C indicate that the temperature reduction

and concentration changes make demixing possible, but for the other curve demixing does not happen, even if the temperature reduction is significant. Another interesting result can be obtained by determining a critical line in the phase space, which separates the initial conditions for which demixing will occur after some time, from those for which no demixing will ever take place. This critical line is represented in Fig. 5-3-b a red dashed curve.

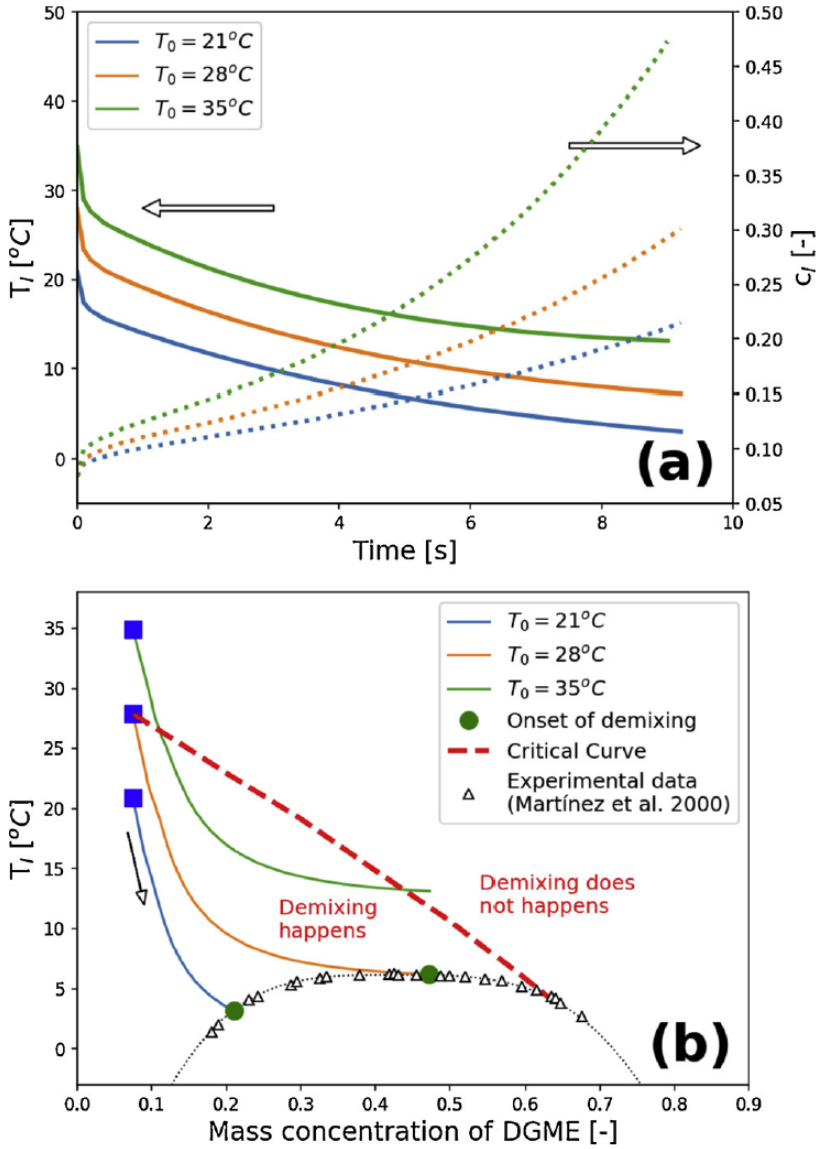

Fig. 5-3. a) Time evolution of temperature (solid lines) and DGME mass fraction (dotted lines) at liquid–gas interface, b) coexistence curve and variation of temperature and DGME mass faction at interface. Three initial temperatures of 21 °C, 28 °C and 35 °C are considered.

To highlight the importance of the substrate in the calculations, we now wonder what is the effect of neglecting its own thermal dynamics. In other words, the liquid film and air exchange heat through the substrate, while the top boundary conditions remain the same as above. Therefore Eq. (3) is replaced by the following:

$$-\beta_l \left.\frac{\partial T_l}{\partial z}\right|_{z=0} = h_{amb}(T_{amb} - \left. T_l\right|_{z=0}) \tag{10}$$

The green dash line curve in Fig. 5-4 corresponds to this case. Comparing the two critical curves shows that the thermal inertia of the substrate has a strong influence on the dynamics of the system. According to Fig. 5-4, demixing may take place even at temperatures as high as 340 K when the glass substrate is neglected. For the same initial concentration and considering the glass in the boundary conditions, the maximum temperature, where demixing may happen is 300 K. Thus, the glass substrate acts as a heat reservoir that prevents the liquid mixture from significant dropping of temperature.

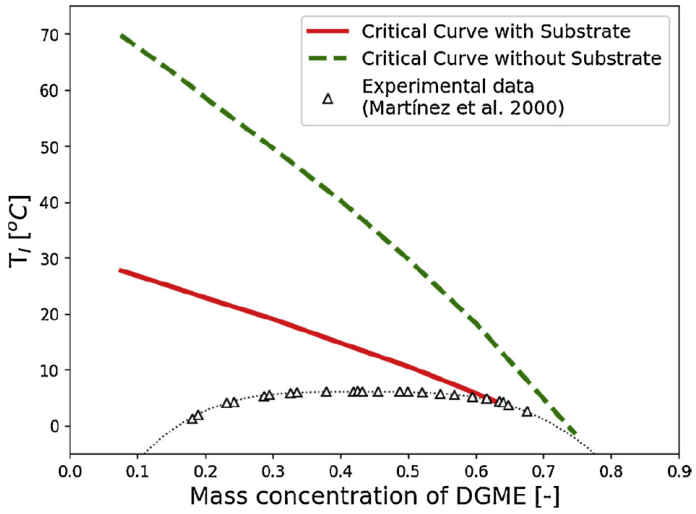

Fig. 5-4. Two critical curves; the limit where demixing occurs. The solid line shows the critical curve considering the glass substrate, and the dash line shows the critical curve neglecting the glass substrate.

5.4.2 Stages of demixing

Fig. 5-5 shows a sessile drop of a binary mixture of n-hexane and DGME (initial volume of 1.5 µl and $c_{0,\mathrm{DGME}}$=2%) on a glass substrate. Fig. 5-5-a corresponds to the time of deposition ($t^* = \frac{t}{t_{evap,h}} = 0$, where t is time and $t_{evap,h}$ is the evaporation time of n-hexane in the bulk liquid observed experimentally). The initial radius of the sessile drops shown in Fig. 5-5-a is 1.93 mm. Next, the first "fingers" around the contact line and isolated micro-drops within the main drop appear at t^*~0.05 (Fig. 5-5-b). Fig. 5-5-c shows the system at approximately half of the evaporation time of n-hexane (t^*~0.5). The micro-drops grow in size, coalesce, sediment and form macro-drops on the substrate. The radius of the macro-drop in the middle of the main drop on Fig. 5-5-c is approximately 166 µm. Meanwhile, the DGME content is continuously pushed outwards and form fingers around the contact line. Finally, Fig. 5-5-d shows the deposition of DGME on the substrate when the nhexane content in the n-hexane-rich phase is fully evaporated (t^*=1). After this time, the remaining DGME continues to evaporate. However, the evaporation time of DGME-rich residue is 1 to 2 orders of magnitude larger than that of n-hexane, depending on the initial concentration of DGME.

Because the evaporation rate of n-hexane at the contact line is higher than elsewhere in a sessile droplet, the concentration of DGME at this region is greater than that of n-hexane. As the surface tension is higher for DGME (see Table 5-1), there is a surface tension gradient towards this region, which generates a solutal Marangoni flow from the apex towards the contact line. It appears that the DGME-rich phase flows outwards in the form of fingers. As the evaporation of n-hexane proceeds, more DGME-rich liquid flows outwards, resulting in further growth of fingers at the contact line. Even

though looking similar, this mechanism is different from the observations of Troian et al. [26], where the liquid was pulled outwards and formed a fingering pattern at the contact line as a result of an external water film around the sessile drop.

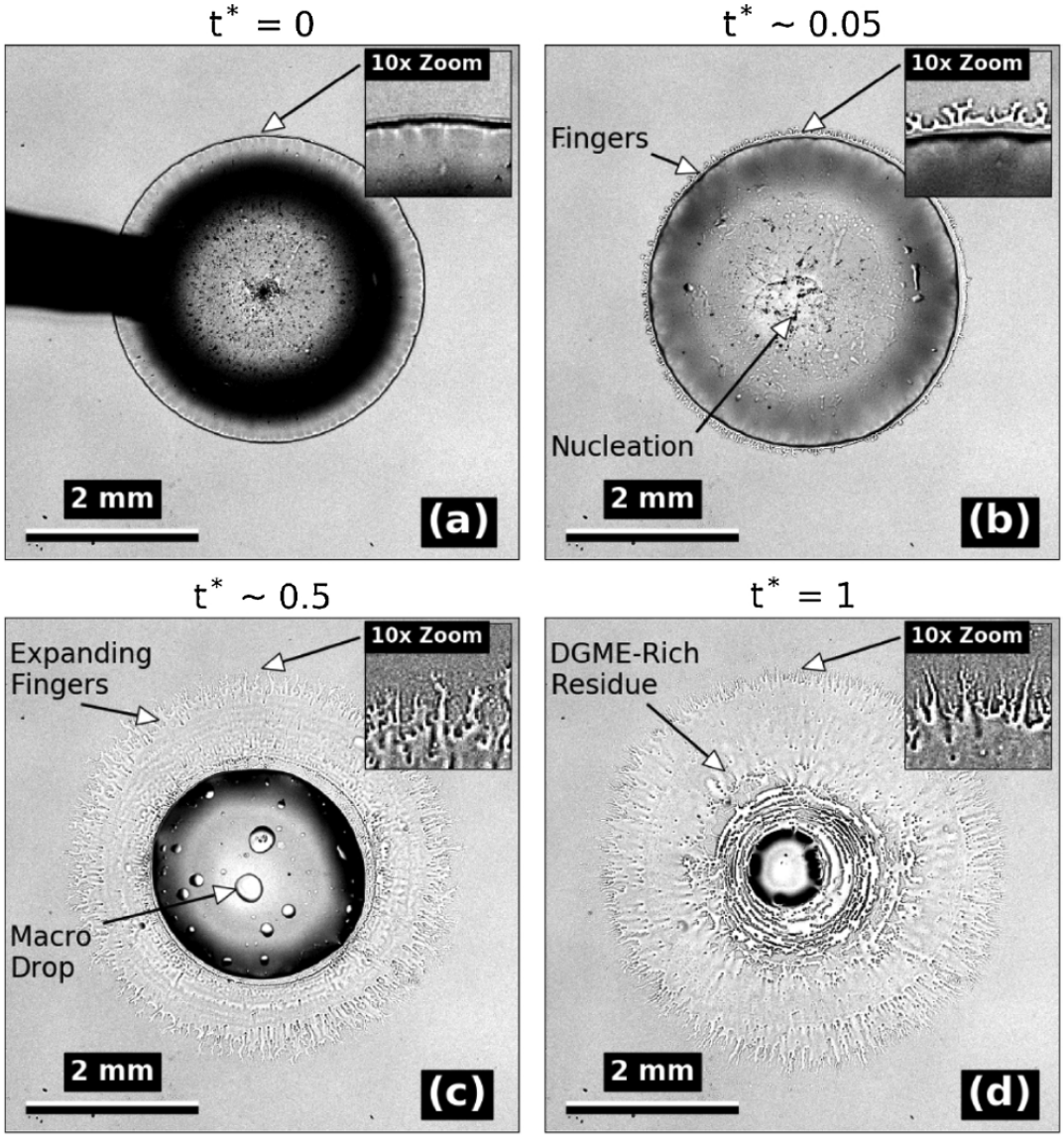

Fig. 5-5. Evaporation and demixing in a sessile binary drop of DGME and n-hexane with initial concentration of 2% by volume.

Based on the experimental results of this research using the inverted microscope and the double telecentric method, different stages of the process can be introduced as follows:

1. Pure evaporation: n-hexane evaporates at the contact line and drop surface (Fig. 5-6-a). The existence and duration of this stage depend on the initial concentration and temperature.

2. Nucleation: after reaching the coexistence curve, the local concentration of DGME at the contact line and drop surface increases, and first micro-drops nucleate (Fig. 5-6-b and b'). The dark lines in Fig. 5-6-b' are the boundaries of Benard-Marangoni cells. The fingering pattern at the contact line appears at this stage. It should be noted that Fig. 5-6-b' does not correspond exactly to the onset of nucleation, but shows a later point where the micro-drops are observable using our experimental device. This point may be a few seconds after the start of nucleation stage.

3. Coalescence: the DGME micro-drops coalesce and form larger isolated drops (macro-drops) within the main solution sessile drop (Fig. 5-6-c and c'). Fig. 5-6-c' shows a large drop (macro-drop) surrounded by a number of smaller drops (micro-drops).

4. Sedimentation and expanding fingers: as the macro-drops grow in size, they fall and sediment on the substrate (Fig. 5-6-d and d'). In Fig. 5-6-d' the large blur droplet that is out of focus is a falling macro-drop, while the plane on the surface including the micro-drops is in-focus. Meanwhile, due to surface tension difference at the contact line, the DGME content flows outwards and the fingers at the contact line expand due to solutal Marangoni effect (Fig. 5-6-d").

5. Emerging and drying: as the evaporation continues the thickness of the n-hexane-rich phase decreases and the isolated macro-drops emerge (Fig. 5-6-e and e'). Then, the n-hexane content in the mixture evaporates and only the DGME rich phase remains (Fig. 5-6-f and f'). Finally, the remaining DGME

dries out at a much longer time scale compared to the time of evaporation of n-hexane.

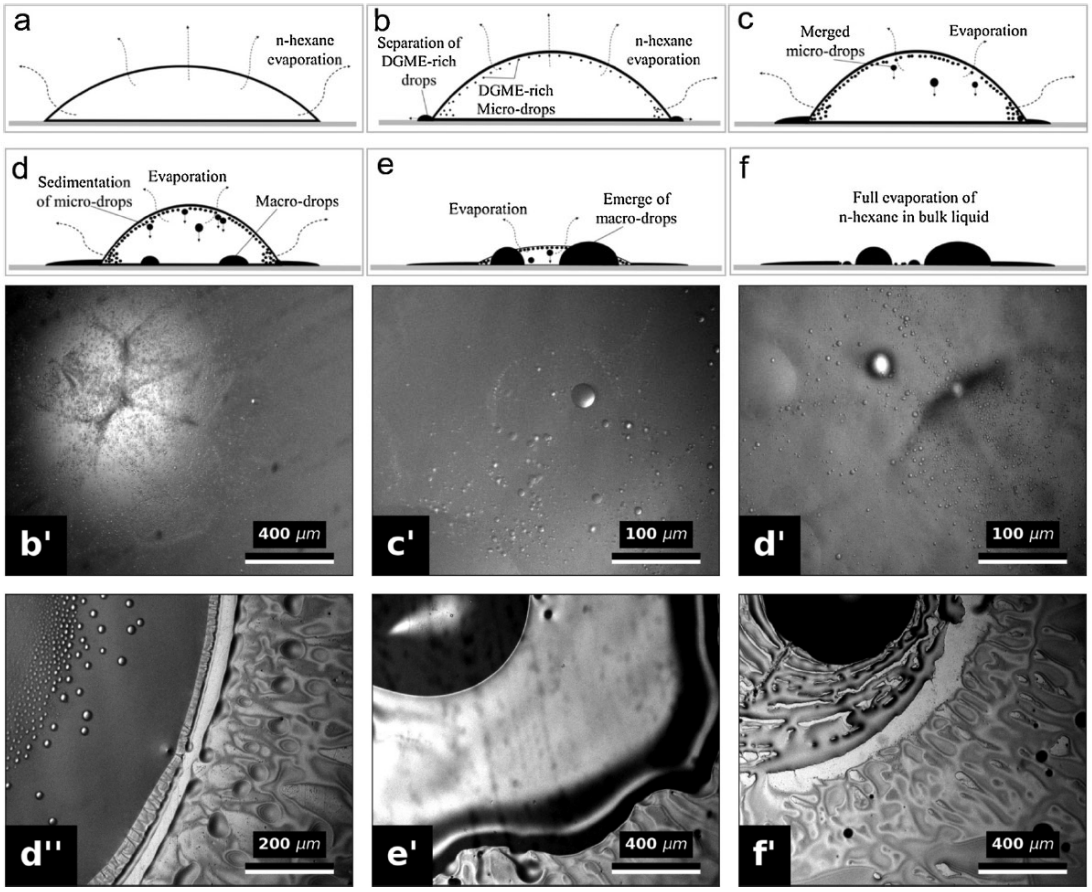

Fig. 5-6. Stages of demixing in an evaporating sessile binary drop of DGME and n-hexane (see text for details): (a) pure evaporation, (b, b') nucleation, (c, c') coalescence, (d, d', d") sedimentation and expanding fingers, (e, e') emergence of macro-drops from the bulk, (f, f') final pattern of deposition after full evaporation of n-hexane in the bulk mixture (snapshots b' to f' correspond to different experimental tests using the inverted microscope).

5.4.3 Influence of the initial concentration on spreading

Fig. 5-7 shows the final patterns (after full evaporation of n-hexane in the n-hexane-rich phase, t^* =1) for different initial concentrations of DGME. The initial volume of all drops ranged between 1.5 and 2 μl. As the initial concentration increases, the total area of deposition and the length of fingers

rise. To determine the total area the Canny edge detection method [43] is used.

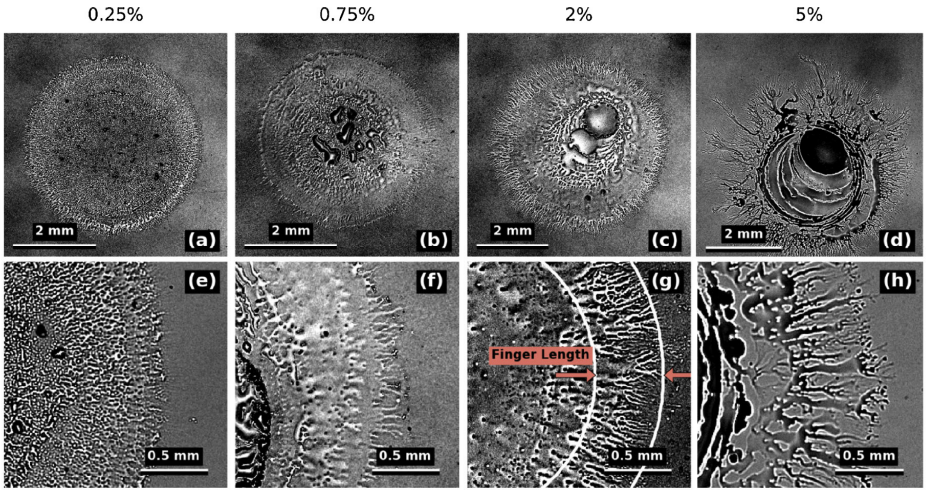

Fig. 5-7. Final pattern of sessile binary drops on glass substrate at t^* =1, where the n-hexane content in the bulk liquid is evaporated and a DGME-rich phase is deposited on the substrate; initial concentrations of DGME: 0.25%, 0.75%, 2% and 5%.

Fig. 5-8-a shows the normalized deposition area of sessile drops with different initial concentrations of DGME. The vertical axis is the normalized deposition area (deposition area divided by the wetted area of the sessile drop when fingers form). The horizontal axis is the normalized time, using the time when the total n-hexane content in the bulk liquid is evaporated. At this point, a still residue of DGME-rich liquid remains behind. The normalized total area of deposition increases with the initial concentration of DGME. As such, the final normal area of deposition for 3.5% initial concentration is approximately 1.9 times its initial wetting area, while this ratio is only 1.1 for 0.25% initial concentration of DGME. For the initial concentrations of up to 1%, it was often observed that before the n-hexane content is fully evaporated, the area of deposition slightly decreases after the initial dominant rise. One reason for this behavior is the evaporation of ultra thin fingers at the border of the deposition area. In contrast to the drops with larger initial concentrations, lack of a continuous outwards flow of DGME

prevents the fingers to expand. Fig. 5-8-b shows a linear trend between the normalized final area of deposition ($\frac{A_{\text{final}}}{A_0}$) at t^* =1 and the initial concentration of DGME binary sessile drops on glass substrates. The slope of the fitted line is 0.26.

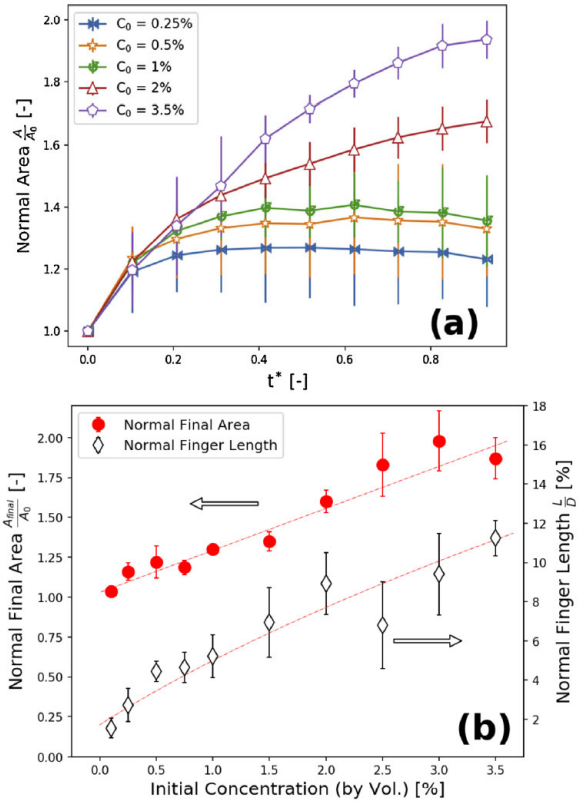

Fig. 5-8. (a) Normalized wetted area versus dimensionless time; the vertical axis is the deposition area divided by the wetted area, and time is non-dimensionalised using the time when the total n-hexane content in the bulk liquid is evaporated, (b) normal final area of deposition ($\frac{A_{\text{final}}}{A_0}$) and normal finger length versus initial concentration.

Each fingering pattern consists of a main interior area, where is the origin of fingers, and an exterior area corresponding the tips of the fingers. To determine the length of fingers, the two best circles fitted to the interior area and the maximum area of deposition are considered (Fig. 5-7-g). Fig. 5-8-b also shows the average length of fingers at t^* =1. The finger lengths are normalized against the diameter of the main interior area. The normalized finger length increases with the initial concentration of DGME. This is

mainly because for high concentrations of DGME, we expect a larger surface tension difference between the hexane-rich bulk liquid and the DGME-rich contact line. Therefore, the continuous Marangoni flow pushing the DGME-rich content outwards through the fingers is stronger. The finger growth loses its axisymmetrical behavior for concentrations larger than 3.5% (final deposited DGME-rich phase is not axisymmetric, see Fig. 5-7-d).

5.5 Conclusion

The evaporation dynamics of a binary mixture of partially miscible liquids is investigated and characterized. Considering sessile drops of such mixtures, five stages of the phenomenon are identified including: pure evaporation, nucleation, and coalescence, sedimentation, expanding fingers, emerging and drying. As the solute has higher surface tension and density than the volatile solvent, the fingering pattern develops at the contact line, while demixing proceeds through nucleation, growth and coalescence. It is shown that the total area of deposition and the finger length increase with the initial concentration. We have also proposed a simple numerical model for the very first stages of the evolution of the system. This model has allowed understanding the large temperature decrease observed in the experiments and has also emphasized that for some initial conditions the mixture can never reach the miscibility gap. The effect of the change of temperature due to evaporation seemed to be quite significant and the temperature drop due to evaporation, calculated by the model, explains why a mixture at 21 °C is able to demix, whilst the demixing upper critical temperature is at 6.3 °C.

Acknowledgments

The authors gratefully thank financial support from European Space Agency (ESA) and the Belgian Federal Science Policy Office (BELSPO) through PRODEX and IAP 7/38 μMAST contracts and Fonds de la Recherche Scientifique – F.N.R.S. (PDR - DITRASOL contract T.0123.16 and Research Director position of PC).

5.6 References

[1] C. Koller, J. Ramm, S. Kolozsvári, J. Paulitsch, P. Mayrhofer, Role of droplets and iron on the phase formation of arc evaporated Al–Cr-oxide coatings, Surface and Coatings Technology, 276 (2015) 735-742.

[2] J. Park, J. Moon, Control of colloidal particle deposit patterns within picoliter droplets ejected by ink-jet printing, Langmuir, 22 (2006) 3506-3513.

[3] B. Sobac, Z. Larbi, P. Colinet, B. Haut, Mathematical modeling of the drying of a spherical colloidal drop, Colloids and Surfaces A: Physicochemical and Engineering Aspects, 576 (2019) 110-122.

[4] M. Farid, A new approach to modelling of single droplet drying, Chemical Engineering Science, 58 (2003) 2985-2993.

[5] F. Debaste, V. Halloin, L. Bossart, B. Haut, A new modeling approach for the prediction of yeast drying rates in fluidized beds, Journal of food engineering, 84 (2008) 335-347.

[6] W. Wang, J. Lin, D.C. Schwartz, Scanning force microscopy of DNA molecules elongated by convective fluid flow in an evaporating droplet, Biophysical journal, 75 (1998) 513-520.

[7] M. Sadafi, I. Jahn, K. Hooman, Cooling performance of solid containing water for spray assisted dry cooling towers, Energy Conversion and Management, 91 (2015) 158-167.

[8] M. Sadafi, J. Ruiz, M. Lucas, I. Jahn, K. Hooman, Numerical and experimental study on a single cone saline water spray in a wind tunnel, International Journal of Thermal Sciences, 120 (2017) 190-202.

[9] A. Oppermann, M. Renssen, A. Schuch, M. Stieger, E. Scholten, Effect of gelation of inner dispersed phase on stability of (w1/o/w2) multiple emulsions, Food Hydrocolloids, 48 (2015) 17-26.

[10] T.P. Lodge, A.L. Maxwell, J.R. Lott, P.W. Schmidt, J.W. McAllister, S. Morozova, F.S. Bates, Y. Li, R.L. Sammler, Gelation, phase separation, and fibril formation in aqueous hydroxypropylmethylcellulose solutions, Biomacromolecules, 19 (2018) 816-824.

[11] J.L. Keddie, R.A. Jones, R.A. Cory, Size-dependent depression of the glass transition temperature in polymer films, EPL (Europhysics Letters), 27 (1994) 59.

[12] F. Kremer, M. Tress, E.U. Mapesa, Glassy dynamics and glass transition in nanometric layers and films: A silver lining on the horizon, Journal of Non-Crystalline Solids, 407 (2015) 277-283.

[13] M. Sadafi, I. Jahn, A. Stilgoe, K. Hooman, Theoretical and experimental studies on a solid containing water droplet, International Journal of Heat and Mass Transfer, 78 (2014) 25-33.

[14] M. Sadafi, I. Jahn, A. Stilgoe, K. Hooman, A theoretical model with experimental verification for heat and mass transfer of saline water droplets, International Journal of Heat and Mass Transfer, 81 (2015) 1-9.

[15] P. Atkins, J. de Paula, Physical Chemistry, Volume 1: Thermodynamics and Kinetics, Macmillan Higher Education2016.

[16] T. Inoue, Reaction-induced phase decomposition in polymer blends, Progress in Polymer Science, 20 (1995) 119-153.

[17] C.K. Haas, J.M. Torkelson, Two-dimensional coarsening and phase separation in thin polymer solution films, Physical Review E, 55 (1997) 3191.

[18] S. Jeon, H. Karkhanechi, L.-F. Fang, L. Cheng, T. Ono, R. Nakamura, H. Matsuyama, Novel preparation and fundamental characterization of

polyamide 6 self-supporting hollow fiber membranes via thermally induced phase separation (TIPS), Journal of Membrane Science, 546 (2018) 1-14.

[19] C. Martinez-Perez, P. Garcia-Casillas, P. Romero, C. Juárez, C.A. Martínez-Villafañe, A.D. Moller, J. Romero-García, Porous biodegradable polyurethane scaffolds prepared by thermally induced phase separation, Journal of Advanced Materials (Special Edition), 1 (2006) 5-11.

[20] H. Tan, C. Diddens, P. Lv, J.G. Kuerten, X. Zhang, D. Lohse, Evaporation-triggered microdroplet nucleation and the four life phases of an evaporating Ouzo drop, Proceedings of the National Academy of Sciences, 113 (2016) 8642-8647.

[21] C. Diddens, H. Tan, P. Lv, M. Versluis, J. Kuerten, X. Zhang, D. Lohse, Evaporating pure, binary and ternary droplets: thermal effects and axial symmetry breaking, arXiv preprint arXiv:1706.06874, (2017).

[22] A. Benusiglio, N.J. Cira, M. Prakash, Two-component marangoni-contracted droplets: friction and shape, Soft matter, 14 (2018) 7724-7730.

[23] Y. Tsoumpas, S. Dehaeck, A. Rednikov, P. Colinet, Effect of Marangoni flows on the shape of thin sessile droplets evaporating into air, Langmuir, 31 (2015) 13334-13340.

[24] L. Keiser, H. Bense, P. Colinet, J. Bico, E. Reyssat, Marangoni bursting: evaporation-induced emulsification of binary mixtures on a liquid layer, Physical review letters, 118 (2017) 074504.

[25] Y. Li, P. Lv, C. Diddens, H. Tan, H. Wijshoff, M. Versluis, D. Lohse, Evaporation-triggered segregation of sessile binary droplets, Physical review letters, 120 (2018) 224501.

[26] S. Troian, X. Wu, S. Safran, Fingering instability in thin wetting films, Physical Review Letters, 62 (1989) 1496.

[27] M. Cachile, A. Cazabat, S. Bardon, M. Valignat, F. Vandenbrouck, Spontaneous spreading of surfactant solutions on hydrophilic surfaces, Colloids and Surfaces A: Physicochemical and Engineering Aspects, 159 (1999) 47-56.

[28] M. Cachile, M. Schneemilch, A. Hamraoui, A. Cazabat, Films driven by surface tension gradients, Advances in colloid and interface science, 96 (2002) 59-74.

[29] R. Rabani, H. Machrafi, P. Dauby, Effect of including a gas layer on the gel formation process during the drying of a polymer solution, The European Physical Journal E, 40 (2017) 89.

[30] A.B. Mikishev, A.Y. Rednikov, P. Colinet, Impact of an insoluble surfactant on the thresholds of evaporative Bénard-Marangoni instability under air, The European Physical Journal E, 40 (2017) 90.

[31] R. Rabani, H. Machrafi, P. Dauby, Influence of Composition Dependent Diffusion Coefficient, Viscosity and Relaxation Time on Evaporative Rayleigh-Bénard-Marangoni Instabilities Induced by Solvent Evaporation in a Polymer Solution, Microgravity Science and Technology, 31 (2019) 615-628.

[32] F. Doumenc, T. Boeck, B. Guerrier, M. Rossi, Transient Rayleigh-Bénard-Marangoni convection due to evaporation: a linear non-normal stability analysis, arXiv preprint arXiv:0911.2088, (2009).

[33] G.A. Zoumpouli, S.G. Yiantsios, Hydrodynamic effects on phase separation morphologies in evaporating thin films of polymer solutions, Physics of Fluids, 28 (2016) 082108.

[34] J. Cummings, J.S. Lowengrub, B.G. Sumpter, S.M. Wise, R. Kumar, Modeling solvent evaporation during thin film formation in phase separating polymer mixtures, Soft Matter, 14 (2018) 1833-1846.

[35] C. Schaefer, P. van der Schoot, J.J. Michels, Structuring of polymer solutions upon solvent evaporation, Physical Review E, 91 (2015) 022602.

[36] P. Dayal, T. Kyu, Porous fiber formation in polymer-solvent system undergoing solvent evaporation, Journal of applied physics, 100 (2006) 043512.

[37] R. Martínez, J.A. Gonzalez, I. Garcia de la Fuente, J.C. Cobos, Thermodynamic properties of n-alkoxyethanols+ organic solvent mixtures. XIV. Liquid− liquid equilibria of systems containing 2-(2-ethoxyethoxy)

ethanol and selected alkanes, Journal of Chemical & Engineering Data, 45 (2000) 1036-1039.

[38] P. Colinet, J.C. Legros, M.G. Velarde, Nonlinear dynamics of surface-tension-driven instabilities, Wiley-vch Berlin2001.

[39] Dortmund Data Bank, www.ddbst.com.

[40] P. Talbot, B. Sobac, A. Rednikov, P. Colinet, B. Haut, Thermal transients during the evaporation of a spherical liquid drop, International Journal of Heat and Mass Transfer, 97 (2016) 803-817.

[41] F.-M. Raoult, Loi générale des tensions de vapeur des dissolvants, CR Hebd. Seances Acad. Sci, 104 (1887) 1430-1433.

[42] G. Toussaint, H. Bodiguel, F. Doumenc, B. Guerrier, C. Allain, Experimental characterization of buoyancy-and surface tension-driven convection during the drying of a polymer solution, International Journal of Heat and Mass Transfer, 51 (2008) 4228-4237.

[43] J. Canny, A computational approach to edge detection, IEEE Transactions on pattern analysis and machine intelligence, (1986) 679-698.

Chapter 6

Paper4: Morphology of phase separation during the evaporation of a thin film of a partially miscible binary mixture [1]

Abstract

In this paper, we develop numerical and experimental analyses of the different morphologies that can be created by the phase separation phenomena that are induced by solvent evaporation in a thin film of a partially miscible binary mixture. Disregarding hydrodynamic effects, the Cahn–Hilliard–Cook and temperature equations are used to describe the thermodynamics of non-isothermal phase separation in 2D thin film. Numerical simulations are performed to investigate the interplay between evaporation and phase separation and we examine the effect of several parameters such as the initial thickness of the thin film, or the initial temperature and concentration, on the morphology evolution. Interestingly,

[1] Ramin Rabani, Hosein Sadafi, Hatim Machrafi, Monavar Abbasi, Benoit Haut, Pierre Dauby, Morphology of phase separation during the evaporation of a thin film of a partially miscible binary mixture, Colloids and Surfaces A: Physicochemical and Engineering Aspects (Submitted).

the results show that for moderate evaporation rate, the spinodal instability takes place only close to the evaporating interface and that a lateral structure is formed. For stronger evaporation, the spinodal instability does not occur at the liquid-gas interface and a lamellar structure is created. Our experiments are carried out in a Hele-Shaw cell and nicely confirm the numerical results.

Keywords: thin film, partially miscible binary mixture, evaporation, phase separation morphology, lateral and lamellar structures, coalescence

6.1 Introduction

6.1.1 Physical concept of phase separation

Phase separation takes place in many industrial processes related to semiconductors [1, 2], binary alloys [3, 4], polymer blends [5, 6], … For a binary mixture of partially miscible liquids consisting of a solvent and a solute, demixing is associated with a "miscibility gap" in the phase diagram of the mixture (see Fig. 6-1). This phase diagram has three regions: the stable (mixed), metastable, and unstable (demixed) ones. The phase diagram is defined by two curves: the binodal and the spinodal curves. The binodal curve defines the boundary between the stable and the metastable regions while the spinodal curve is the boundary between the metastable and the unstable regions [7, 8]. When the representative point of a mixture crosses one of these curves and enters either in the metastable or in the unstable region, phase separation occurs. It means that the solution separates to create two phases of different compositions. In the metastable region, phase separation occurs through nucleation and growth, while spinodal decomposition happens in the unstable region [7, 8]. When a mixture is suddenly quenched below the spinodal curve, the phase separation

mechanism may be divided into the following three stages: (a) early stage, (b) intermediate stage, and (c) late stage [9-11]. In the early stage of the spinodal decomposition, the concentration fluctuations are small and weakly nonlinear. Therefore, the characteristic wavelength of the domain's size does not change with time while the amplitude of the concentration fluctuations increases with time. The phase separation at this stage can be described by the linearized Cahn–Hilliard equation [9-13]. In the intermediate stage, the concentration fluctuations and the characteristic wavelength both increase with time. The nonlinear effects on the time evolution of the concentration fluctuations become increasingly important in this stage. As a consequence, growth of the concentration fluctuations is governed by a nonlinear time evolution equation [9-11]. In the late stage, the equilibrium concentrations are reached and the domain size is coarsening without a change in concentration, whereas the wavelength increases with time due to coarsening [9-11].

The kinetics of phase separation by demixing has been the focus of many theoretical and experimental studies [14-17]. In the absence of surface effects, the phase separation of a binary mixture in a bulk can typically generate two types of morphologies according to the average concentration. If the concentration of the binary mixture is not the critical concentration (i.e. if the solvent volume fraction $\emptyset_{sl} \neq 0.5$, see Fig. 6-1), a droplet-type morphology forms [18-20]. On the contrary, an interconnected-type morphology forms for the critical concentration [18-20]. The presence of a surface may also alter the morphology type and preferential wetting of the surface by one of the components becomes a relevant parameter [21-23].

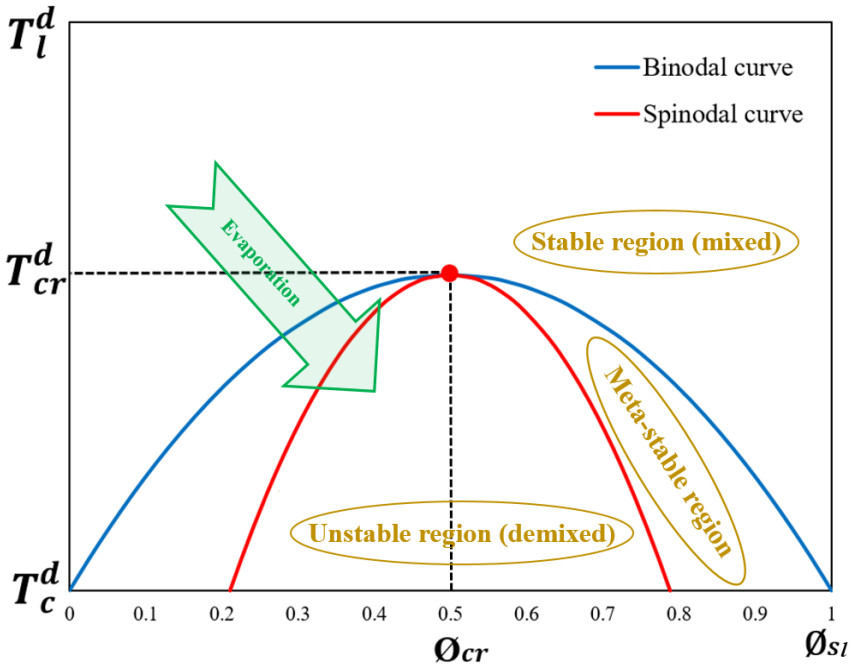

Fig. 6-1. Binodal and spinodal curves in a phase diagram. $\emptyset_{sl}$ is the solute volume fraction. T_l^d, T_{cr}^d, and T_c^d are respectively the liquid phase temperature, the critical temperature, and the minimum temperature, which corresponds to $\emptyset_{sl} = 0$ and $\emptyset_{sl} = 1$ in the binodal curve.

Both temperature and concentration can be changed in the phase diagram to induce phase separation (see Fig. 6-1). Phase separation induced by a decrease in temperature is known as thermally-induced phase separation and is usually performed by cooling down the binary mixture, while the mean concentration of the mixture remains constant [24-26]. Phase separation can also be induced by a change in the concentrations of the different components of a mixture. This process can be performed by directly adding some components in the mixture [27, 28]. Evaporation can also induce concentration changes in the system, and this phenomenon is the object of the present paper. Note however that in this situation, temperature changes are also expected because evaporation induces a cooling of the system.

6.1.2 Phase separation in a thin evaporating film

The evaporation of thin films has attracted many interests because it commonly happens in natural phenomena and in many industrial processes such as drying of paint films [29-31] ink-jet printing [32-34], packaging [35, 36], heat exchangers [37, 38], and fabrication of solar cells [39, 40]. When a thin film consists of a binary mixture of partially miscible liquids, either a temperature gradient [41], or a concentration gradient [42], or both as in the case of evaporation [43], can induce demixing. The situation of evaporation, which is analyzed in the present paper, provides an example of phase separation induced by phase change. The interplay between surface and bulk behavior for the phase separation in a thin film can lead to different types of morphologies, such as the lateral and lamellar structures [44-46]. The lamellar structure is characterized by a horizontal homogeneity and the separated phases form superposed layers within the film. On the contrary, the lateral structure consists of arrangements of columns, or vertical stripes of the separated components. These morphologies occur when altering the system characteristics such as the composition [47], or changes in the external conditions including the wetting behavior on the surfaces [48] and the temperature [24]. These conditions directly control the formation and the evolution of the demixing process and thus create the different types of morphologies.

Evaporation induced phase separation in a partially miscible mixture has received rather little attention so far in the literature. Zoumpouli et al. [49] performed a numerical analysis of the phase separation morphology developed in a thin film containing a volatile solvent and two dissolved polymers. They modeled the evaporation by a purely empirical model. They observed that, for a system with preferential wetting, diffusion alone favors

a lamellar structure for the separated phases in the film. However, hydrodynamic effects may deform and transform the lamellar structure to a lateral structure. Negi et al. [50] developed three-dimensional simulations of evaporation-induced phase separation in a polymer solution. They observed that phase separation for fast evaporation rates proceeds in an inhomogeneous manner, with droplets appearing first at the top of the film. For a slow evaporation rate, the solvent has enough time to diffuse from the bulk and, thus, phase separation occurs uniformly in the bulk. Another analysis of an evaporating and demixing fluid layer is provided by Cummings et al. [51]. In this study, a thermodynamic deduction of the equations is proposed for a mixture of two polymers and a solvent, but the system is assumed isothermal. Some ad hoc coefficients are also introduced to describe evaporation. Dayal and Kyu [52] examined numerically the competition between the dynamics of phase separation and the rate of solvent evaporation and its effect on the morphology of a single polymer-solvent in a cylindrical geometry. They observed a skin layer of polymer at the outer surface of the cylindrical fiber for fast evaporation, while a porous structure was obtained for slow evaporation. Another study of an evaporating and isothermal phase separation for a binary mixture consisting of a single polymer and solvent is provided by Schaefer et al. [53]. In this study, the authors examined theoretically and numerically the impact of the solvent evaporation on the dynamics of the isothermal phase separation of a binary mixture in order to explain how solvent evaporation affects the appearance and development of structural length scales. They solved their model only in the limit of small Biot numbers (expressing the ratio between the rate of external mass transport by evaporation and internal mass transport by diffusion), where the system is uniform along the height of the thin film. In the early stages of demixing, they observed a spinodal length scale that

decreases with time under the influence of the solvent evaporation. They also achieved a good agreement between the theoretical model and numerical simulations for the early stages of demixing.

According to our knowledge and to the literature review presented above, demixing in the evaporation process of a thin film of a partially miscible binary mixture has been mainly studied in the case of an isothermal situation. There is limited information in the literature on non-isothermal demixing induced by evaporation, in particular on the path to the unstable zone in the phase diagram. In our previous work [43], we analyzed experimentally and theoretically the evaporation induced demixing in sessile drops of binary mixtures of partially miscible liquids. We proposed a simple model with the aim to analyze the influence of the initial conditions on the possible onset of demixing (but we did not model the demixing phase separation itself). Notably, we showed that demixing can be induced even if the initial temperature of the system is above the critical temperature, due to the cooling generated by its evaporation.

6.1.3 Objective of this work

The main purpose of the present study is to analyze the demixing phenomenon induced by the evaporation of a volatile solvent in a two-dimensional thin film of a partially miscible binary mixture consisting of a solvent and a solute (the solute is assumed nonvolatile). The model is based on a non-isothermal phase field approach to describe the behavior of phase separation in a multicomponent system. Hydrodynamics effects and convective flow are not modeled in the present paper and will be considered in a future study. Therefore, we focus solely on the diffusive dynamics and the morphology evolution in the system. We present and solve a numerical model based on the Cahn–Hilliard–Cook and heat transfer equations. We

perform numerical simulations to examine the competition between the evaporation and the phase separation and we analyze the role of the initial temperature, the initial solvent concentration, and the initial thickness of the film. Additionally, we describe an experimental set-up that has been used to show that the trends regarding the morphology highlighted by the numerical simulations can also be observed experimentally.

6.2 Methods and model formulation

In this section, we describe the phase field model and the heat transfer equation used to simulate the morphology of phase separation during the evaporation of a thin film of a partially miscible binary mixture of solvent-solute, of which solely the solvent evaporates into an inert gas, air (Fig. 6-2). As discussed in the introduction, convection is disregarded in the present study. A 2D rectangular domain is considered, with x the horizontal coordinate and z the vertical one.

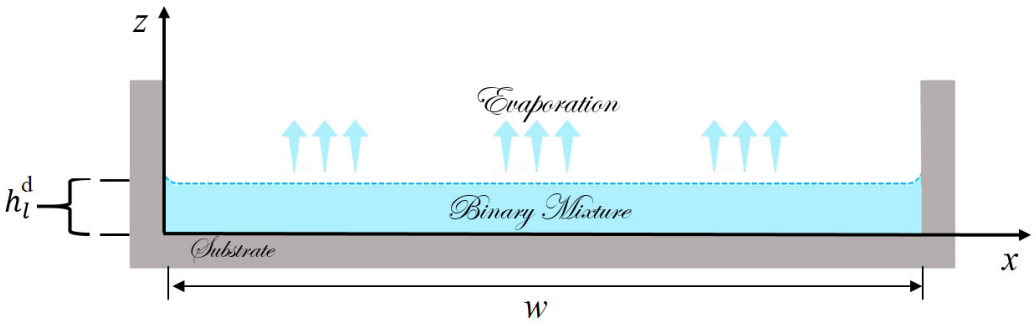

Fig. 6-2. Schematic of the studied configuration.

6.2.1 Order parameters

The local composition of the binary mixture can be described by the mass fractions of the components C_{sv} and C_{sl} ($C_{\mathrm{sl}} = 1 - C_{\mathrm{sv}}$). The subscripts "$sv$" and "$sl$" stand for the solvent and the solute, respectively. The local

composition can also be expressed in terms of the solvent volume fraction $\emptyset_{\mathrm{sv}}$ with

$$C_{\mathrm{sv}} = \frac{\rho_{\mathrm{sv}}\,\emptyset_{\mathrm{sv}}}{\rho_{\mathrm{sv}}\,\emptyset_{\mathrm{sv}} + \rho_{\mathrm{sl}}(1-\emptyset_{\mathrm{sv}})} \tag{1}$$

where ρ_{sv} and ρ_{sl} are the densities of the solvent and the solute, respectively. Since, in our system, we assume that the densities of solvent and solute are not too different, C and $\emptyset$ are almost identical. Therefore, all equations are presented in this paper in terms of the volume fraction $\emptyset$.

6.2.2 Free energy and governing equations

General theories on phase field models have been developed in several papers (see for instance [54-57]) and we recall here the basic ingredients only. The free energy density F of a non-isothermal mixture of two fluids can be written in the Ginzburg-Landau form:

$$F\left(\emptyset_{\mathrm{sv}}, \nabla\emptyset_{\mathrm{sv}}, T_l^d\right) = f_0(\emptyset_{\mathrm{sv}}, T_l^d) + \frac{1}{2}\varepsilon^2|\nabla\emptyset_{\mathrm{sv}}|^2 \tag{2}$$

with T_l^d the local liquid phase temperature. Note that the superscript "d" indicates that the quantity is dimensional. The first term in Eq. (2) is called the potential function and it depends on the local concentration and temperature. The interfacial energy, described by the second term in Eq. (2), depends on the concentration gradient and ε, the capillary width characterizing the thickness of the diffuse interface (interfacial thickness) between the two phases [58-60]. It is worth mentioning that the interfacial thickness may range from 10^{-9} m up to 10^{-7} m for two partially miscible substances [61-63].

We need a double-well potential function in order to describe the possible separation of the binary mixture into two distinct phases. For convenience, we use the simplest way to describe this double-well potential function and

introduce a fourth order polynomial with respect to $\emptyset_{\mathrm{sv}}$, taking the following form [64, 65]:

$$f_0(\emptyset_{\mathrm{sv}},T_l^d) = \frac{1}{4}((2\emptyset_{\mathrm{sv}} - 1)^2 + (\frac{T_l^d - T_{cr}^d}{T_{cr}^d - T_c^d}))^2 \tag{3}$$

where T_{cr}^d, and T_c^d are the critical and the minimum temperature, respectively (see Fig. 6-1). The minima of the double-well potential function determine the concentrations of the separated phases at equilibrium, as functions of the temperature, and, subsequently, the binodal curve (see Fig. 6-1). In addition, the spinodal curve can be built by plotting, as a function of the temperature, the inflection points of the double-well potential function (see Fig. 6-1).

Based on Eq. (2), the governing equations can be formulated. A generalized chemical potential for a binary mixture can be defined: $\mu = \delta F/\delta\emptyset_{\mathrm{sv}}$, where $\delta/\delta\emptyset_{\mathrm{sv}}$ is the functional derivative. Using the continuity equation $\frac{\partial\emptyset_{\mathrm{sv}}}{\partial t} = -\vec{\nabla}\cdot\vec{J}$ and Fick's law for the mass flux $\vec{J} = -M\vec{\nabla}\mu$, where M is the mobility, which is assumed constant, the Cahn–Hilliard equation is obtained:

$$\begin{aligned}\frac{\partial\emptyset_{\mathrm{sv}}}{\partial t} &= M\nabla^2\mu \\ &= M\nabla^2\left(-\varepsilon^2\nabla^2\emptyset_{\mathrm{sv}} + 2(2\emptyset_{\mathrm{sv}} - 1)((2\emptyset_{\mathrm{sv}} - 1)^2 + (\frac{T_l^d - T_{cr}^d}{T_{cr}^d - T_c^d}))\right)\end{aligned} \tag{4}$$

To introduce a possible thermal noise ξ_{s} in the description, an additional term is added to the equation above and one obtains the Cahn–Hilliard–Cook equation [66]:

$$\begin{aligned}\frac{\partial\emptyset_{\mathrm{sv}}}{\partial t} = M\nabla^2\Big(&-\varepsilon^2\nabla^2\emptyset_{\mathrm{sv}} + 2(2\emptyset_{\mathrm{sv}} - 1)((2\emptyset_{\mathrm{sv}} - 1)^2 + \\ &(\frac{T_l^d - T_{cr}^d}{T_{cr}^d - T_c^d}))\Big) + \sigma\xi_{\mathrm{s}}\end{aligned} \tag{5}$$

The thermal noise ξ_s is assumed to obey the fluctuation-dissipation theorem, i.e. $\langle \xi_s(r,t) \rangle = 0,$ and $\langle \xi_s(r,t)\xi_s(r',t') \rangle = -M\nabla^2\delta(r-r')\delta(t-t')$ [66, 67]. The dimensionless parameter $\sigma > 0$ describes the strength of this noise.

Finally, according to Fourier's law, the heat transfer equation in this study is expressed by:

$$\frac{\partial T_l^d}{\partial t} = \kappa_l \nabla^2 T_l^d \tag{6}$$

where κ_l is the thermal diffusivity of the liquid phase.

6.2.2.1 Boundary conditions

The boundary conditions for solving Eqs. (5) and (6) are the following. A zero-mass flux and an adiabatic boundary condition are applied at the bottom substrate. Moreover, we consider that the substrate is neutral with respect to the two components of the binary mixture [41, 68], in that there is no wetting preference for either of them. These 3 boundary conditions are respectively written as:

$$\mathbf{n}.\nabla\mu = 0 \tag{7}$$

$$\mathbf{n}.\nabla T_l^d = 0 \tag{8}$$

$$\mathbf{n}.\nabla\emptyset_{sv} = 0 \tag{9}$$

where **n** is the unit vector normal to the substrate.

Considering that the inert gas absorption in the liquid is negligible and that only the solvent is volatile, the evaporation flux J calculated at the liquid-gas interface takes the following form [69-71]:

$$\mathbf{n}.M\nabla\mu = J(1\text{-}\emptyset_{sv}) \tag{10}$$

where **n** is the unit vector normal to the gas-liquid interface.

Concerning the physics of the evaporation at the interface, we consider a simple representation in which the evaporation flux is directly proportional to the volume fraction of the volatile component at the liquid-gas interface [72-75]:

$$J = J_o \emptyset_{\mathrm{sv}}|_{z=h_l^d} \tag{11}$$

where J_o is a global mass transfer coefficient and $h_l^d(t)$ is the thickness of the liquid layer.

Assuming that the liquid-gas interface remains flat during the evaporation, the time evolution of $h_l^d(t)$ due to the evaporation is described by:

$$\begin{aligned} \frac{dh_l^d}{\partial t} &= -\bar{J} \\ \bar{J} &= J_o \overline{\emptyset}_{\mathrm{sv}}\big|_{z=h_l^d} \end{aligned} \tag{12}$$

where $\overline{\emptyset}_{\mathrm{sv}}$ and $\bar{J}$ are the average of the solvent volume fraction and evaporation flux at the liquid-gas interface.

Moreover, we consider that the liquid-gas interface is neutral with respect to the two components of the binary mixture and one thus gets a condition similar to Eq. (9):

$$\mathbf{n}.\nabla \emptyset_{\mathrm{sv}} = 0 \tag{13}$$

Assuming the characteristic thermal time in the gas is much smaller than in the liquid, we can consider that the temperature of the upper gas phase is homogeneous, constant and equal to the ambient temperature. Therefore, the energy conservation at the liquid-gas interface takes the following form [70, 71]:

$$JL\rho_l = -\alpha_l \frac{\partial T_l^d}{\partial z} \tag{14}$$

where ρ_l and α_l are respectively the density and thermal conductivity of the liquid and L is the latent heat of evaporation of the solvent (all these parameters are assumed constant).

Note that we also introduce periodic boundary conditions in the horizontal x-direction, in a domain of width equal to w (see Fig. 6-2).

6.2.2.2 Initial conditions

The initial concentration and temperature fields in the film are assumed spatially uniform and chosen in such a way that the system is in the stable region (i.e. the representative point is above the binodal curve).

6.2.3 Non-dimensional equations

It is convenient to rewrite the equations in a non-dimensional form. The following scaling factors are used for this purpose. The length scale is taken to be ε and ε^2/M is used as the time scale. The local dimensionless temperatures T_l of the liquid is defined as $T_l = (\frac{T_l^d - T_{cr}^d}{T_{cr}^d - T_c^d})$. In these new units, the equations take the form

$$\frac{\partial \emptyset_{\mathrm{sv}}}{\partial t} = \nabla^2(-\nabla^2 \emptyset_{\mathrm{sv}} + 2(-1 + 2\emptyset_{\mathrm{sv}})((1 - 2\emptyset_{\mathrm{sv}})^2 + T_l)) + \sigma\eta_{\mathrm{s}} \qquad (15)$$

$$\frac{\partial T_l}{\partial t} = Le\nabla^2 T_l \qquad (16)$$

where $Le = \frac{\kappa_l}{M}$ is a Lewis number and η_{s} is the dimensionless form of ξ_{s}, with $\langle \eta_{\mathrm{s}}(r,t) \rangle = 0$ and $\langle \eta_{\mathrm{s}}(r,t)\eta_{\mathrm{s}}(r',t') \rangle = -\nabla^2 \delta(r - r')\delta(t - t')$. The boundary conditions at the bottom are:

$$\mathbf{n}.\nabla\,(-\nabla^2 \emptyset_{\mathrm{sv}} + 2(-1 + 2\emptyset_{\mathrm{sv}})((1 - 2\emptyset_{\mathrm{sv}})^2 + T_l)) = 0 \qquad (17)$$

$$\mathbf{n}.\nabla T_l = 0 \qquad (18)$$

$$\mathbf{n}.\nabla \emptyset_{\mathrm{sv}} = 0 \qquad (19)$$

At the top, the boundary conditions become:

$$\mathbf{n}.\nabla\left(-\nabla^2\emptyset_{\mathrm{sv}}+2(-1+2\emptyset_{\mathrm{sv}})((1-2\emptyset_{\mathrm{sv}})^2+T_l)\right)=\ Pe\emptyset_{\mathrm{sv}}\ (1-\emptyset_{\mathrm{sv}}) \tag{20}$$

$$\frac{dh_l}{dt}=-Pe\overline{\emptyset}_{\mathrm{sv}} \tag{21}$$

$$\mathbf{n}.\nabla\emptyset_{\mathrm{sv}}=0 \tag{22}$$

$$\beta Pe\emptyset_{\mathrm{sv}}\ =-\frac{\partial T_l}{\partial z}\ ,\ \beta=\frac{ML\rho_l}{\alpha_l(T_{cr}^d-T_c^d)} \tag{23}$$

where $h_l(t)$ is the dimensionless height of the liquid layer, whose initial value is written H_l. β is the dimensionless latent heat of evaporation and $Pe=J_o/(\frac{M}{\varepsilon})$ is a Peclet number. This non-dimensional number allows comparing the evaporation with the mobility coefficient, which describes both the diffusion when the components are miscible and their separation in the miscibility gap. Note that the dimensionless domain width is written *W*.

6.2.4 Numerical implementation

The numerical simulations have been carried out using the commercial CFD software COMSOL Multiphysics. This software allows solving any partial differential equations (PDE) system using the finite-element method (FEM) and adaptive time steps [76]. FEM has been applied widely for solving the Cahn-Hilliard equation [77-79], notably via COMSOL Multiphysics [68, 80-83], and for investigating solvent evaporation induced phase separation in ternary systems [74]. For time stepping, a Backward Differential Formula (BDF) method was implemented with time steps taken by the solver [76]. In this regard, the solver automatically modifies the time step to satisfy the convergence criteria.

From a computational point of view, an evaporation process is a problem with a moving boundary, since the liquid thickness decreases over time (h_l =$h_l(t)$). COMSOL Multiphysics is able to deal with moving boundaries [84-86] and the Arbitrary Lagrangian–Eulerian (ALE) module implemented in COMSOL Multiphysics was used to manage the moving interface [76]. The phase field model and the temperature equation have been coupled with moving mesh, allowing an automatic remeshing procedure during the time evolution of the physical domain. A mesh-independency test has been carried out to determine the optimal number of elements and to ensure that the solution is independent of the mesh size. We generated unstructured meshes using COMSOL Multiphysics (free triangular meshes) for different non-dimensional widths of the elements: 1/3, 1/4, 1/5, 1/6 and 1/8. These choices correspond to about 3, 4, 5, 6 and 8 elements across the capillary width. In Fig. 6-3, the time evolution of the average value of the solvent volume fraction at the liquid–gas interface, for Pe = 0.02, $Le = 20$, $\beta = 0.4$, $\sigma = 0.005$, a dimensionless width W = 80 and an initial dimensionless height H_l= 20, is evaluated for these different meshes. The initial volume fraction of the solvent and the initial temperature of the liquid phase are $\emptyset_{sv} = 0.9$ and $T_l = 0.2$, respectively. Our analysis clarifies that decreasing the dimensionless size of the elements from 1/4 to 1/8 hardly changes the results. Therefore, to minimize the computational time, we carried out the rest of our simulations with a dimensionless size of the elements equal to 1/5.

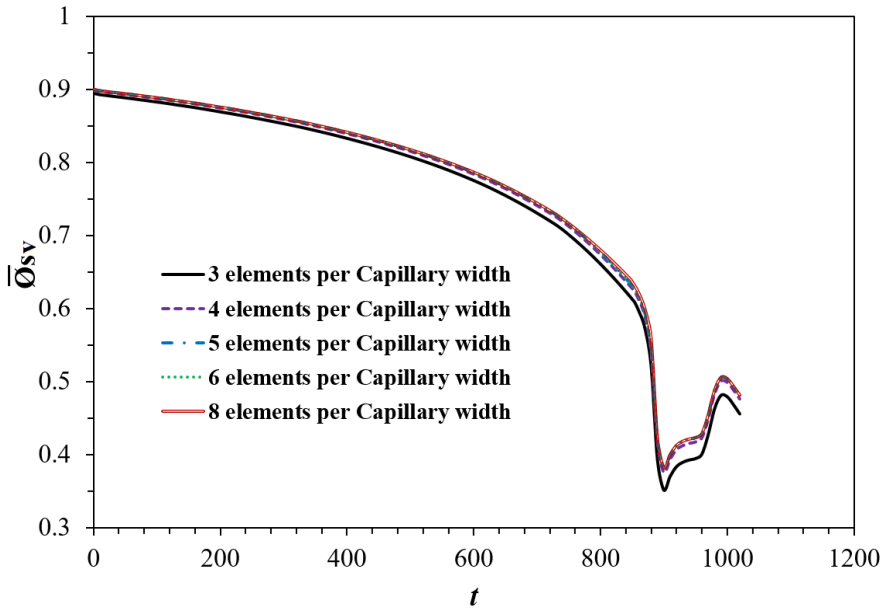

Fig. 6-3. Time evolution of the average value of the solvent volume fraction at the liquid-gas interface, for different mesh widths.

6.2.5 Experimental set-up

To experimentally investigate the mechanism of 2-D phase separation in a thin evaporating film of a partially miscible binary mixture, a Hele Shaw cell was used with a double telecentric setup, as shown in Fig. 6-4. The Hele Shaw cell confines a liquid in a shallow volume with an open upper side. In this research, the Hele Shaw cell was built using two Plexiglas plates, and the confinement at the bottom and along the lateral sides was realized thanks to a thin elastic strip (see Fig. 6-5). To ensure a uniform gap of 1.4 mm between the plates, the Plexiglas plates and the elastic band were maintained using an aluminum casing and 16 M3 bolts. A LED light (1) passing through a telecentric lens (2) goes through the Hele Shaw Cell (4) placed on the sample holder (3) as shown in Fig. 6-4. Before being captured by the camera (6), the light beam goes through another adjustable telecentric lens (5). The two lenses with adjustable openings make the visualization technique very sensitive to the change of refractive index, which is relevant here as the partially miscible liquids refract light differently.

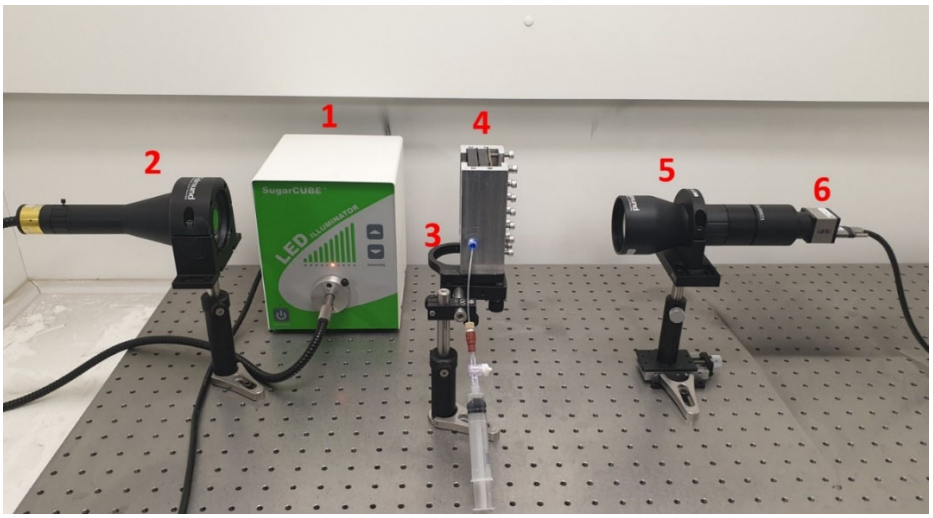

Fig. 6-4. Double telecentric setup; 1) LED light source, 2) adjustable telecentric lens connected to light source, 3) sample holder, 4) Hele Shaw cell, 5) adjustable telecentric lens connected to camera and 6) camera.

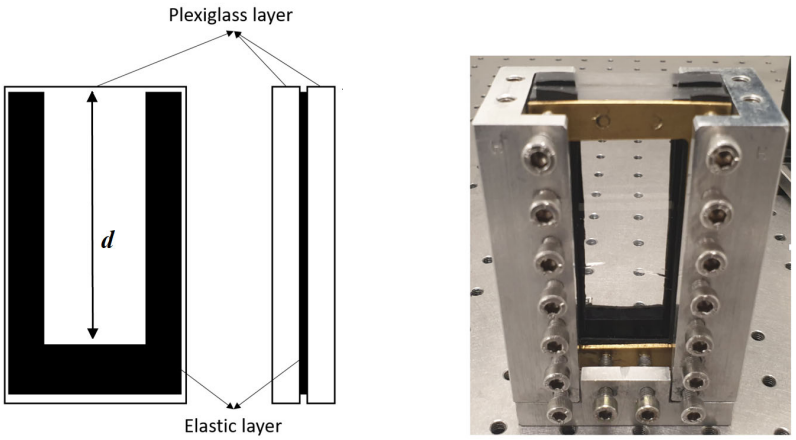

Fig. 6-5. Hele Shaw cell.

The liquids used in this work are n-hexane and 2-(2-Ethoxyethoxy)ethanol, also known as Diethylene Glycol Monoethyl Ether (DGME), used as purchased from Sigma-Aldrich company. The components are partially miscible and there is a considerable difference between their volatility [43], which allows considering that only the n-hexane evaporates. The binodal curve defining the miscibility gap in the phase space of the two partially miscible liquids is available in the literature [87].

Before each test, the Hele Shaw cell was disassembled, washed by ethanol and optical tissue and left to dry. The mixture was injected from the bottom of the cell using a syringe connected to a Polytetrafluoroethylene tube fixed to the cell. The tests were performed during different days at atmospheric pressure, for an initial liquid thickness of 10 mm, and with the room temperature between 19°C and 21°C. This is above the upper critical temperature of the system (6.3°C [87]). The relative humidity of the air was between 43% and 52%. Each test was repeated at least three times. The distance from the bottom of the Hele Shaw cell to the open air is denoted *d* and this distance has been varied from one test to another in order to change the evaporation rate (see below).

6.3 Results and discussion

The fluids properties used in the model are those corresponding to our experiments and already described previously in [43] (see section 6.3 in [43] for more details). They give $Le \approx 20$ and $\beta \approx 0.4$ and these two values are used throughout this work. Note that we assume that the values of these properties are not substantially modified by the concentration and temperature changes in the mixture induced by the evaporation and thus that they can be considered as constant during the time evolution of the system. We consider a noise strength $\sigma = 0.005$, to make sure that phase separation occurs in the system [88].

6.3.1 Interplay between the evaporation rate and the phase separation

Evaporation is the key phenomenon driving the phase separation in the studied system. Indeed, since the system is initially in the stable region, evaporation leads the system to approach the binodal curve by decreasing

the temperature and increasing the solute concentration close to the upper surface (see Fig. 6-1). Then, the binodal curve, and later the spinodal one, are crossed, which makes the system unstable and allows the beginning of phase separation. Note that some initial conditions (for instance high temperature, see [43] for more details) could prevent the system from crossing these curves. In such situations, phase separation does not occur. Note also that, depending on the initial temperature and concentration, the system will reach the demixing region at different locations in the phase diagram (i.e. at different temperature and concentration), and phase separation will thus start at a temperature that varies with the initial conditions. This point is very important, because it is well known that phase separation proceeds faster at lower temperatures, due to the higher driving force for phase separation (see [89-91] for more details on the effect of different quench depths in the phase separation process).

For the simulations presented in this section, the computational domain is rectangular, with a dimensionless width $W = 80$ and an initial dimensionless height $H_l = 20$. Fig. 6-6 and Fig. 6-7 describe the interplay between evaporation and the phase separation dynamics for an initial solvent volume fraction $\emptyset_{sv} = 0.9$ and an initial temperature $T_l = 0.2$. Different evaporation rates are considered by choosing the following different values of the Peclet number: Pe = 0.002, Pe = 0.02, and Pe = 0.08.)

For Pe = 0.002 (Fig. 6-6), which corresponds to a low evaporation rate, the system remains almost vertically uniform and thus the phase separation occurs everywhere across the bulk of the thin film when the system enters the miscibility gap.

For Pe = 0.02, which corresponds to a moderate evaporation rate, the liquid close to the liquid-gas interface enters the spinodal before the bottom of the

layer (see the time labels in Fig. 6-7-c). For this reason, the spinodal instability takes place only in the upper part of the system, which creates a lateral structure in the film, characterized by a well-defined wavelength. Then as time increases, this lateral structure progressively invades the whole thickness of the fluid. In Fig. 6-7-c, the paths in the phase diagram describing the time evolution of the average values of the temperature and of the solute volume fraction at the liquid-gas interface and at the substrate are presented. We clearly see in this figure that the top of the layer enters the unstable region before the bottom of the layer. Moreover, we see that the evolution of the average solute volume fraction at the liquid-gas interface and at the bottom of the film is not monotonous. Notably, while the bottom of the film is in the metastable region, we observe a decrease of the solute concentration there (i.e. an increase of the solvent concentration). It is due to the phase separation taking place at the top of the layer, transferring some solvent towards the bottom of the film.

Finally, in the case of a "fast" evaporation with Pe = 0.08, phase separation appears only in the vertical direction as a result of the concentration gradient imposed by the evaporation. The spinodal instability and the resulting formation pattern characterized by a typical wavelength do not occur at liquid-gas interface and the so-called lamellar morphology is observed, with a thin horizontal skin of solute in the upper part of the layer. As evaporation continues, the lower part of the layer enters the unstable region (see Fig. 6-7-d) and a spinodal instability takes place in the neighborhood of the substrate, similar to the spinodal instability at the liquid-gas interface for the lateral structure. Some solvent-rich droplets are formed but they finally disappear.

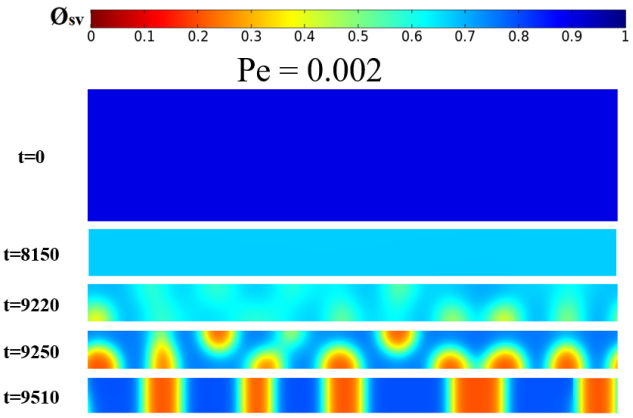

Fig. 6-6. Time evolution of the phase separation morphology for Pe = 0.002. $H_l = 20$, $W = 80$, $\emptyset_{sv} = 0.9$ and $T_l = 0.2$ at $t = 0$.

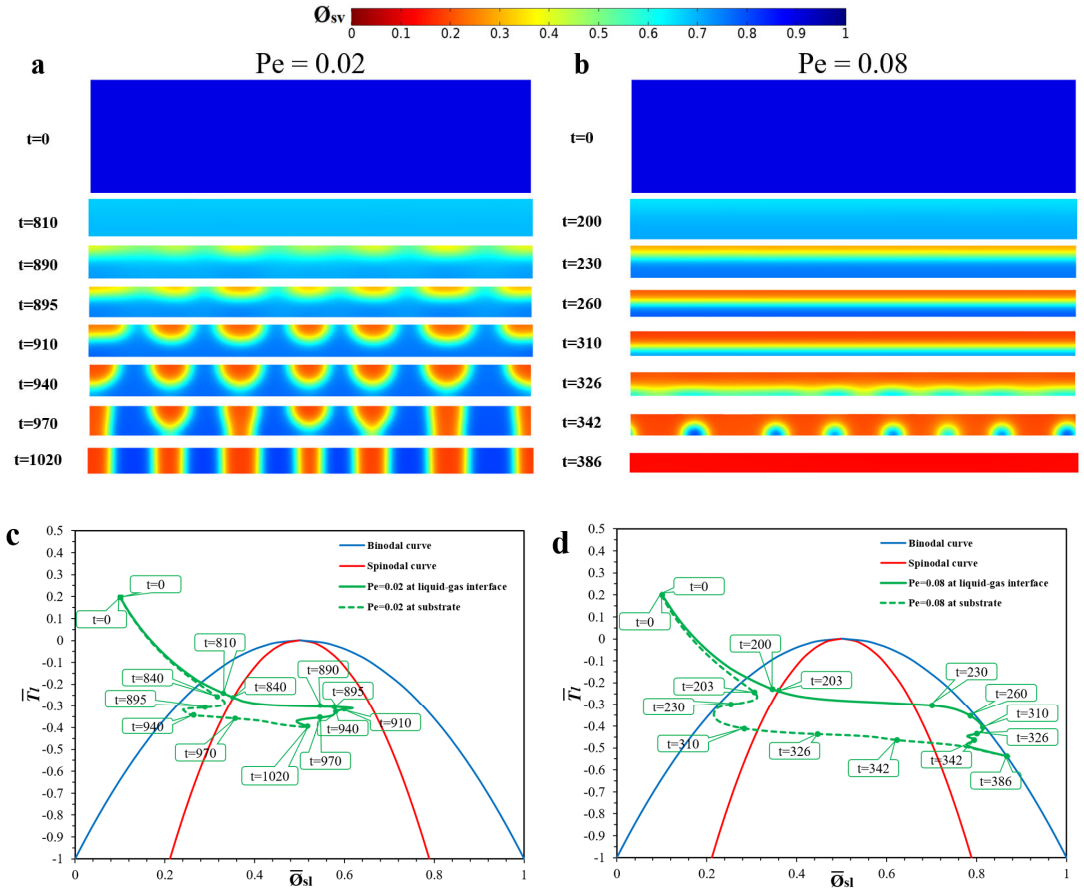

Fig. 6-7. a and b: time evolution of the phase separation morphology. c and d: paths in the phase diagram describing the evolution with time of the average values of the temperature and of the solute volume faction at the liquid-gas interface and at the substrate. Pe = 0.02 and 0.08, $\emptyset_{sv} = 0.9$ and $T_l = 0.2$ at $t = 0$, $H_l = 20$, $W = 80$.

Another interesting global indicator of the evolution of the system is the evaporation flux Pe $\overline{\emptyset}_{sv}$. This quantity, rescaled by Pe, is plotted versus time in Fig. 6-8 for three values of the Peclet number: Pe = 0.02, 0.03, and 0.08. As expected, the evaporation flux decreases over time due to the removal of solvent at the liquid-gas interface. However, the decrease of the evaporation flux is not monotonous and some sudden changes are also observed, which are emphasized by circles in the figure. These changes are further discussed in the next section.

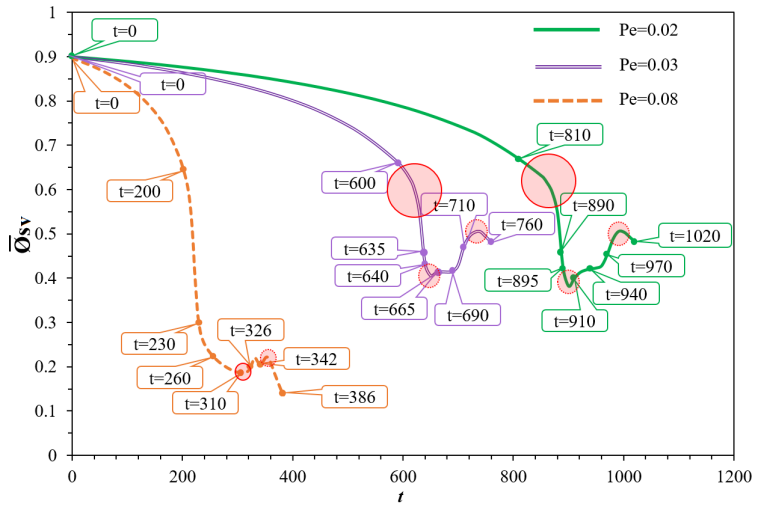

Fig. 6-8. Time evolution of the average evaporation flux at the gas-liquid interface, rescaled by Pe, for three values of the Peclet number: Pe = 0.02, 0.03, and 0.08. $\emptyset_{sv} = 0.9$ and $T_l = 0.2$ at $t = 0$, $H_l = 20$, $W = 80$.

6.3.2 Beginning of the phase separation

As already mentioned, the Peclet number is a measure of the competition between evaporation and phase separation. The results shown above for 3 values of Pe clearly emphasize the important role of this parameter on the behavior of the system.

Low evaporation rates have been considered first, with Pe = 0.002. In that situation, the system is almost uniform in the vertical direction when it enters the unstable region in the phase diagram. For this reason, the spinodal

instability takes place through the whole layer at the same time, as observed in Fig. 6-6. Note that this expected behavior has already been studied in [53], where the isothermal demixing of a polymer-solvent mixture, induced by the solvent evaporation, was analyzed at a very low evaporation rate. This slow evaporation and the corresponding phase separation are not analyzed further in the present paper.

The case of a moderate evaporation rate, with Pe = 0.02, is described by Fig. 6-7-a. In this situation, a moderate vertical concentration gradient is present in the liquid film. Its upper part enters the unstable region while its bottom part is in the metastable region. For this reason, the spinodal instability takes place only close to the top surface, which gives rise to the lateral morphology that appears in Fig. 6-7-a for $t \sim 890$. The appearance of this instability is also related to a rather sudden decrease of the evaporation rate versus time, which is emphasized by Fig. 6-8 for Pe = 0.02 and 0.03 (see the first red circle for Pe = 0.02 and 0.03). As already mentioned above, the instability is also related to an increase of the solvent concentration close to the bottom substrate.

The Peclet number has also an interesting effect on the wavelength (or wavenumber) that characterizes the lateral pattern generated by the spinodal instability in the upper part of the system. In our numerical approach, the wavelength λ can be estimated from the number n of cells that appear close to the interface, with $\lambda = W/n$. To have a more precise numerical estimation of this quantity, it is of course preferable to decrease the constraining influence of the (periodic) lateral boundaries of the layer and we use $W = 160$ for the results presented in the present discussion. Using the same initial conditions as previously (H_l = 20, $\emptyset_{sv} = 0.9$ and $T_l = 0.2$), we consider three values of the Peclet number, Pe = 0.02, 0.03, and 0.04, and the associated patterns observed right after the instability are represented in Fig.

6-9. The numbers of cells are respectively 12, 14 and 15, which emphasizes that the increase of the Peclet number (i.e. of the evaporation rate) corresponds to an increase of the observed wavenumber.

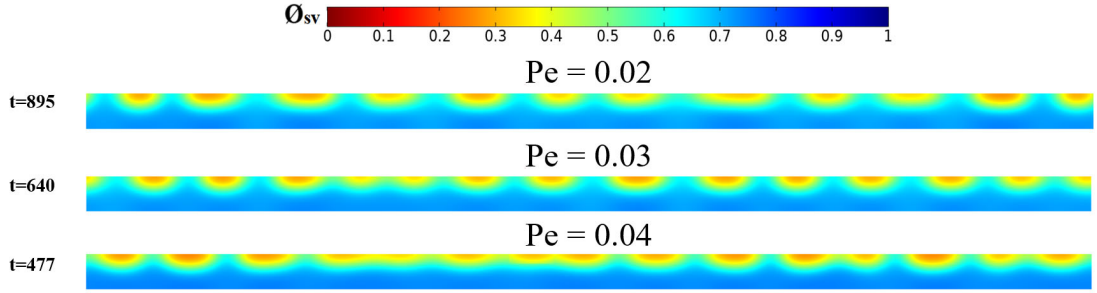

Fig. 6-9. Phase separation pattern for three different values of the Peclet number: Pe = 0.02, 0.03, and 0.04. $\emptyset_{sv} = 0.9$ and $T_l = 0.2$ at $t = 0$, $H_l = 20$, $W = 160$.

To understand this behavior, it is worth recalling briefly the linear Cahn–Hilliard theory of spinodal instability in quenching experiments [13, 92, 93]. When a system is suddenly quenched into the miscibility gap, a band $[0, k_c]$ of wavenumbers becomes unstable, with:

$$k_c^2 = -\left(\frac{\partial^2 f_0}{\partial \emptyset_{sv}{}^2}\right) \tag{24}$$

Remember also that the dominant wavenumber k_m, and its growth rate ω_m, which is the maximum value over the unstable band, are given by:

$$k_m^2 = \frac{1}{2}k_c^2 \qquad \omega_m = \frac{1}{4}k_c^4 \tag{25}$$

The situation analyzed in our work is of course more complex than quenching, notably because the entrance in the miscibility gap is progressive. Since the instability takes place close to the upper surface, we consider the average temperature and concentration at the interface as global indicators of the state of the system. When the representative point given by these indicators is below the spinodal curve, one can consider that they define unstable bands of wavenumbers, but these are now time-dependent because evaporation let the indicators move inside the miscibility gap. When the

system crosses the spinodal curve on the left (see Fig. 6-7-c), the band has first a zero width. Then, as time passes, the width of the unstable band increases, and the corresponding k_m and ω_m also increases, until the system reaches the critical concentration $\emptyset_{sv} = 0.5$. Besides this point, k_c, k_m and ω_m start to decrease.

Fig. 6-10 shows the time evolution of k_m and ω_m, calculated using Eqs. (24) and (25) and the average temperature and concentration at the interface, for the three Peclet numbers Pe = 0.02, 0.03, and 0.04. It is interesting to stress that the curves corresponding to the 3 values of Pe are quite similar, except that the time scale is shorter for large Pe, as expected. In particular, note that the time interval Δt between the crossing of the spinodal and reaching the critical concentration $\emptyset_{sv} = 0.5$ decreases when the evaporation is stronger. Note also that these time intervals are larger than the typical growing time τ of the perturbations, which can be estimated by calculating 2π divided by the maximum value of ω_m in Fig. 6-10, which gives $\tau \approx 17$. As a result, larger wavenumbers will be excited and amplified by larger evaporation rates, as observed in Fig. 6-9.

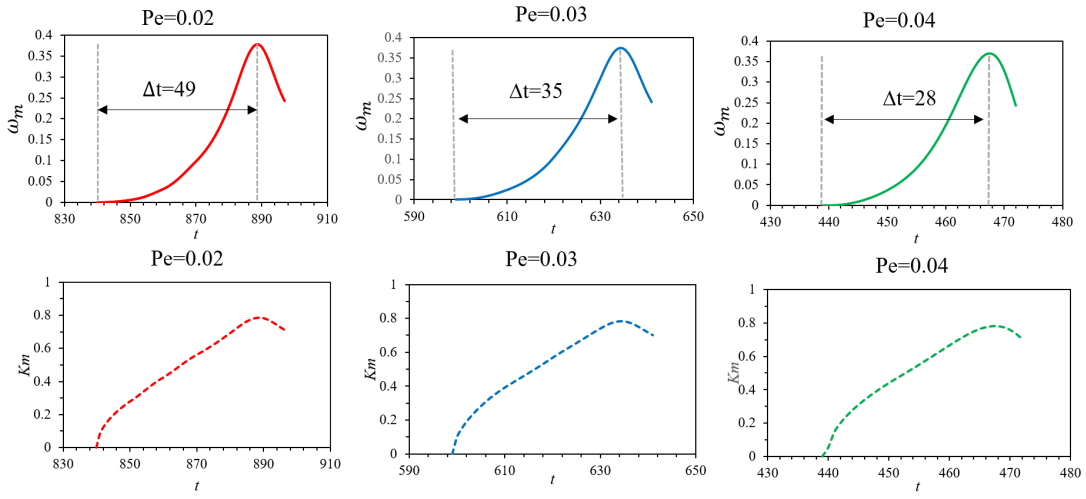

Fig. 6-10. Growth rate and wavenumber for the average values of the solvent volume fraction and the temperature at the liquid-gas interface and for Pe = 0.02, 0.03, and 0.04. H_l = 20, W = 160, $\emptyset_{sv} = 0.9$ and $T_l = 0.2$ at t = 0.

Finally, a Peclet number equal to 0.08 corresponds to a large evaporation rate. In that situation, Fig. 6-7-b shows that the phase separation occurs only in the vertical direction, as a consequence of the vertical gradient imposed by the evaporation. No spinodal instability appears in the upper part of the system when it enters the unstable region and a so-called lamellar morphology is created. Note that this layered morphology was also observed in [52] for the isothermal phase separation induced by a fast solvent evaporation of a single polymer-solvent binary mixture in a cylindrical geometry. This behavior can be explained as follows. First, it is interesting to note generally that a spinodal instability close to the upper surface induces the development of horizontal concentration gradients. Since the evaporation flux is proportional to the solvent concentration at the interface, the evaporation then reduces the horizontal concentration gradients between the solvent-rich and solute-rich areas and thus participates in the damping of the perturbations. This argument clearly emphasizes the competition between separation and evaporation and the important role of the Peclet number. It is also interesting to note the rather complex role played by evaporation in the phenomenon under analysis. On the one side, evaporation brings the fluid in the demixing area, which allows for the spinodal instability, and it is worth noting that the path in the phase space depends only slightly on the Peclet number, i.e. on the intensity of the evaporation. On the other side, evaporation can damp the perturbations generated by the instability and, if Pe is large enough, this damping can finally prevent the appearance of the lateral morphology, which allows understanding the lamellar morphology for Pe = 0.08. Using again the linear Cahn–Hilliard theory of spinodal instability as above provides also another more technical explanation for the behavior corresponding to large evaporation rates. In Fig. 6-11, the time evolution of k_m and ω_m for Pe = 0.08 is given and the corresponding typical

growth time of the perturbation is $\tau \approx 19$. Since this time is larger than the time interval $\Delta t = 16$ between crossing the spinodal curve and reaching the critical concentration, one can deduce that the system does not have enough time to create the pattern and no spinodal instability occurs in the system.

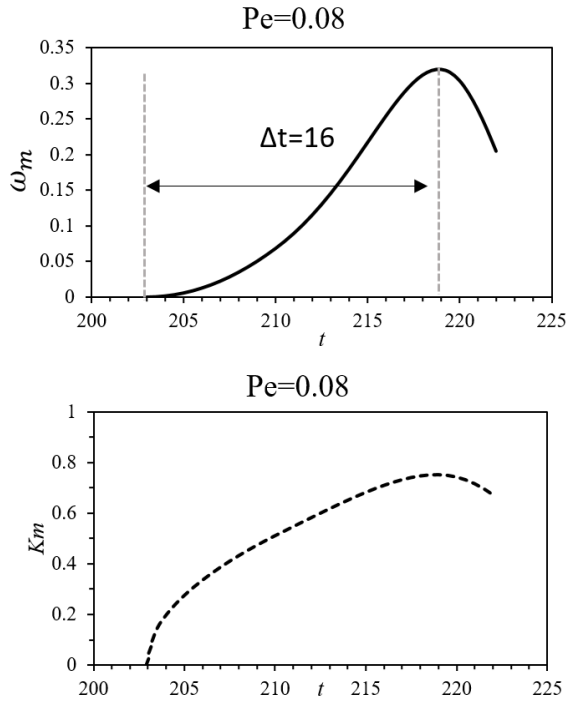

Fig. 6-11. Growth rate and wavenumber for the average values of the solvent volume fraction and the temperature at the liquid-gas interface and for Pe = 0.08. H_l = 20, W = 160, $\emptyset_{sv} = 0.9$ and $T_l = 0.2$ at t = 0.

6.3.3 Mid- and long-term evolution of the phase separation morphology

Here, we analyze the mid- and long-term evolution of the system, (far) after the beginning of the phase separation, described in the previous subsection. We consider only moderate and high evaporation rates, for which phase separation starts close to the liquid-gas interface.

For Pe = 0.02 (moderate evaporation rate), we show the time evolution of the morphology and of the evaporation flux in Fig. 6-7-a and in Fig. 6-8, respectively. As mentioned in subsection 6.3.2, the first sudden change in

the curve describing the evolution with time of the evaporation flux is related to the time when the spinodal instability occurs in the system. This instability, which is emphasized by the first red circle in Fig. 6-8, close to $t = 870$, is associated with a sudden change of the slope of the curve. A sharp decrease of the evaporation flux is then observed, whose duration is of the order of the growing time τ of the instability. Then a second drastic change of the slope appears in Fig. 6-8, which is emphasized by the second red circle close to t = 900. From that moment, the nonlinear evolution of the phase separation pattern takes places and the solute-rich (red) droplets start to grow (see the growing red zones in Fig. 6-7-a), while the solvent is rejected towards the bottom or between the red drops (see the blue that gets darker close to the substrate or between the red zones). During this stage, the evaporation flux increases but note that this increase is not completely regular because the growth of the solute-rich drops let the red zones touch the substrate one after the other. Finally, close to the third red circle in Fig. 6-8, all the red drops have reached the bottom and a new evolution stage starts, with a decreasing evaporation flux. However, it is important to stress that this stage of the evolution of the system cannot be studied with our model and we have thus stopped the numerical calculations then. More precisely, the flat surface assumption would artificially squeeze the “red pillars” and prevent a possible dewetting of the substrate and the creation of isolated pure solute droplets on the substrate, as observed experimentally in [43].

For Pe = 0.08 (fast evaporation, see Fig. 6-7-b), the evaporation flux decreases importantly when the phase separation starts, owing to the lamellar structure created by the evaporation induced vertical gradient (see Fig. 6-8). Close to t = 320, the lower parts of the layer enter the demixing region and a spinodal instability takes place in the neighborhood of the substrate (see also

Fig. 6-7-b for t = 326). As a result of this phenomenon, a sudden slope change appears in Fig. 6-8 (first red circle) and the evaporation flux starts to increase. After some time, the solvent-rich (blue) droplets disappear and the final stage of the evolution starts close to t = 350 (second red circle), with only solute-rich (red) fluid remaining in the system and the progressive evaporation of the remaining solvent.

Another interesting phenomenon that could appear after the spinodal instability is the coalescence of solute-rich (red) droplets. In fact, the growth of the solute-rich drops takes place both in the vertical and horizontal directions and it is easy to understand that if the thickness of the layer is large enough, the drops could coalesce horizontally before touching the substrate. To illustrate this, we consider the same system as in Fig. 6-7-a (Pe = 0.02, initial solvent volume fraction $\emptyset_{sv} = 0.9$ and initial temperature $T_l = 0.2$), but we use three different initial heights H_l= 20 (the height already considered before), H_l = 28, and H_l = 38. The corresponding results are presented in Fig. 6-12. For the 3 cases, a lateral structure is created first close to the interface. The case H_l = 20 is already discussed above and no coalescence is observed before the red pillars are formed. Fig. 6-12 then shows that, for H_l = 28, coalescence occurs between some droplets and a smaller number of pillars than for H_l = 20 is formed later. Finally, for H_l = 35 the coalescence of all the drops happens, which gives rise to a secondary lamellar structure. The subsequent evolution of this lamellar structure is then similar to what is observed in Fig. 6-7-b, with the appearance of a spinodal instability close to the substrate, before only solute-rich (red) fluid remains in the system. Finally, note that the possibility of coalescence is linked to an appropriate relation between the dimension of the drops (i.e. the wavelength of the pattern) and the thickness of the layer when the instability takes place. Indeed, Fig. 6-12-b (that corresponds to an initial thickness equal to 28)

shows the coalescence of drops when the thickness is around 8, which is of the order of half the wavelength of the pattern (this wavelength is 160/13 ~ 13.3, see above).

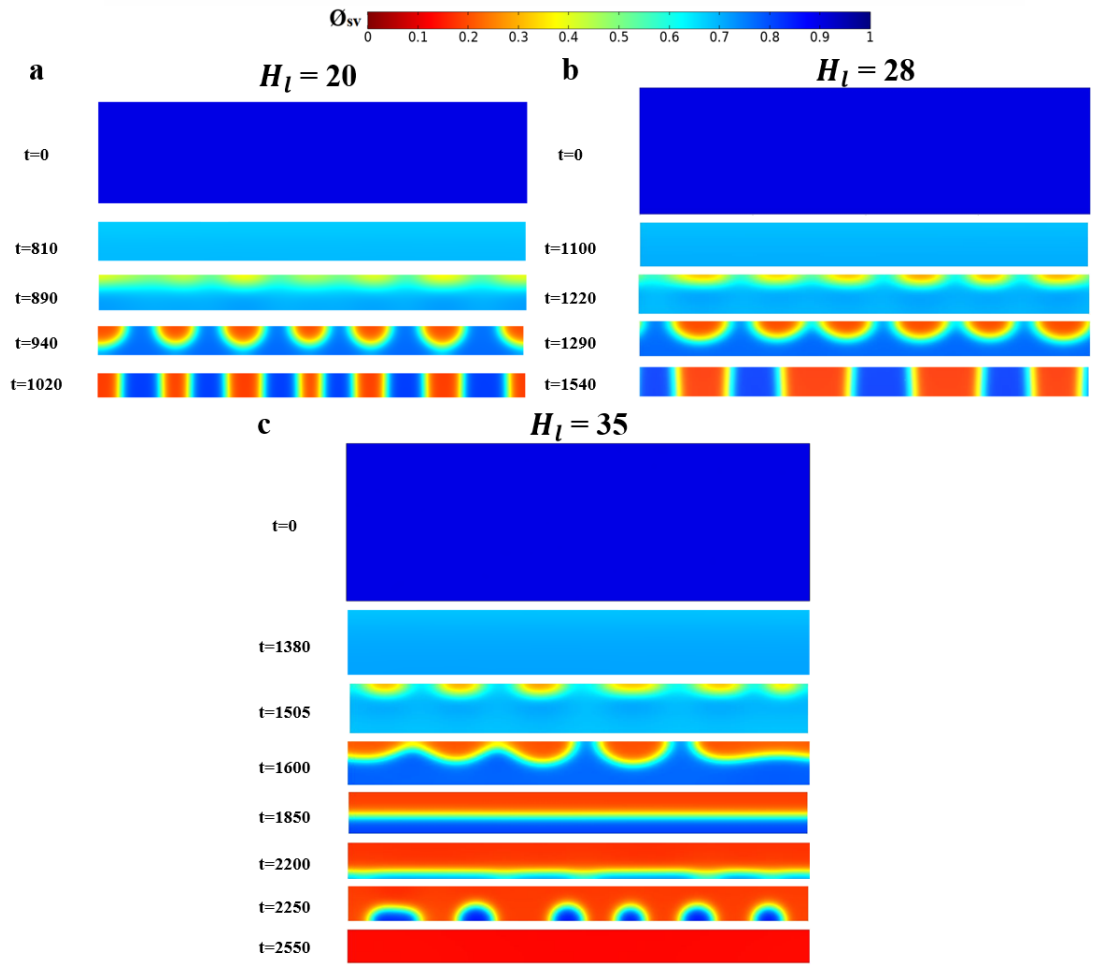

Fig. 6-12.Time evolution of the phase separation morphology for Pe = 0.02 and for three initial dimensionless heights H_l = 20, 28, and 35. $\emptyset_{sv} = 0.9$ and $T_l = 0.2$ at $t = 0$, $W = 80$.

6.3.4 Influence of the initial conditions on the phase separation morphology

The initial temperature and concentration are parameters that can influence the phase separation morphology in the binary mixture. In fact, a change of the initial temperature or concentration can lead the system to enter the unstable region at different conditions, which can affect significantly the

driving force of the phase separation and its competition with the evaporation. To emphasize this, we consider two examples in this section. First, for Pe = 0.08, we consider a change in the initial temperature with respect to the situation in Fig. 6-7-b. In Fig. 6-13, we observe that reducing the initial temperature to T_l = -0.3 induces logically an entry in the unstable region at a lower temperature, resulting in higher driving force for the phase separation. Therefore, the phase separation proceeds much faster and eventually overcomes the strong evaporation to form a lateral structure, in contrast to what was observed in Fig. 6-7-b, for the same Pe number and T_l = 0.2. It is also interesting to note that in contrast to what was observed in Fig. 6-12-a (same initial thickness as in the present situation), coalescence is possible here because the wavelength is smaller than in Fig. 6-12-a and also because the thickness when the instability takes place is larger (around 9, instead of 6).

The second example consists in changing the initial concentration with respect to the case of Fig. 6-7-a (Pe = 0.02). The corresponding results, for an initial concentration for $\emptyset_{sv}$= 0.85, are represented in Fig. 6-14. They show that the reduced initial concentration of the solvent leads to a reduced driving force for the separation, when compared to the case with $\emptyset_{sv}$ = 0.9 as initial value. Consequently, the phase separation is overcome by the evaporation and the lateral morphology obtained for $\emptyset_{sv}$ = 0.9 (see Fig. 6-7-a) is transformed into a lamellar pattern.

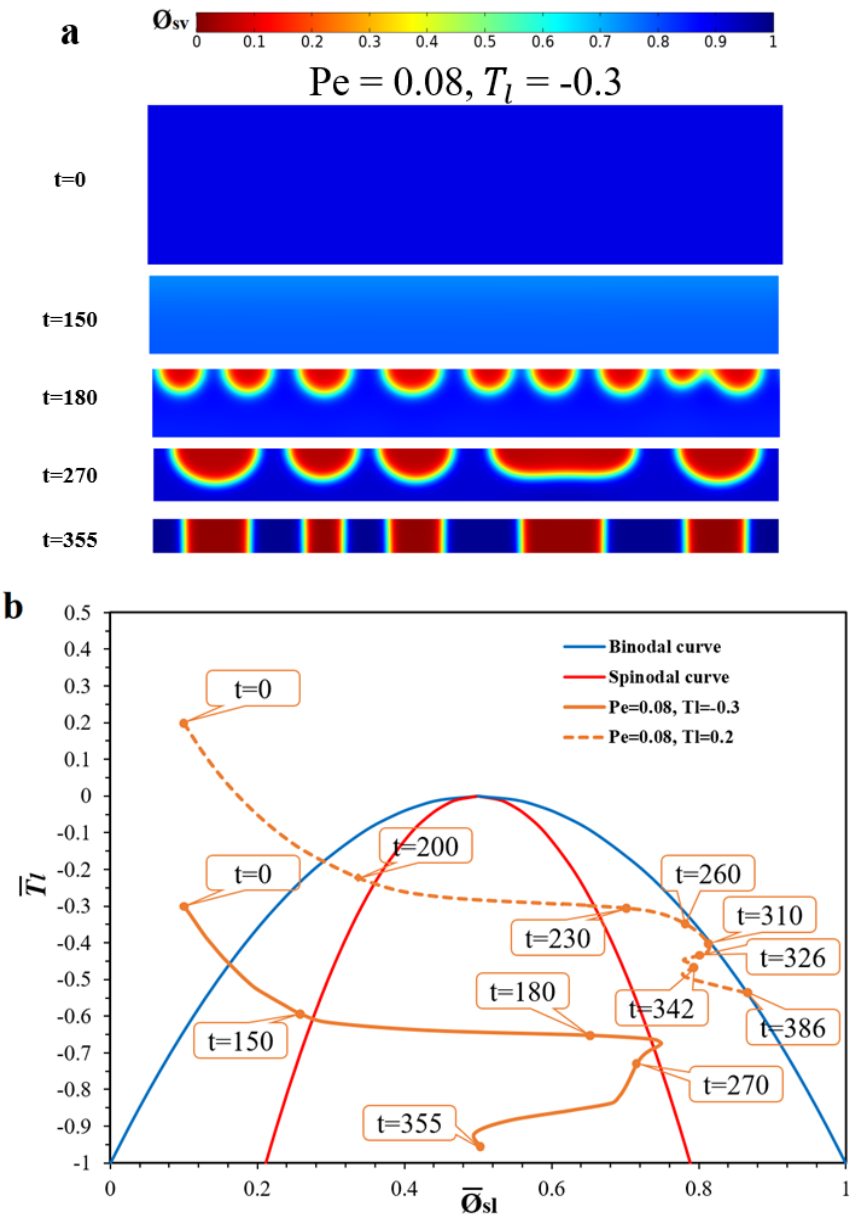

Fig. 6-13. a: time evolution of the phase separation morphology for Pe = 0.08 and T_l = -0.3. b: path in the phase diagram describing the evolution with time of the average values of the temperature and of the solute volume faction at the liquid-gas interface for T_l = -0.3 and T_l = 0.2. H_l = 20, W = 80, $\emptyset_{sv} = 0.9$ (initial value).

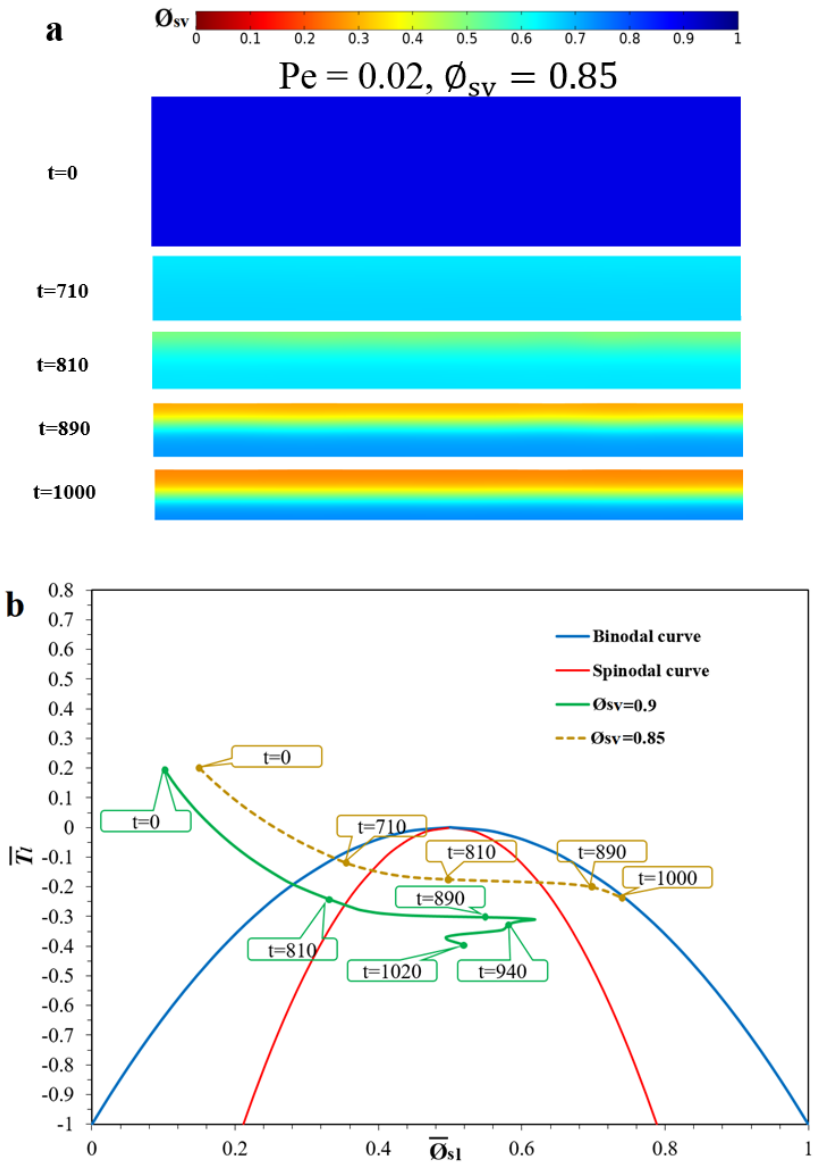

Fig. 6-14. a: time evolution of the phase separation morphology for initial solvent volume fraction $\emptyset_{sv} = 0.85$. b: path in the phase diagram describing the evolution with time of the average values of the temperature and of the solute volume faction at the liquid-gas interface for $\emptyset_{sv} = 0.9$ and $\emptyset_{sv} = 0.85$. $H_l = 20$, $W = 80$, and $T_l = 0.2$ at $t = 0$.

6.4 Experimental results

In this section, we present the experimental results obtained with the Hele Shaw set-up presented in subsection 6.2.5 and compare them with our numerical analysis. Since the distance between the plexiglass plates is small,

it is assumed that convection is very weak in the system, which allows the comparison with the numerical purely diffusive approach. Note also that the experimental evaporation rate can be changed by varying the thickness d of the gas layer above the thin film. In our set up, we consider d = 78 mm and d = 32 mm, corresponding to "moderate" and "fast" evaporation rates, respectively. In the results presented below, the red and green colors correspond to n-hexane-rich and DGME-rich phases, respectively. The experiment tests were performed with a liquid at the initial room temperature (between 19°C and 21°C). This is above the critical temperature (6.3°C [87]).

For an initial mass fraction of DGME in the liquid of 8%, the experimental results indicate that a moderate evaporation rate (d = 78 mm) leads to the lateral structure (Fig. 6-15-a) while a fast evaporation rate (d = 32 mm) induces the development of the skin layer (lamellar structure) at the liquid-gas interface (Fig. 6-15-b). This is in very good qualitative agreement with the numerical results discussed earlier.

Fig. 6-15-a and Fig. 6-15-c compare the time evolution of the phase separation for two different initial concentrations of DGME in the solution (8% and 12%), in the case of the moderate evaporation rate (d = 78 mm). The lateral structure is obtained for the low initial concentration and the lamellar structure for the high initial concentration. This is again in qualitative agreement with the numerical results presented at the end of subsection 6.3.4.

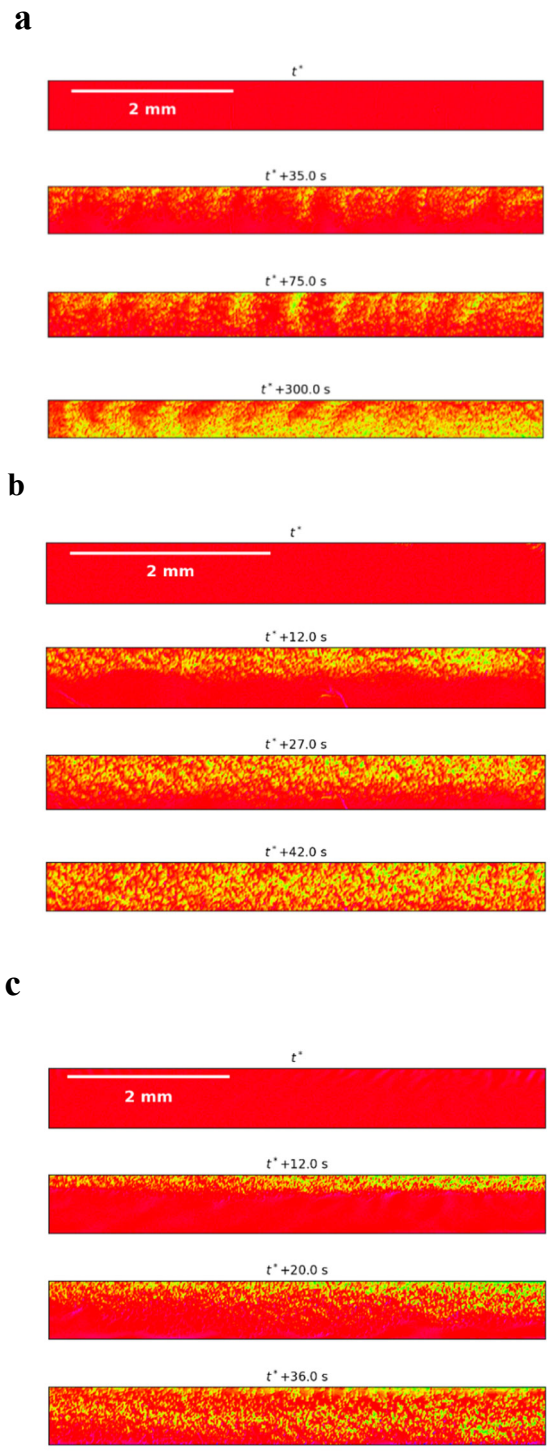

Fig. 6-15. Time evolution of the phase separation for: a moderate evaporation and 8% of DGME (a), a fast evaporation and 8% of DGME (b), and a moderate evaporation and 12% of DGME (c).

6.5 Conclusion

Thin layers of evaporating binary mixture of partially miscible components are commonly encountered in a number of industrial contexts. Therefore, it is of great practical interest to further understand the relationship between the physical processes that occur during the evaporation process and to analyze the morphological changes in the evaporating thin film. In this study, we developed a numerical description, based on a non-isothermal diffusive phase field model. We also built an experimental framework to study two-dimensional morphology evolution during solvent evaporation in a thin film of a partially miscible binary mixture. Our main findings are the following. First, it is worth stressing that the Peclet number, which allows quantifying the competition between evaporation and phase separation, is a very important parameter of the system. For low Peclet numbers, which corresponds to small evaporation rates, demixing occurs throughout the whole film at the same time, as the bottom of the layer and its top enter the unstable region together. Consequently, a bulk structure is formed. On the other hand, for larger values of Pe, i.e. at moderate and high evaporation rates, the top of the layer enters the unstable zone before the bottom and a vertical concentration gradient is formed. For the moderate evaporation rate, the spinodal instability occurs close to the top surface, which results in a lateral structure. For high evaporation rates, no spinodal instability takes place in the system close to the top surface and a lamellar structure is formed. Note that our analysis has also emphasized an interesting effect of Peclet number on the wavelength of the lateral structure generated by the spinodal instability in the upper part of the system. The results show indeed that the increase of the Peclet number (i.e. of the evaporation rate) corresponds to a decrease of the observed wavelength. As far as the mid- and long-term

evolution of the system is concerned, our main observations are the following.

When a lateral structure is first created close to the surface, we have emphasized the possibility of coalescence of solute-rich droplets. This coalescence is observed only in thick enough layer, for which the growth of the drops can induce their coalescence before these drops reach the bottom. It is also interesting to note that more and more drops can coalesce if the thickness is larger and finally a lamellar morphology can appear in very thick films. We have also emphasized that after the creation of a lamellar structure, a spinodal instability can subsequently appear close to the substrate, as a result of the bottom part of the film crossing the spinodal curve in the phase space. A momentary lateral morphology, made up of solvent rich droplets, then appears close to the substrate, but this structure disappears in the long term and only solute rich fluid remains in the film. Interestingly, we have also shown that the morphology evolution is affected by the initial conditions (initial temperature and concentration). In fact, a change of the initial temperature or concentration can lead the system to enter the demixing region at different locations in the phase diagram, which can affect notably the driving force of the phase separation and its competition with the evaporation. Finally, we want to stress that our numerical results regarding the lateral and lamellar structures were validated experimentally. The experimental results showed a very good qualitative agreement with the numerical results.

Let us also recall that our present study was restricted to the study of phase separation of a binary mixture in a two-dimensional situation and without considering the hydrodynamic effects and the wetting/dewetting behavior (or surface preferences) of the two components along the boundaries. It is important to mention that these effects could of course play a role in the

competition between the different possible morphologies, but the analysis of the associated physical mechanisms is postponed to a future work.

Acknowledgements

Financial support from F.R.S.-FNRS ("DITRASOL" PDR T.0123.16) and from BELSPO ("EVAPORATION" MAP-PRODEX project) is cordially acknowledged.

6.6 References

[1] A. van Breemen, T. Zaba, V. Khikhlovskyi, J. Michels, R. Janssen, M. Kemerink, G. Gelinck, Surface Directed Phase Separation of Semiconductor Ferroelectric Polymer Blends and their Use in Non-Volatile Memories, Advanced Functional Materials, 25 (2015) 278-286.

[2] G.M. Su, E. Lim, E.J. Kramer, M.L. Chabinyc, Phase Separated Morphology of Ferroelectric–Semiconductor Polymer Blends Probed by Synchrotron X-ray Methods, Macromolecules, 48 (2015) 5861-5867.

[3] M. Haataja, F. Léonard, Influence of mobile dislocations on phase separation in binary alloys, Physical Review B, 69 (2004).

[4] P. Krasnochtchekov, R.S. Averback, P. Bellon, Homogeneous phase separation in binary alloys under ion irradiation conditions: Role of interstitial atoms, Physical Review B, 75 (2007).

[5] L. Xue, Y. Han, Pattern formation by dewetting of polymer thin film, Progress in Polymer Science, 36 (2011) 269-293.

[6] E. Kiran, K. Liu, The miscibility and phase behavior of polyethylene with poly (dimethylsiloxane) in near-critical pentane, Korean Journal of Chemical Engineering, 19 (2002) 153-158.

[7] T. Inoue, Reaction-induced phase decomposition in polymer blends, Progress in Polymer Science, 20 (1995) 119-153.

[8] L.M. Robeson, Polymer blends, A Comprehensive Review, (2007).

[9] P.K. Chan, A.D. Rey, Computational analysis of spinodal decomposition dynamics in polymer solutions, Macromolecular theory and simulations, 4 (1995) 873-899.

[10] P.K. Chan, A.D. Rey, A numerical method for the nonlinear Cahn-Hilliard equation with nonperiodic boundary conditions, Computational materials science, 3 (1995) 377-392.

[11] K.-W.D. Lee, P.K. Chan, X. Feng, Morphology development and characterization of the phase-separated structure resulting from the thermal-induced phase separation phenomenon in polymer solutions under a temperature gradient, Chemical Engineering Science, 59 (2004) 1491-1504.

[12] J.W. Cahn, Phase Separation by Spinodal Decomposition in Isotropic Systems, The Journal of Chemical Physics, 42 (1965) 93-99.

[13] S. Asai, S. Majumdar, A. Gupta, K. Kargupta, S. Ganguly, Dynamics and pattern formation in thermally induced phase separation of polymer–solvent system, Computational Materials Science, 47 (2009) 193-205.

[14] Y.C. Li, R.P. Shi, C.P. Wang, X.J. Liu, Y. Wang, Predicting microstructures in polymer blends under two-step quench in two-dimensional space, Phys Rev E Stat Nonlin Soft Matter Phys, 83 (2011) 041502.

[15] K. Zhao, G. Zhou, Q. Wang, Y. Han, L. Wang, D. Ma, Phase Separation in Poly(9,9-dioctylfluorene)/Poly(methyl methacrylate) Blends, Macromolecular Chemistry and Physics, 211 (2010) 313-320.

[16] A. Charas, Q. Ferreira, J. Farinhas, M. Matos, L.s. Alcácer, J. Morgado, Insoluble Patterns of Cross-Linkable Conjugated Polymers from Blend Demixing in Spin Cast Films, Macromolecules, 42 (2009) 7903-7912.

[17] T.L. Tran, P.K. Chan, D. Rousseau, Morphology control in symmetric polymer blends using spinodal decomposition, Chemical Engineering Science, 60 (2005) 7153-7159.

[18] S. Puri, Kinetics of phase transitions, Kinetics of Phase Transitions, CRC Press2009, pp. 13-74.

[19] K.W.D. Lee, P.K. Chan, X. Feng, A computational study into thermally induced phase separation in polymer solutions under a temperature gradient, Macromolecular theory and simulations, 11 (2002) 996-1005.

[20] K. Binder, P. Fratzl, Spinodal decomposition, Phase transformations in materials, (2001) 409-480.

[21] K. Binder, Surface effects on polymer blends and block copolymer melts: theoretical concepts of surface enrichment, surface induced phase separation and ordering, Acta polymerica, 46 (1995) 204-225.

[22] L.T. Yan, X.M. Xie, Wetting-layer formation mechanisms of surface-directed phase separation under different quench depths with off-critical compositions in polymer binary mixture, J Chem Phys, 126 (2007) 064908.

[23] L.-T. Yan, J. Li, Y. Li, X.-M. Xie, Kinetic pathway of pattern-directed phase separation in binary polymer mixture films, Macromolecules, 41 (2008) 3605-3612.

[24] M. Tabatabaieyazdi, P.K. Chan, J. Wu, A computational study of short-range surface-directed phase separation in polymer blends under a linear temperature gradient, Chemical Engineering Science, 137 (2015) 884-895.

[25] V.-N. Tran Duc, P.K. Chan, Using the Cahn–Hilliard Theory in Metastable Binary Solutions, ChemEngineering, 3 (2019).

[26] S. Puri, Phase separation in an off-critical quench, Physics Letters A, 134 (1988) 205-210.

[27] X. Li, M.A. Kanjwal, K. Stephansen, I.S. Chronakis, Preparing poly (caprolactone) micro-particles through solvent-induced phase separation, Materials Letters, 75 (2012) 189-191.

[28] M. Dai, L. Song, W. Nie, Y. Zhou, Golf ball-like particles fabricated by nonsolvent/solvent-induced phase separation method, Journal of Colloid and Interface Science, 391 (2013) 168-171.

[29] P.L. Evans, L.W. Schwartz, R.V. Roy, A Mathematical Model for Crater Defect Formation in a Drying Paint Layer, J Colloid Interface Sci, 227 (2000) 191-205.

[30] S. Howison, J. Moriarty, J. Ockendon, E. Terrill, S. Wilson, A mathematical model for drying paint layers, Journal of Engineering Mathematics, 32 (1997) 377-394.

[31] P. Mokarian-Tabari, M. Geoghegan, J.R. Howse, S.Y. Heriot, R.L. Thompson, R.A. Jones, Quantitative evaluation of evaporation rate during spin-coating of polymer blend films: Control of film structure through defined-atmosphere solvent-casting, Eur Phys J E Soft Matter, 33 (2010) 283-289.

[32] B.-J. de Gans, U.S. Schubert, Inkjet printing of well-defined polymer dots and arrays, Langmuir, 20 (2004) 7789-7793.

[33] T. Kawase, T. Shimoda, C. Newsome, H. Sirringhaus, R.H. Friend, Inkjet printing of polymer thin film transistors, Thin Solid Films, 438-439 (2003) 279-287.

[34] B.J. de Gans, P.C. Duineveld, U.S. Schubert, Inkjet Printing of Polymers: State of the Art and Future Developments, Advanced Materials, 16 (2004) 203-213.

[35] S. Walheim, E. Schäffer, J. Mlynek, U. Steiner, Nanophase-separated polymer films as high-performance antireflection coatings, Science, 283 (1999) 520-522.

[36] A. Münch, C.P. Please, B. Wagner, Spin coating of an evaporating polymer solution, Physics of Fluids, 23 (2011).

[37] M.H. Sadafi, I. Jahn, K. Hooman, Cooling performance of solid containing water for spray assisted dry cooling towers, Energy Conversion and Management, 91 (2015) 158-167.

[38] M.H. Sadafi, J. Ruiz, M. Lucas, I. Jahn, K. Hooman, Numerical and experimental study on a single cone saline water spray in a wind tunnel, International Journal of Thermal Sciences, 120 (2017) 190-202.

[39] F.-C. Chen, Y.-K. Lin, C.-J. Ko, Submicron-scale manipulation of phase separation in organic solar cells, Applied Physics Letters, 92 (2008).

[40] K. Zhao, O. Wodo, D. Ren, H.U. Khan, M.R. Niazi, H. Hu, M. Abdelsamie, R. Li, E.Q. Li, L. Yu, B. Yan, M.M. Payne, J. Smith, J.E.

Anthony, T.D. Anthopoulos, S.T. Thoroddsen, B. Ganapathysubramanian, A. Amassian, Vertical Phase Separation in Small Molecule:Polymer Blend Organic Thin Film Transistors Can Be Dynamically Controlled, Advanced Functional Materials, 26 (2016) 1737-1746.

[41] P.K. Jaiswal, S. Puri, K. Binder, Phase separation in thin films: Effect of temperature gradients, EPL (Europhysics Letters), 103 (2013).

[42] P.K. Jaiswal, K. Binder, S. Puri, Phase separation of binary mixtures in thin films: Effects of an initial concentration gradient across the film, Phys Rev E Stat Nonlin Soft Matter Phys, 85 (2012) 041602.

[43] H. Sadafi, R. Rabani, S. Dehaeck, H. Machrafi, B. Haut, P. Dauby, P. Colinet, Evaporation induced demixing in binary sessile drops, Colloids and Surfaces A: Physicochemical and Engineering Aspects, (2020) 125052.

[44] S.Y. Heriot, R.A. Jones, An interfacial instability in a transient wetting layer leads to lateral phase separation in thin spin-cast polymer-blend films, Nat Mater, 4 (2005) 782-786.

[45] M. Sprenger, S. Walheim, A. Budkowski, U. Steiner, Hierarchic structure formation in binary and ternary polymer blends, Interface Science, 11 (2003) 225-235.

[46] S. Walheim, M. Böltau, J. Mlynek, G. Krausch, U. Steiner, Structure formation via polymer demixing in spin-cast films, Macromolecules, 30 (1997) 4995-5003.

[47] A.D. Dunbar, P. Mokarian-Tabari, A.J. Parnell, S.J. Martin, M.W. Skoda, R.A. Jones, A solution concentration dependent transition from self-stratification to lateral phase separation in spin-cast PS:d-PMMA thin films, Eur Phys J E Soft Matter, 31 (2010) 369-375.

[48] J. Jaczewska, A. Budkowski, A. Bernasik, E. Moons, J. Rysz, Polymer vs solvent diagram of film structures formed in spin-cast poly (3-alkylthiophene) blends, Macromolecules, 41 (2008) 4802-4810.

[49] G.A. Zoumpouli, S.G. Yiantsios, Hydrodynamic effects on phase separation morphologies in evaporating thin films of polymer solutions, Physics of Fluids, 28 (2016).

[50] V. Negi, O. Wodo, J.J. van Franeker, R.A.J. Janssen, P.A. Bobbert, Simulating Phase Separation during Spin Coating of a Polymer–Fullerene Blend: A Joint Computational and Experimental Investigation, ACS Applied Energy Materials, 1 (2018) 725-735.

[51] J. Cummings, J.S. Lowengrub, B.G. Sumpter, S.M. Wise, R. Kumar, Modeling solvent evaporation during thin film formation in phase separating polymer mixtures, Soft Matter, 14 (2018) 1833-1846.

[52] P. Dayal, T. Kyu, Porous fiber formation in polymer-solvent system undergoing solvent evaporation, Journal of Applied Physics, 100 (2006).

[53] C. Schaefer, P. van der Schoot, J.J. Michels, Structuring of polymer solutions upon solvent evaporation, Physical Review E, 91 (2015).

[54] R. Ball, R. Essery, Spinodal decomposition and pattern formation near surfaces, Journal of Physics: Condensed Matter, 2 (1990) 10303.

[55] J. Kim, A numerical method for the Cahn–Hilliard equation with a variable mobility, Communications in Nonlinear Science and Numerical Simulation, 12 (2007) 1560-1571.

[56] M. Dehghan, V. Mohammadi, The numerical solution of Cahn–Hilliard (CH) equation in one, two and three-dimensions via globally radial basis functions (GRBFs) and RBFs-differential quadrature (RBFs-DQ) methods, Engineering Analysis with Boundary Elements, 51 (2015) 74-100.

[57] J.F. Blowey, C.M. Elliott, The Cahn–Hilliard gradient theory for phase separation with non-smooth free energy Part I: Mathematical analysis, European Journal of Applied Mathematics, 2 (2009) 233-280.

[58] J.W. Cahn, J.E. Hilliard, Free Energy of a Nonuniform System. I. Interfacial Free Energy, The Journal of Chemical Physics, 28 (1958) 258-267.

[59] C. Zhou, P. Yue, J.J. Feng, C.F. Ollivier-Gooch, H.H. Hu, 3D phase-field simulations of interfacial dynamics in Newtonian and viscoelastic fluids, Journal of Computational Physics, 229 (2010) 498-511.

[60] P. Yue, C. Zhou, J.J. Feng, C.F. Ollivier-Gooch, H.H. Hu, Phase-field simulations of interfacial dynamics in viscoelastic fluids using finite

elements with adaptive meshing, Journal of Computational Physics, 219 (2006) 47-67.

[61] A. Bertei, R. Mauri, Dynamics of phase separation of sheared inertialess binary mixtures, Physics of Fluids, 32 (2020).

[62] A. Das, S.M. Ali, Understanding of interfacial tension and interface thickness of liquid/liquid interface at a finite concentration of alkyl phosphate by molecular dynamics simulation, Journal of Molecular Liquids, 277 (2019) 217-232.

[63] D.M. Saylor, C.S. Kim, D.V. Patwardhan, J.A. Warren, Diffuse-interface theory for structure formation and release behavior in controlled drug release systems, Acta Biomater, 3 (2007) 851-864.

[64] T. Araki, H. Tanaka, Hydrodynamic delocalization of phase separation in a locally cooled fluid mixture, Europhysics Letters (EPL), 65 (2004) 214-220.

[65] O. Wodo, B. Ganapathysubramanian, Computationally efficient solution to the Cahn–Hilliard equation: Adaptive implicit time schemes, mesh sensitivity analysis and the 3D isoperimetric problem, Journal of Computational Physics, 230 (2011) 6037-6060.

[66] H. Cook, Brownian motion in spinodal decomposition, Acta metallurgica, 18 (1970) 297-306.

[67] J.S. Langer, Theory of spinodal decomposition in alloys, Annals of Physics, 65 (1971) 53-86.

[68] A. Bertei, B. Tellini, R. Mauri, Dynamic transition of dendrite orientation in the diffusive spinodal decomposition of binary mixtures under a thermal gradient, Chemical Engineering Science, 203 (2019) 450-463.

[69] R. Rabani, H. Machrafi, P. Dauby, Effect of including a gas layer on the gel formation process during the drying of a polymer solution, Eur Phys J E Soft Matter, 40 (2017) 89.

[70] R. Rabani, H. Machrafi, P. Dauby, Influence of Composition Dependent Diffusion Coefficient, Viscosity and Relaxation Time on Evaporative Rayleigh-Bénard-Marangoni Instabilities Induced by Solvent Evaporation in

a Polymer Solution, Microgravity Science and Technology, 31 (2019) 615-628.

[71] P. Colinet, J.C. Legros, M.G. Velarde, Nonlinear dynamics of surface-tension-driven instabilities, Wiley-vch2001.

[72] M.G. Hennessy, G.L. Ferretti, J.T. Cabral, O.K. Matar, A minimal model for solvent evaporation and absorption in thin films, J Colloid Interface Sci, 488 (2017) 61-71.

[73] K.y. Ozawa, T. Okuzono, M. Doi, Diffusion Process during Drying to Cause the Skin Formation in Polymer Solutions, Japanese Journal of Applied Physics, 45 (2006) 8817-8822.

[74] O. Wodo, B. Ganapathysubramanian, Modeling morphology evolution during solvent-based fabrication of organic solar cells, Computational Materials Science, 55 (2012) 113-126.

[75] C.S. Kim, D.M. Saylor, M.K. McDermott, D.V. Patwardhan, J.A. Warren, Modeling solvent evaporation during the manufacture of controlled drug-release coatings and the impact on release kinetics, J Biomed Mater Res B Appl Biomater, 90 (2009) 688-699.

[76] COMSOL Multiphysics, User's Guide Version 5.5, (2019).

[77] C.M. Elliott, D.A. French, F. Milner, A second order splitting method for the Cahn-Hilliard equation, Numerische Mathematik, 54 (1989) 575-590.

[78] C.M. Elliott, H. Garcke, On the Cahn–Hilliard equation with degenerate mobility, Siam journal on mathematical analysis, 27 (1996) 404-423.

[79] S. Zhang, M. Wang, A nonconforming finite element method for the Cahn–Hilliard equation, Journal of Computational Physics, 229 (2010) 7361-7372.

[80] P. Yazgan-Birgi, H.A. Arafat, M.I. Hassan Ali, Implementation of two multiphase flow methods in modeling wetting of microporous hydrophobic membranes, Sci Total Environ, 691 (2019) 1251-1261.

[81] M.A. Zaeem, S.D. Mesarovic, Morphological instabilities in thin films: Evolution maps, Computational Materials Science, 50 (2011) 1030-1036.

[82] M. Krivilyov, D. Aflyatunova, V. Lebedev, P.K. Galenko, Phase-field simulation of non-isothermal phase separation in rapidly quenched Co-Cu melts, Computational Materials Science, 158 (2019) 289-295.

[83] M. Liang, X. Xin, W. Fan, H. Wang, W. Sun, Phase field simulation and microscopic observation of phase separation and thermal stability of polymer modified asphalt, Construction and Building Materials, 204 (2019) 132-143.

[84] G. Fayaz, S. Kazemzadeh, Towards additive manufacturing of compressor impellers: 3D modeling of multilayer laser solid freeform fabrication of nickel alloy 625 powder mixed with nano-CeO 2 on AISI 4140, Additive Manufacturing, 20 (2018) 182-188.

[85] A. Adrover, A. Brasiello, G. Ponso, A moving boundary model for food isothermal drying and shrinkage: General setting, Journal of Food Engineering, 244 (2019) 178-191.

[86] M.-A. Xue, O. Kargbo, J. Zheng, Seiche oscillations of layered fluids in a closed rectangular tank with wave damping mechanism, Ocean Engineering, 196 (2020).

[87] R. Martínez, J.A. Gonzalez, I. Garcia de la Fuente, J.C. Cobos, Thermodynamic properties of n-alkoxyethanols+ organic solvent mixtures. XIV. Liquid− liquid equilibria of systems containing 2-(2-ethoxyethoxy) ethanol and selected alkanes, Journal of Chemical & Engineering Data, 45 (2000) 1036-1039.

[88] X. Li, G. Ji, H. Zhang, Phase transitions of macromolecular microsphere composite hydrogels based on the stochastic Cahn–Hilliard equation, Journal of Computational Physics, 283 (2015) 81-97.

[89] Y.C. Li, R.P. Shi, C.P. Wang, X.J. Liu, Y. Wang, Phase-field simulation of thermally induced spinodal decomposition in polymer blends, Modelling and Simulation in Materials Science and Engineering, 20 (2012).

[90] S.S. Kim, T.H. Sanders, Phase-field simulation of spinodal phase separation in the Na2O-SiO2 glasses, Journal of Non-Crystalline Solids, 528 (2020).

[91] Y. Li, Thermodynamic and kinetic study of spinodal phase separation in heptane–phenol system, Calphad, 50 (2015) 113-117.

[92] K. Binder, Spinodal Decomposition in P. Haasen (Ed.): Material Science and Technology, Vol. 5, Phase Transitions in Materials, (1991).

[93] P. Papon, J. Leblond, P.H. Meijer, Physics of Phase Transitions, Springer2002.

Chapter 7

Conclusion and future work

In this thesis, we explored several problems which provide a better understanding of the couplings that exist between convective instabilities, evaporation and phase separation or gel formation in thin films of liquid mixtures. The approach was theoretical, numerical and experimental and the results showed the competition between the different basic physical mechanisms that determine the behavior of the system.

7.1 Summary of thesis

This thesis was divided into the following two parts:

- Thin evaporating film of a polymer solution
- Phase separation in thin evaporating film of a partially miscible binary mixture

In the first part of the thesis, which is introduced in Chapter 1 and developed in Chapters 2 and 3, we studied a mechanism of skin formation and the hydrodynamic thermal and solutal instabilities that can take place in a thin

film of an evaporative polymer solution. In the following paragraphs, we discuss our central conclusions related to the aforementioned problems.

In Chapter 2, we developed a one-dimensional model for a thin evaporating film of a polymer solution, considering the physics of the gas layer and its interaction with the liquid, to describe the effect of solvent evaporation on the formation of a polymer-rich skin below the free surface. A composition-dependent diffusion coefficient in the liquid layer and the local equilibrium hypothesis at the liquid-gas interface were introduced, which allowed describing gelation and the formation of a skin layer and the evaporation process, respectively.

A skin layer starts forming as soon as the surface concentration reaches the so-called gelation mass fraction during the evaporation process, after which the evaporation rate considerably starts decreasing. As evaporation proceeds, the polymer-rich/gel layer can grow from the surface down to the substrate.

Another interesting result of our study was the possible immediate gelation at the liquid-gas interface when evaporation is induced in a rather sudden way. This immediate gelation is associated with the very fast (theoretically infinite) evaporation predicted by our model and impossible with the other previous approaches (see [20, 22] in Chapter 2) for which a phenomenological law was introduced to describe the evaporation flux. This gelation and its formation can freeze the motion of the liquid at the free surface and consequently prevent Marangoni convection in the system.

In Chapter 3, we analyzed the solutal and thermal Rayleigh-Bénard-Marangoni instabilities in a thin evaporating film of a polymer solution. These instabilities are caused by temperature and concentration gradients in buoyancy forces and/or surface tension. To conduct our study, we considered a horizontal polymer solution layer consisting of a volatile solvent, which

evaporates into air, and a single non-volatile polymer. The approach was based on general thermodynamic principles as well as on the physics of the gas phase and its interactions with the liquid phase.

The main difficulty of the problem stemmed from the time dependence of the one-dimensional reference solution, and also from the need to consider in our stability analysis the variations of the viscosity, diffusion and relaxation time with the solvent mass fraction in the liquid phase.

Carrying out a frozen-time linear stability analysis revealed that not one, but two modes of instability can occur during the drying process. One of these modes (monotonic mode) corresponds to the onset of stationary convection cells within the bulk of the layer. For this mode of instability, our results indicated that the concentration dependent diffusion and viscosity makes the system more stable in comparison with constant diffusion and viscosity. Moreover, for the monotonic mode of the instability, our results emphasized that there is a minimum liquid thickness (turning point in the curve), below which no instability ever occurs. A comparison was also carried out between our numerical approach and the experimental data provided by Doumenc et al. (see [43] in Chapter 3) and our stability results for thick gas layers showed a good agreement with the experimental work.

The other mode corresponds to the onset of oscillatory convection and is a consequence of the viscoelastic behavior of polymer solutions. For this oscillatory mode, a turning point also appeared in the stability curve, but this turning point defines a maximal thickness above which no oscillatory instability is possible. Moreover, this maximal thickness is in the micrometer range, which means that oscillatory instabilities would be possible only in very thin layers.

Finally, we developed an approximate model of our system by keeping only the most important physical phenomena and the findings showed that the corresponding results are in a very good agreement with the complete analysis. From this comparison, it is concluded that the thermal and Rayleigh effects can safely be neglected, since these are not strong enough to induce an instability on their own. This supports the fact that the solutal Marangoni effect is much stronger than the thermal and Rayleigh effects and is the actual main physical mechanism generating the instability. Note also that the comparison between the complete and simplified models has also shown that the gas phase can be considered as a purely diffusive medium for the solvent vapor.

In the second part of the thesis, which is introduced in Chapter 4 and developed in Chapters 5 and 6, we focused on the relationship between evaporation and phase separation in a partially miscible binary mixture in order to understand the onset of phase separation and to analyze the different types of morphologies that can appear in the system. In the following paragraphs, we highlight the main results regarding these topics.

In Chapter 5, we presented the experimental results that have been carried out in collaboration with the TIPs research group in ULB regarding the phase separation in an evaporating sessile binary drop of DGME and n-hexane. The results provided a useful insight into the physical mechanisms for different stages of demixing including: pure evaporation, nucleation, coalescence, sedimentation, expanding fingers, emerging and drying. Beside the experimental results, our aim was also to analyze theoretically the diffusive behavior of the system before phase separation starts and, in particular, to determine the conditions for which demixing would never happen in a partially miscible binary mixture. To analyze this matter, we built a one-dimensional model for a thin film of a binary mixture considering purely

diffusive equations for heat and mass transports in the liquid phase and in the upper gas layer.

The numerical results provided a foundation for understanding how a binary mixture at ambient temperature, initially above the critical temperature of the coexistence curve, is able to demix due to the evaporation. The evaporation induces a temperature decrease at the free surface, alongside a decrease of the solvent concentration in the upper part of the liquid layer. Consequently, the representative point in the phase space for the mixture at the interface rapidly approaches and enters the coexistence curve and subsequently demixing starts in the upper part of the system.

Although we studied the system in an idealized context, without using a phase field model for the phase separation between components of the binary mixture, our results suggest an interesting critical line in the phase diagram. This critical line separates the initial conditions for which phase separation will take place after some time, from those for which no phase separation will ever occur.

Finally in Chapter 6, the aim was to determine different types of morphologies that can be created by the phase separation phenomena induced by solvent evaporation in a thin film of a partially miscible binary mixture. The mathematical model was based on a non-isothermal phase field approach of a binary mixture to describe the thermodynamics of phase separation. Hydrodynamics effects were not considered. Instead, the evolution of the two phases was driven purely by diffusion. The binary mixture was confined in a thin film with a periodic boundary conditions in the horizontal direction, an impermeable and adiabatic substrate, and a free surface at liquid-gas interface. We also assumed that the substrate and liquid-gas interface are neutral with respect to each component of the binary

mixture, leading to a diffuse interface perpendicular to the surfaces upon phase separation. Finally, we described an experimental framework in a Hele-Shaw cell that allows studying 2-D phase separation in a thin evaporating film of a partially miscible binary mixture.

In the numerical simulations, we have considered three values of the so-called Peclet number, which describes the competition between evaporation and phase separation. For low Peclet number, which corresponds to small evaporation rate, phase separation takes place everywhere across the bulk of the thin film at the same time and consequently a bulk structure is created. For larger values of the Peclet number, i.e. at moderate and high evaporation rates, the liquid close to the liquid-gas interface enters the unstable zone before the bottom and a vertical concentration gradient is formed. For a moderate evaporation rate, the spinodal instability occurs close to the top surface, which creates a lateral structure in the film. For high evaporation rate, no spinodal instability occurs in the system close to the liquid-gas interface and a lamellar structure is formed.

Concerning the mid- and long-term evolution of the system after the beginning of the phase separation, our main findings are the following. When a lateral structure is initially formed close to the liquid-gas interface, we highlighted the possibility of coalescence of solute-rich droplets. This coalescence was observed only in thick enough layer, for which the growth of the drops can lead to their coalescence before these drops reach the substrate. We also observed that after the formation of a lamellar morphology, a spinodal instability can subsequently appear close to the substrate, with the formation of solvent rich droplets, when the lower parts of the layer enter the demixing region. After some time, these drops disappear in the long term and only solute rich fluid remains in the film.

The initial temperature and concentration of the binary mixture are possible adjustable variables that allow controlling the morphology evolution. In fact, a change of the initial temperature or concentration can lead the system reach the spinodal curve at different locations in the phase diagram, which can affect notably the driving force of the phase separation and its competition with the evaporation.

Finally, we showed experimentally the mechanism of 2-D phase separation in a thin evaporating film of a partially miscible binary mixture using a Hele Shaw cell with a double telecentric setup. The experimental results indicated a very good qualitative agreement with the numerical results regarding the lateral and lamellar structures.

7.2 Limitations of our approach and recommendations for future work

The investigations carried out in this thesis provide some novel insights into the key processes that can occur in a thin evaporative film of a binary mixture. However, they also have some limitations and have led to several interesting questions, which remain unanswered and which will be briefly introduced now.

The results of Chapter 3 revealed that two modes of instability (monotonic and oscillatory modes) can occur in a thin evaporative film of a polymer solution. Our approach was based on the frozen time assumption, which remains a questionable hypothesis. Therefore, other techniques of stability analyses could also be used and compared with ours. For instance, it would be interesting to implement and asses the amplification approach (see [25, 26] in Chapter 3), which fully considers the transient behavior of the

reference solution, or the non-normal approach described in ref. [27] of Chapter 3, which is an extension of the amplification approach. Other possible extensions would consist in carrying out a nonlinear analysis or two- or three-dimensional numerical simulations to study the long-term evolution of the instability in the system. Beside the theoretical and numerical approaches, it would also be interesting to perform an experimental work to determine if the oscillatory instability actually takes place, as predicted by our theory. Such a study could also be used to refine the model for linear stability analysis.

The removal of solvent from the upper surface can also possibly lead to an unstable density stratification, whereby a heavier layer fluid appears on top of a lighter fluid. Such systems are often subject to a Rayleigh-Taylor instability. This leads to a fingering pattern, which can subsequently develop into plumes that sink. The question of whether a Rayleigh-Taylor instability can occur in a thin evaporative film of a polymer solution was not addressed in our work, because the polymer and the solvent were assumed to have the same density. Considering components with different densities would therefore be important to analyze the possibility of Rayleigh-Taylor instabilities, but it is worth emphasizing that such a study would face the same challenges as those we met because of the time-dependence of the reference solution whose stability is analyzed. For this reason, numerical simulations of the full problem might also be useful for understanding the long-term evolution of the fluid and, in particular, the development of plumes.

In Chapter 6, we investigated phase separation phenomena in a thin evaporative film of a binary mixture and different types of morphologies were emphasized. These investigations were based on a phase field model of

the binary mixture, but it is important to remember that several important assumptions were introduced in our analysis.

First, we neglected all hydrodynamic effects, with the consequence that Rayleigh-Bénard-Marangoni, or Rayleigh-Taylor instabilities were not considered. Some other studies have already emphasized that convection can interact with phase separation and therefore, it would be very interesting to analyze how the different physical mechanisms we have observed in our purely diffusive description would be affected by taking hydrodynamics into account. In particular, it would be important to analyze how the spinodal instability, and the competition between phase separation and evaporation, would be modified by considering motion in the fluid layer.

Then, we did not consider the possibility of deformations of the free surface of the layer in our simulations. In fact, deformations of the liquid-gas interface can be induced by the inhomogeneous evaporation when phase separation has begun and is also linked with convection in the layer. Moreover, imposing a flat interface prevents dewetting along the substrate and imposes an artificial coalescence of solute drops that have reached the substrate in the long-term evolution of the system. Since dewetting is actually observed in experiments, describing surface deformations is really an important additional step that should be considered.

In our description, we have also considered equal attractions of the two components by the free upper surface and by the substrate. However, we believe that preferential attraction could greatly affect the creation of structure during phase separation and its influence on the final morphology of the film should therefore be analyzed in future work.

Finally, let us remind that we restricted our simulations, and also the experimental set-up, to two-dimensional situations. Clearly, it would be

interesting to run simulations and build experiments in a three-dimensional thin film, since dimensionality can have a direct effect on the coalescence of separated phases and thus the formation of lateral and lamellar structures.